UNIVERSITÄTSKLINIKUM HAMBURG-EPPENDORF

The impact of general anesthesia on memory consolidation, hippocampal network activity and spine dynamics and the application of genetically-encoded tools for mapping neuronal and synaptic activity in vivo.

Dissertation

zur Erlangung des Doktorgrades PhD

an der Medizinischen Fakultät der Universität Hamburg.

vorgelegt von:

Wei Yang

aus Liaoning, China

Hamburg 2021

(wird von der Medizinischen Fakultät ausgefüllt)

Angenommen von der

Medizinischen Fakultät der Universität Hamburg am: 17.02.2022

Veröffentlicht mit Genehmigung der

Medizinischen Fakultät der Universität Hamburg.

Prüfungsausschuss, der/die Vorsitzende: Prof.Dr. Simon J.Wiegert

Prüfungsausschuss, zweite/r Gutachter/in: Prof.Dr. Tobias Donner

Prüfungsausschuss, dritte/r Gutachter/in:

TABLE OF CONTENTS

Acknowledgment

First of all, I thank Prof. Simon Wiegert for providing me with the opportunity to be a PhD student in his lab. My PhD journey in Germany was smooth but full of difficulties and obstacles, and due to the unfortunate passing of my previous PhD supervisor, prof. Frotscher, I joined Simon's recently established lab in 2017. Probably because it was newly established, in my eye, he works not only as a supervisor but also as a super postdoc, who was always available for discussing projects, dealing with platform problems, showing me experiments by himself, basically for any difficulties. All these offered me precious opportunities to learn lab skills and strengthen my scientific capacities. I would like to thank him for his kind supports over these years. Also, I do appreciate the freedom he gave me to look for my interests. Under his guidance, I saw myself improve by leaps and bounds. Thanks very much again.

I thank Prof. Thomas Oertner for his effort as a member of my thesis committee and a reviewer of the thesis. What’s more, I thank Prof. Thomas Oertner for offering me the opportunity to work on the collaborative SynTagMA project. I am also so impressed by his great passion for research that, I remind myself, I should always follow my heart and find my interests.

I thank Prof. Matthias Kneussel not only for his support and effort as a member of my thesis committee and reviewer of this thesis but also for helping me study in the ZMNH family. Also, I would like to thank prof. Tobias H. Donner for joining the dissertation committee and for his careful and professional advice and guidance.

I want to thank Mattia Chini, Jastyn A. Pöpplau, Andrey Formozov, Alexander Dieter. The anesthesia project would not be proceeding so well without their support and help. Even though I didn't enjoy the analysis challenge, we work together, complement each other's strengths, learn from each other and finally complete this project.

I want to thank Dr. Alberto Perez-Alvarez and Dr. Brenna C Fearey for having me in the SynTagMA project. I really enjoyed the time spent together with them.

I would like to thank our collaborators, specifically Prof. Thomas Oertner, Prof. Dr. Ileana Hanganu-Opatz, Dr. Fabio Morellini and Prof. Olaf Sporns. It's been a pleasure working with you all.

Especially, I want to thank all the Wiegert and Oertner lab members. The time spent with each individual in this big family was the most precious memory of my PhD study.

Mauro, thank you for all your support and encouragement over the years. I feel you are reliable so that you were always the person I turn to when I wanted to complain about the mess in my life and work. I do appreciate the friendship with you. Through spending time with you and Celine, I have come to realize that one of the very, very important abilities is the ability to be emotionally stable, being patient with oneself and being confident in life.

Silvia, I cannot tell you how happy I am to know you here. In my heart, you are attractive, full of sunshine and courage. It seems that just talking to you fills me with the courage to face life again when I am down. Despite you told me that you are not always positive either, you always try to stay positive. That's already a lot I could learn.

Cynthia, you are so determined. How I wish I had known what I wanted to do much earlier, although for me, now is the earliest moment. I am so grateful for your friendship.

Alex, you are a very influential person. If I had met you earlier, I would have made more progress. Your dedication to your work, your balance in life, and your thoughtfulness in helping others are influencing me. Thank you for your unlimited help in this limited time.

Paul, I am so pleased to meet you here. In one term of time, we were both the only in-vivo person in each group, and I spent a lot of time doing experiments with you. I always received inspiration from your enthusiasm for science, and you always explained to me every detail of every step. Thanks for your patience in helping me.

I cannot individually thank everyone, but I'll thank all the other colleagues who shared their wonderful moments and experience with me. Thanks to: Christine, Stefan, Patrick, Kathrin, Adrianna, Maxime, Chantal, Yasmine, Oana, Andreas, Margo, Tim, Iris.

I would like to thank the China Scholarship Council (CSC) for providing me the scholarship to study abroad, which has allowed me to meet so many lovely people and had such a wonderful experience in my life.

Last but not least, I would like to express my most sincere gratitude to my parents, Yunxiu Jia and Chengyi Yang, and my husband, Xuekun Wu, for their unreserved and unlimited supports. Because of them, I am growing towards a better myself.

Abbreviations

ACh	acetylcholine
AMPAR	α-amino-3-hydroxy-5-methyl-4-isoxazolepropionic acid receptor
AP	action potential
CA	cornus ammonis
CaMPARI	calcium-modulated photoactivatable ratiometric integrator
DG	dentate gyrus
Dox	doxycycline
ECFP	enhanced cyan fluorescent protein
EMG	electromyography
FAB	Flumazenil, Atipamezole and Buprenorphine,
FOV	field of view
FRET	Förster resonance energy transfer
GABA	γ-aminobutyric acid
GABAR	γ-aminobutyric acid receptor
GAs	general anesthetics
GECI	genetically encoded calcium indicator
GRASP	GFP reconstitution across synaptic partners
H.M.	Henry Molaison
hSyn	Human synapsin 1 gene promoter
IEG	immediate early gene
Iso	isoflurane
K2P	two-pore domain potassium
KAR	kainic acid receptor
Keta/Xyl	ketamine/xylazine

LC	locus coeruleus
LFP	local field potential
MMF	medetomidine/midazolam/fentanyl
NMDARs	N-methyl-D-aspartate receptors
NREM	non-rapid eye movement
PC	principal component
POCD	postoperative cognitive dysfunction
PRF	pontine reticular formation
REM	rapid eye movement
s.o.	stratum oriens
s.p.	stratum pyramidale
s.r.	stratum radiatum
s.l.m.	stratum lacunosum-moleculare
SUA	single-unit activity,
SynTagMA	synaptic tag for mapping activity
tTA	tetracycline-controlled transactivator
VLPO	ventrolateral preoptic nucleus
VTA	ventral tegmental area

Abstract

Learning and memory are important to brain functions that are essential for the survival of animals and humans. Amnesia refers to memory loss caused by brain diseases, injuries, or pharmacological interventions such as the use of general anesthetics. In this thesis, I presented two projects related to the hippocampus, a brain region central to memory formation and consolidation.

In the first project, I investigated the effects of three different general anesthetics (GAs), isoflurane (Iso), medetomidine/midazolam/fentanyl (MMF), and ketamine/xylazine (Keta/Xyl) on memory consolidation, hippocampal network activity and spine dynamic. First, using Morris Water Maze, I found that anesthesia with MMF or Keta/Xyl, but not Iso, impaired memory consolidation. Using in vivo calcium imaging with the genetically encoded indicator GCaMP6f, I imaged the same field of view of CA1 of each individual mouse under different anesthetics to compare the population dynamics and recovery timeline for each condition. I found that different GAs induced highly distinct network states. Iso induced 0.1 Hz oscillations, Keta/Xyl had the strongest reduction in calcium dynamics, and MMF strongly impaired population dynamics for many hours. Furthermore, I found different long-term effects on dendritic spine dynamics, with Keta/Xyl having the strongest effect, by imaging the formation and elimination of dendritic spines under each condition. Finally, to compare general anesthesia with sleep, I performed calcium imaging under NREM and REM sleep states and found that sleep modifies CA1 activity to a much lower degree than anesthesia. Taken together, this study revealed distinct effects of Iso, MMF and Keta/Xyl on network activity and structural spine dynamics in the hippocampal CA1 of adult mice.

In the second part of this thesis, I tested a photoconvertible fluorescent probe, postSynTagMA, in vivo by mapping active neurons and synapses during behavior. SynTagMA is developed by my colleagues in order to rapidly and stably label synapses with high calcium levels. After injecteing hSyn-postSynTagMA or mDlx-postSynTagMA in dorsal

CA1 of the mouse hippocampus, I found that there was a small percentage of photoconverted CA1 neuronal nuclei or photoconverted synapses after illumination with 405 nm light under anesthesia. Then, I made the behavioral application to investigate active neuronal populations under goal-directed navigation with 405 nm light illumination triggered by the reward. In sum, these results show that postSynTagMA photoconversion could selectively map behaviorally relevant neurons and synapses with high calcium transients in behaving mice.

Taken together, the findings in this thesis 1) demonstrate that different anesthetics, despite inducing similar physiological states, differ significantly in their effects on synaptic stability, hippocampal network activity and memory consolidation; and 2) validate that postSynTagMA photoconversion selectively maps behaviorally relevant neurons and synapses with high calcium transients in behaving mice.

ZUSSAMMENFASSUNG

Lernen und Gedächtnisbildung sind wichtige Funktionen des Gehirns und essentiell für das Überleben von Tieren und Menschen. Amnesie bezeichnet den Verlust des Gedächtnisses, welcher durch Krankheit, Verletzung, oder pharmazeutische Intervention, wie z.B. Narkosemittel, verursacht werden kann. In dieser Arbeit vereine ich zwei Projekte, welche sich mit dem Hippocampus, einer der Schlüsselregionen des Hirns in Bezug auf Gedächtnisformation und -konsolidierung, beschäftigen.

Im ersten Projekt habe ich die Effekte dreier Anästhetika, Isofluran (Iso), Medetomidine/Midazolam/Fentanyl (MMF), sowie Ketamin/Xylazin (Keta/Xyl), auf Gedächtniskonsolidierung, hippocampale Netzwerkaktivität, und die Dynamik dendritischer Spines untersucht. Mittels des Morris-Wasserlabyrinths habe ich herausgefunden, dass MMF- und Keta/Xyl-vermittelte Narkosen, nicht aber die Iso-Narkose, die Gedächtnisbildung beeinträchtigen. Durch in vivo 2-Photonenmikroskopie genetisch kodierter Kalziumindikatoren konnte ich einen definierten Teil des neuronalen Netzwerkes der CA1-Region des Hippocampus in einzelnen Mäusen chronisch verfolgen, und den Einfluss der verschiedenen Narkosemittel auf die Populationsdynamiken der neuronalen Aktivität vergleichen. Hierdurch konnte ich zeigen, dass verschiedene Narkosemittel zu verschiedenen Netzwerkzuständen führen: Während Iso Oszillationen mit 0.1 Hz induziert hat, verursachte Ket/Xyl die stärkste Reduktion der Kalziumdynamiken MMF, hingegen, hatte den stärksten Einfluss auf die Populationsdynamik, welcher für mehrere Stunden andauerte. Zusätzlich konnte ich durch Bildgebung der Formation und Eliminierung dendritischer Spines zeigen, dass die verschiedenen Konditionen verschiedene Langzeiteffekte der Spine-Stabilität zur Folge hatten, wobei Keta/Xyl die stärksten Effekte hervorgerufen hat. Durch zusätzliche Messungen der Kalziumaktivitäten während natürlichen Schlafs konnte ich zeigen, dass die CA1-Aktivtät durch Schlaf deutlich geringer verändert wurde als durch die verschiedenen Narkosemittel. Zusammengenommen offenbart diese Studie die

verschiedenen Effekte von Iso, MMF, und Keta/Xyl auf die Netzwerkaktivität und Dynamik der Spine-Strukturen in der CA1-Region des Hippocampus adulter Mäuse.

Im zweiten Teil meiner Arbeit habe ich das photokonvertierbare Werkzeug postSynTagMA bezüglich seiner Anwendbarkeit zur Kartierung aktiver Neurone und Synapsen in einem wachen, sich verhaltenden Tier, getestet. Hierzu habe ich entweder hSyn-postSynTagMA oder mDlx-postSynTagMA in die CA1-Region des dorsalen Hippocampus der Maus injiziert und einen kleinen Prozentsatz photokonvertierter, neuronaler Nuclei oder Synapsen in der CA1-Region beobachten können, nachdem der Hippocampus des narkotisierten Tieres mit violettem Licht beleuchtet wurde. Anschließend habe ich an der Anwendung im wachen, sich verhaltenden Tier gearbeitet, um die durch eine Belohnung aktivierte Population hippocampaler Neurone während einer zielgerichteten Navigationsaufgabe zu untersuchen. Die Ergebnisse dieser Experimente zeigen, dass die Photokonversion von postSynTagMa zur Kartierung spezifischer, verhaltensrelevanter Neurone und Synapsen mit hohen Kalziumtransienten in sich verhaltenden Mäusen genutzt werden kann.

Zusammengenommen zeigen die Ergebnisse dieser Arbeit 1), dass verschiedene Anästhetika, obwohl sie ähnliche physiologische Zustände hervorrufen, sich in ihren Auswirkungen auf die synaptische Stabilität, die Aktivität des hippocampalen Netzwerks und die Gedächtniskonsolidierung erheblich unterscheiden; und 2) bestätigen, dass die postSynTagMA-Photokonversion selektiv verhaltensrelevante Neuronen und Synapsen mit hohen Kalziumtransienten in Mäusen abbildet.

1 Introduction

1.1 Hippocampal structure and function

1.1.1 Structure

The hippocampus, located in the medial temporal lobe, is part of the limbic system. The C-shaped structure of the hippocampus consists of the dentate gyrus (DG), cornus ammonis 1, 2 and 3 (CA1, CA2 and CA3) (Bourne and Harris 2008). A unique feature of the hippocampal circuit is its unidirectional excitatory pathway in DG, CA3 and CA1. First, the axons of the performant path carry sensory information from neurons in layer II of the entorhinal cortex to the dendrites of granule cells in DG. Second, granule cells project to the proximal apical dendrites of CA3 pyramidal cells through mossy fibers. Third, CA3 pyramidal neurons project to apical dendrites of ipsilateral CA1 pyramidal cells through Schaffer collateral pathway and to contralateral CA1 and CA3 pyramidal cells through commissural connections (Neves, Cooke, and Bliss 2008).

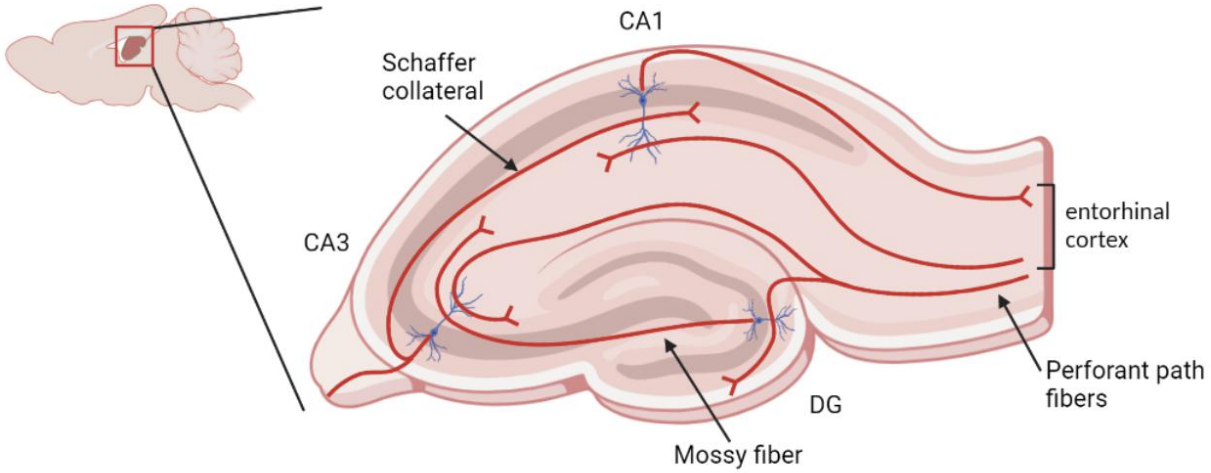

Figure 1. The main hippocampalsynaptic circuits. Left, location of the hippocampus in the mouse brain. A magnified section of the hippocampus (right) highlights the principal neurons and their major connections. Blue, cell bodies and dendrites; red, axons. Synapses can form where blue and red lines intersect. Perforant pathway axons from entorhinal cortex can reach hippocampal CA1 pyramidal neurons directly via a monosynaptic connection, or indirectly via a trisynaptic connection through the dentate gyrus granule cells and CA3 pyramidal neurons. Granule cells project to the proximal apical dendrites of CA3 pyramidal cells through mossy

fibers. Then, CA3 pyramidal neurons project to apical dendrites of ipsilateral CA1 pyramidal cells through the Schaffer collateral pathway. (Image made using BioRender)

The imaging experiments in this thesis focus on the dorsal CA1 region. The CA1 region has been divided into stratum oriens, stratum pyramidale, stratum radiatum and stratum lacunosum-moleculare. In principle, the cell bodies of CA1 pyramidal neurons are located in the stratum pyramidale. The basal dendrites of pyramidal neurons occupy the stratum oriens and form synapses mainly with axons from CA3 pyramidal cells. At the opposite pole, the apical dendrites of pyramidal neurons make up the stratum radiatum and receive input primarily from the Schaffer collateral pathway, whereas the apical tuft dendrites make up the stratum lacunosum-moleculare and receive a direct input from layer III cells of the entorhinal cortex.

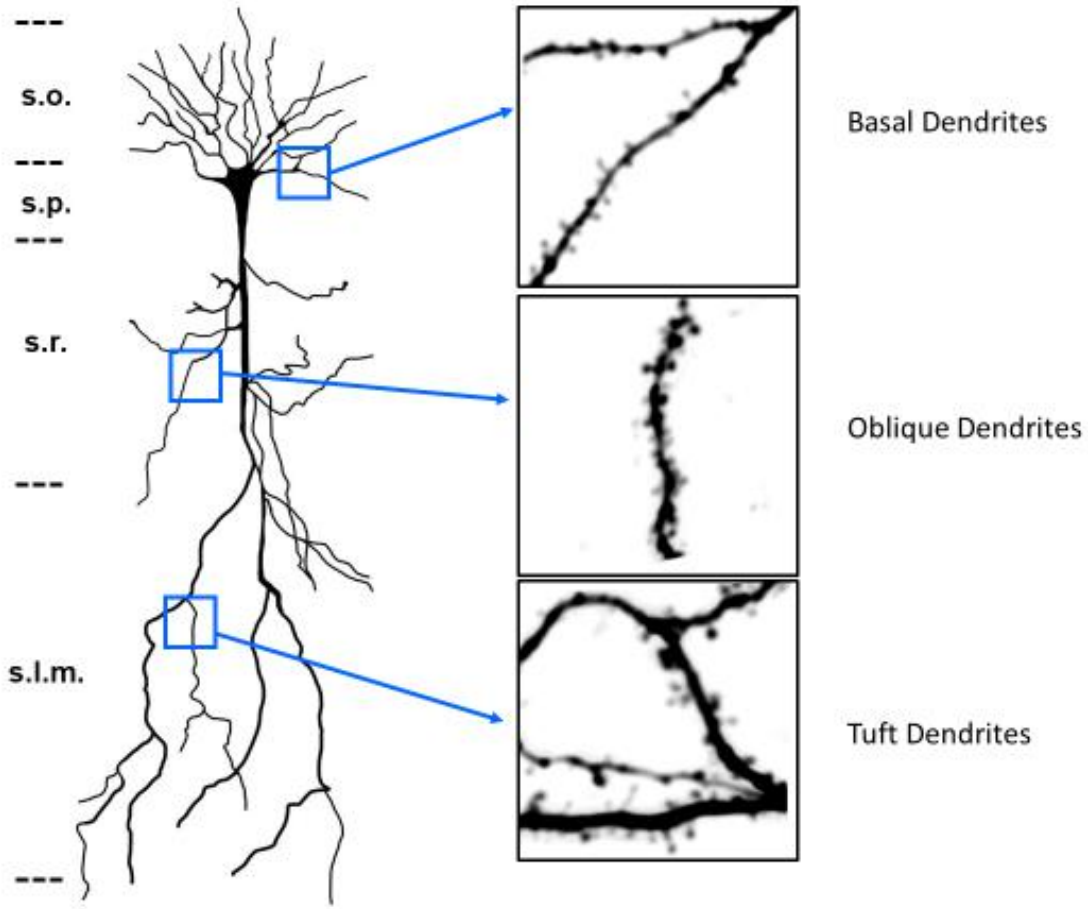

Figure 2. Morphology of the CA1 pyramidal neuron. Left, indicating the layer structure in CA1. s.o.,stratum oriens, s.p., stratum pyramidale, s.r., stratum radiatum, s.l.m., stratum lacunosum moleculare. Middle, representative camera lucida drawings of a CA1 pyramidal neuron (adapted from Ishizuka, Cowan, and Amaral 1995). **Right**, representative 2-photon images of basal dendrites in s.o., oblique dendrites in s.r. and tuft dendrites in s.l.m aquired in the mouse in vivo.

Previous studies of the dendritic morphology of pyramidal neurons in the CA1 region of the rat hippocampus revealed that the number of dendrites emerging from the base of the pyramidal soma ranges from 2 to 8. Most of these dendrites branch multiple times, forming a basal dendritic tree with approximately 40 terminal segments. Most of the branches in the basal dendrites are close to the soma (Bannister and Larkman 1995). Studies suggest that the apical dendrites of CA1 pyramidal neurons can be divided into two groups based on dendritic morphology. In the first group of neurons, the apical dendrites would extend all the way through the stratum radiatum and branch out in the stratum lacunosum-moleculare. The second group would bifurcate in the stratum radiatum (Bannister and Larkman 1995). Although the apical dendrites of these two types of CA1 neurons differ in morphology, the CA1 pyramidal neurons have been considered to be one class at that time. This view has been challenged by recent studies on hippocampal CA1 heterogeneity that have shown superficial and deep CA1 pyramidal neurons differ in molecular, structural, physiological properties as well as in connectivity (Soltesz and Losonczy 2018). Quantifications of the distribution of spines on different dendritic domains of CA1 pyramidal neurons revealed that the density is highest in the stratum oriens and stratum radiatum but lower in the stratum lacunosum-moleculare (Megias et al. 2001). Also, proximal basal and oblique apical dendrites in the stratum oriens and stratum radiatum are sparsely spiny, while the distal basal and oblique apical dendrites are densely spiny; their excitatory inputs terminate exclusively on dendritic spines, whereas inhibitory inputs target dendritic shafts (Megias et al. 2001). Spine structure is dynamic and may change in response to environmental stimuli. Also, the growth of new spines and changes in the existing spines have been linked to

synaptic plasticity in the hippocampus (Segal 2005; Wiegert et al. 2018), suggesting that synaptic spines may be the subcellular substrates for memory storage ns in neural circuits (Whitlock et al. 2006; Attardo, Fitzgerald, and Schnitzer 2015).

1.1.2 Role in learning and memory

In human studies, the first evidence to show the location of learning and memory came from the famous patient Henry Molaison, widely known as H.M. who underwent a bilateral surgical removal of the medial temporal lobe in order to treat his epileptic seizures. Although the surgery eliminated his seizures, he emerged from the surgery with the lost ability to form new memories (anterograde amnesia), as well as to recall memories of events that occurred just prior to this surgery (retrograde amnesia) (Scoville and Milner 1957). This seminal study has led to the notion that some types of memory may be stored in the medial temporal lobe region.

Afterward, extensive studies using lesion or pharmacological inactivation, neural stimulation and single-cell recordings in rodent animals have further proved the importance of the hippocampus in learning and memory formation, especially episodic-like memory (Squire 1992; Bird and Burgess 2008; Squire, Stark, and Clark 2004) and spatial memory (Burgess, Maguire, and O'Keefe 2002). Episodic-like memory, in non-human animals, is defined as the ability to recall and reexperience a specific event, including information about position of the event (‘where’), sequence of the event (‘when’), and the content of the event (‘what’). Using the natural aversion to the water environment, Morris Water Maze has been used to test for episodic-like memory processes. It is a classic spatial and reversal learning test, in which mice learn to memorize the position of the hidden platform in order to quickly escape the water. In this study, I use the Morris water maze to test for reversal learning, specifically testing the effects of the different anesthetics on the consolidation of the memory of the new platform location. Moreover, the hippocampus has been shown to be involved in many kinds of spatial memory, and, in particular, the formation of cognitive maps and their use in spatial

navigation (Burgess, Maguire, and O'Keefe 2002). A recent study found that a small population of neurons in CA1 and subiculum dedicated to encoding reward locations (Gauthier and Tank 2018). The same cells are active near multiple reward sites in an environment, and can even remain active in different environments, which indicates that neurons in the hippocampus are not only specific to encoding the features of environment but also identifying goal locations. In project II, I used this spatial goal-directed behavior to test the validity of the postSynTagMA.

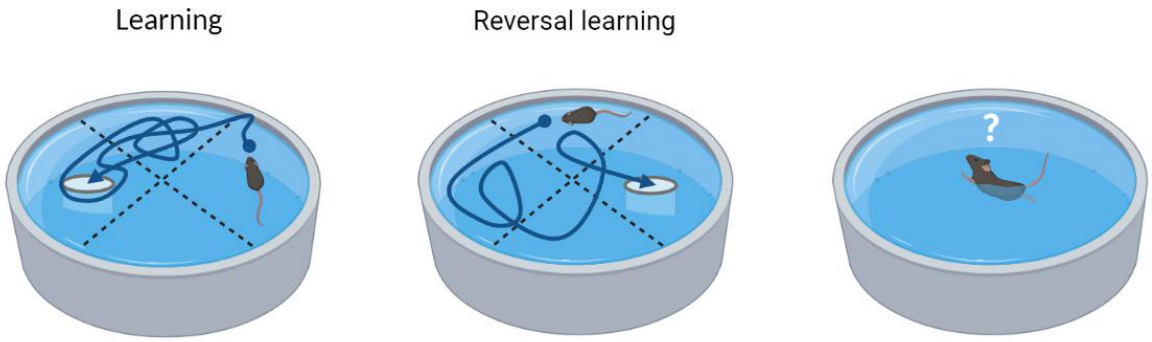

Figure 3. Spatial and reversal learning in the Morris water maze. A schematic representation of the Morris water maze training protocol. In this example, mice were first trained to locate a hidden platform ("Learning"). Next, the hidden platform was moved to the opposite quadrant during reversal training ("Reversal learning"). In the end, a probe trial is performed to assess the strength of the memory. Image made using BioRender.

1.2 Hippocampus-dependent amnesia

1.2.1 Hippocampus-dependent amnesia in humans

Extensive studies have now shown that an increasing number of especially elderly patients experience varying degrees of cognitive deficits in the days and months after surgery (Moller et al. 1998; McDonagh et al. 2010). This deterioration in cognitive performance is often referred to as postoperative cognitive dysfunction (POCD), including post-operative delirium and post-operative cognitive decline. Risk factors associated with POCD can be broadly

grouped into patient-related, procedure- and anesthesia-related. Age and preexisting medical conditions are the most common patient-related risk factors. In elderly patients, the incidence of POCD doesn't decrease from 6 weeks (54.3%) to 1 year (46.1%), suggesting that deficits in this aged group are not easily recovered (McDonagh et al. 2010). Also, patients with mild cognitive impairment have an accelerated progression of POCD compared to patients without mild cognitive impairment (Bekker et al. 2010).

Many surgical factors have been reported to influence cognitive performance in the early postoperative cognitive dysfunction. The type of surgery appears to influence the incidence of POCD, with cardiac surgery having the highest risk (Moller et al. 1998). Other risk factors positively associated with POCD are: duration of anesthesia, postoperative infection, and respiratory complications (Moller et al. 1998). Interestingly, increasing the duration of anesthesia, but not the choice of technique (general versus regional anesthesia), was positively correlated with the incidence of POCD (Moller et al. 1998).

1.2.2 Hippocampal amnesia after general anesthesia in animal models

It is quite challenging to identify specific factors contributing to POCD through studies of patients. For example, the effects of anesthesia cannot be distinguished from the other surgical factors that affect cognitive function. Therefore, it is necessary to use animal models for further in-depth studies. Since learning and memory deficits are the main features of patients with POCD, many of the animal studies conducted to date have focused on amnesia syndrome, which in turn lead to the concept of memory consolidation.

Memory consolidation refers to the transition of a newly formed memory from a fragile short-term state to a stable long-term state. This initial fragile short-term memory can be disrupted by interventions ranging from electroshock (McGaugh and Alpern 1966) to protein synthesis inhibitors (Davis and Squire 1984), which, if delivered specifically before the learning, results in anterograde amnesia or after the learning results in retrograde amnesia. Anterograde amnesia is characterized by the inability to form new memory following the onset of amnesia,

while retrograde amnesia is characterized by the inability to recall past events formed prior to the onset of amnesia.

Many factors may lead to amnesia, such as trauma, brain tumors, stress, general anesthesia, etc. This thesis focuses on the effects by which exposure to general anesthetics triggers lasting memory deficits in an adult mouse model.

Behavioral studies in rats and mice have shown that a single anesthetic dose could induce memory deficits. Aged rats exhibit anterograde amnesia when trained on a radial arm maze spatial memory task 2 weeks after exposure to isoflurane-nitrous oxide anesthetic treatment (Culley et al. 2004). Anterograde memory impairment also occurs in adult mice after a single isoflurane treatment on Barnes maze and contextual fear conditioning tasks (Lin and Zuo 2011) and novel object recognition tasks (Zurek et al. 2014). In other studies, adult mice also showed retrograde amnesia on an object recognition task, which they learned immediately before sevoflurane anesthesia (Wiklund et al. 2009). These studies rely on behavioral performance to investigate the effect of a single anesthetic on the learning and memory function of the animal, and also make effort to figure out the cause of amnesia by using antagonists and agonists. However, there is still the need to systematically investigate at different levels how commonly used general anesthetic protocols affect hippocampal CA1 network dynamics, synaptic structure, and memory performance.

1.3 General anesthesia

General anesthesia is a drug-induced, reversible behavioral condition including unconsciousness, amnesia, sedation, immobility, and analgesia, which all together represent a state where surgery can be tolerated (Urban and Bleckwenn 2002). Among the more than 200 million surgical procedures performed worldwide each year, a proportion of patients exhibit cognitive impairment after surgery and anesthesia (Monk et al. 2008). While the loss of memory is required during anesthetic administration, so that no memories of the surgical

procedure are formed, post-operative cognitive dysfunction is not desired. Combined with the previous introduction of POCD, we could draw the following conclusions. First, a positive correlation between the duration of anesthesia and the incidence of postoperative cognitive deficits in patients is found, pointing to a role for general anesthetics in this phenomenon (Moller et al. 1998). Besides, a single exposure to an anesthetic can cause retrograde and anterograde memory impairment that persists for days to weeks in adult and aged rats (Culley et al. 2003). The purpose of the first part of this thesis is to provide an accurate and detailed assessment of the effects of three general anesthetics commonly used in animal research by linking neuronal network changes and dendritic spine dynamics with the known molecular events of the general anesthetic actions. In the following sections, I will introduce the known molecular and cellular mechanisms of general anesthesia, followed by a brief description of the three general anesthetics we chose, including Iso, Keta/Xyl, and MMF. In the last section, I will compare the anesthesia-induced loss of consciousness and natural sleep.

1.3.1 Molecular mechanisms

Although the exact mechanisms of how general anesthetics work remain elusive, a host of ion channels and intracellular effects on the cytoskeleton, intracellular signaling proteins, and mitochondria have been identified as specific targets of general anesthetics (Kelz and Mashour 2019). Of these, ion channels are the most prominent candidates. They include ligand-gated ionotropic receptors such as γ-aminobutyric acid receptors (GABARs), glutamate receptor and acetylcholine receptors, voltage-gated ion channels such as voltage-gated sodium channels, calcium channels and potassium channels (Campagna, Miller, and Forman 2003; Rudolph and Antkowiak 2004; Kelz and Mashour 2019).

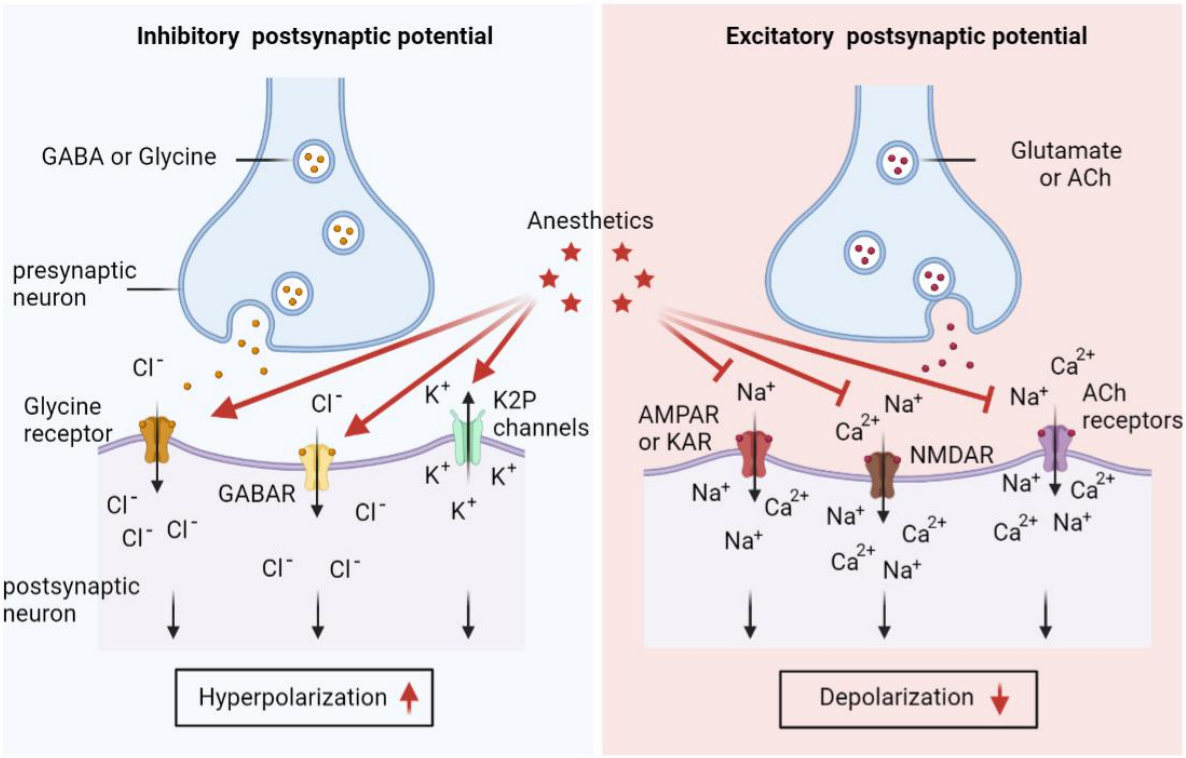

Figure 4. Putative targets of anesthetic action. Anesthetic drugs may **(left)** enhance inhibitory synaptic activity or **(right)** diminish excitatory activity. GABA, γ-aminobutyric acid; GABAR, γ-aminobutyric acid receptor; NMDAR, N-methyl-D-aspartate receptor; AMPAR, α-amino-3-hydroxy-5-methyl-4-isoxazol-propionic acid receptor; KAR, kainic acid receptor; ACh, acetylcholine; K(2P) channels, two-pore domain potassium channels. Image made using BioRender.

$GABA_A$ receptors are the most abundant fast inhibitory neurotransmitter receptors found throughout the central nervous system, and they have long been appreciated as a key target of general anesthetics (Nicoll 1978). In the clinic, low doses of all volatile anesthetics have been proven to enhance $GABA_A$ signaling (Krasowski and Harrison 1999). The most persuasive data have come from in vivo experiments using genetically modified animals. Using gene-targeting technology, results from mice harboring a subtle point mutation (N265M) in the second transmembrane region of the beta3 subunit of the $GABA_A$ receptor show a profound reduction in the loss of righting reflex duration in response to intravenous but not volatile anesthetics, indicating that a point mutation in $GABA_A$ receptor's specific subunit could greatly affect their in vivo anesthetic potencies (Jurd et al. 2003). In addition,

studies from mice carrying a knock-in in their α1 subunit, which retain an unperturbed sensitivity to GABA, show altered loss of righting reflexes in response to volatile agents, such as isoflurane, supporting a role for α1-containing receptors in mediating the effects of these anesthetics (Sonner et al. 2007). There are also studies using α4- and α5-knockout animals linking particular anesthetic to extra-synaptic $GABA_A$ receptors. Mice lacking the α4 subunit, which are thought to be found predominantly in extrasynaptic locations, are insensitive to the ataxic, sedative and analgesic effects of gaboxadol, demonstrating that the key pharmacological effects of the sedative agent gaboxadol are mediated by α4-subunit-containing $GABA_A$ receptors (Chandra et al. 2006). Similarly, Mice lacking the α5 subunit, which is also thought to be mainly extrasynaptic, reduce the amnesic but not the sedative-hypnotic properties of etomidate (Cheng et al. 2006). Almost all general anesthetics have been found to potentiate GABA-induced Cl^- currents, and only the relatively small and apolar anesthetics such as ketamine and xenon have little or no effect on $GABA_A$ receptors (de Sousa et al. 2000).

The examples above indicate that selective enhancement of inhibitory GABAergic neurotransmission induces unconsciousness. Conversely, selective blockade of excitatory glutamatergic neurotransmission in the central nervous system can induce general anesthesia: analgesia, unconsciousness and immobility (Petrenko et al. 2014).

The N-methyl-D-aspartate receptors (NMDARs), being a major component of glutamatergic neurotransmission, are present broadly at excitatory glutamatergic synapses in the central nervous system. Structurally, NMDARs exist as heteromeric complexes composed of four subunits derived from three subtypes: GluN1 (also known asNR1), GluN2A–B (also known as NR2A–B) and GluN3A–B (also known as NR3A–B) (Salussolia et al. 2011). NMDARs have been shown to be inhibited by many intravenous anesthetics, like ketamine, phencyclidine, as well as volatile anesthetics isoflurane and sevoflurane, but the effects vary among different agents (Liu et al. 2001; Hollmann et al. 2001). The data from point mutation studies show that two mutations (F639A in GluN1 and A825W in GluN2A) reduce the

anesthetic sensitivity of NMDA receptors, such as isoflurane, halothane, but not ketamine or benzene (Ogata et al. 2006).

In addition to the targets discussed above, there are a number of other plausible targets that are worth mentioning. First, glycine receptors, which are homologous to, and often colocalized with, $GABA_A$ receptors, are a potential anesthetic target (Downie et al. 1996; Betz and Laube 2006; Brackmann et al. 2004). Glycine receptors have an inhibitory role, particularly in the brainstem and spinal cord, where they might mediate the action of volatile anesthetics. Also, the two-pore domain K+ channel could be another target. Studies have shown that dual pore domain K+ channels can be activated by a variety of volatile general anesthetics (Patel et al. 1999). Stimuli increasing the activity of K2P channels inhibit excitability due to membrane hyperpolarization by reducing the number of channels in the cell membrane, decreasing membrane conductivity. While stimuli blocking K2P channels reduce K+ flux and increase cellular excitability (Ries and Puil 1999; Steinberg et al. 2015). Besides, α2 adrenergic agonists, such as medetomidine, can be used as both a surgical anesthetic and analgesic because of their ability to produce sedation without causing respiratory depression, while promoting cardiovascular stability. In veterinary anesthesia, medetomidine is often used in combinations with opioids, like buprenorphine, which reduces requirements for postoperative analgesics and the dose of anesthetics (Hedenqvist, Roughan, and Flecknell 2000).

1.3.2 Cellular mechanism

Based on the molecular mechanisms described above, the effects of general anesthetics can be further understood at the level of the cellular network. Various general anesthetics may intervene at the cellular network level by following ways: enhancing the activity of sleep-promoting neuronal subpopulations; attenuating the activity of wake-promoting neuronal subpopulations; disruption of cortical-subcortical interactions. One hypothesis is those general anesthetics exert part of their actions by "hijacking" the endogenous arousal circuitry

of the brain. Thus, modulating the activity of the neuroanatomical systems associated with sleep-wake cycle could, to some extent, explain some of the effects of anesthetics (Lydic and Baghdoyan 2005; Franks 2008).

Neurons in the hypothalamic preoptic area, particularly the ventrolateral preoptic nucleus (VLPO), are thought to be important for sleep generation and regulation (Szymusiak and McGinty 2008; Sherin et al. 1996; Chung et al. 2017). Studies have shown that anesthesia could increase the number of active neurons in the VLPO. In addition, destroying VLPO neurons produces an acute resistance to the effects of anesthesia, demonstrating the role of the VLPO in the induction of general anesthesia (Nelson et al. 2003; Moore et al. 2012).

Several brain regions have been shown to promote wakefulness, which includes GABAergic neurons in pontine reticular formation (PRF), noradrenergic neurons in the locus coeruleus (LC), the glutamatergic neurons in parabrachial nucleus, the serotonergic neurons in dorsal raphe, and the dopaminergic neurons in ventral tegmental area (VTA) (Varin and Bonnavion 2019).

Studies have reported that in the PRF during REM sleep, GABA levels decrease and acetylcholine levels increase (Vanini et al. 2008; Vanini et al. 2011), which describes the relationship between GABA and acetylcholine in the PRF, raising the possibility that modulation of these neurotransmitters may modulate sleep. Other studies verified this hypothesis by administration of the GABA agonist muscimol into the PRF, which causes a significant increase of periods of wakefulness and a decrease in rapid eye movement (REM) and non-REM (NREM) sleep. Interestingly, these effects were reversed by coadministration of the $GABA_A$ antagonists bicuculline (Flint et al. 2010). In the same study, results also support the notion that the PRF is an important site of anesthetic action. The injection of $GABA_A$ antagonist bicuculline into the PRF prolonged isoflurane-induced hypnosis (Flint et al. 2010). Similarly, PRF administration of drugs that increase or decrease GABA levels increased or decreased, isoflurane induction time, respectively.

The LC is the main source of noradrenergic projections in the brain and it is implicated in regulating attention and arousal (Sara 2009). There is a frequency-dependent, causal relationship between LC firing and sleep-to-wake transitions. Indeed, optogenetic activation of the LC is sufficient to awaken sleeping animals, while its inhibition would prevent hypocretin-mediated awakening (Carter et al. 2010; Carter et al. 2012).

Recent studies have also verified the role of the dopaminergic system in modulating anesthetic sensitivity. Although dopaminergic neurons in the VTA do not exhibit state-dependent firing, electrical stimulation of the VTA, administration of dopamine D1 receptor agonists, or administration of methylphenidate, a dopamine/norepinephrine reuptake inhibitor, induces emergence from anesthesia (Solt et al. 2011; Chemali et al. 2012; Solt et al. 2014). These studies suggest that also the dopaminergic system has a role in the arousal pathways in the brain.

The preceding sections focused on the subcortical cellular mechanisms by which general anesthetics act by modulating the shared circuit with sleep. Another hypothesis suggests that general anesthetics cause loss of consciousness by modulating cortical and thalamocortical circuits and fragmentating cortical information interactions (Mashour and Hudetz 2017).

The thalamus has long been considered a crucial neuroanatomical target for general anesthetics and is thought to be the "switch" for anesthetic state transitions (Alkire, Haier, and Fallon 2000). The thalamus gates sensory inputs to the cortex and is bidirectionally connected with neocortex. Loss of thalamocortical connectivity is considered a key event underlying loss of consciousness both during anesthesia and sleep (Boveroux et al. 2010; Goupil and Bekinschtein 2012).

A study shows that, by simultaneously recording from thalamus and across layers of the frontoparietal cortex in awake, sleeping, and anesthetized macaques, the firing frequency of deep cortical neurons was significantly decreased and functional cortical connections were fragmented under general anesthesia, while electrical stimulation activating thalamus

significantly increases the electrical activity of deep cortical neurons and the coherence of different frequency field potentials, suggesting thalamus regulates intra- and intercortical information processing as an important mechanism for the loss of consciousness induced by general anesthetics (Redinbaugh et al. 2020).

In the past few years, a large number of studies have reported that during anesthetic-induced loss of consciousness there is a breakdown in effective connectivity with a loss of both spatial and temporal propagation of information across the cerebral cortex (Ferrarelli et al. 2010). Positron-emission tomographic studies in humans revealed that general anesthesia significantly decreases cortical metabolic activity (Alkire et al. 1995). Functional magnetic resonance Imaging (Purdon et al. 2009) and local-field-potential recordings (Velly et al. 2007) in humans also provide supportive evidence of changes in cortical neural activity of unconsciousness induced by general anesthesia. In contrast, studies using two-photon calcium activity imaging in the mouse cortex show that general anesthetic may induce network synchrony and disrupt sensory processing in the cortex (Lissek et al. 2016). A recent study in the mouse somatosensory cortex also reveals that general anesthesia decouples the flow of information between layer 5 pyramidal neuron dendrites and their cell bodies by blocking metabotropic glutamate and cholinergic receptors (Suzuki and Larkum 2020).

1.3.3 Iso, Keta/Xyl, MMF

Project I of the thesis focuses on the three general anesthetics, Iso, Keta/Xyl, and MMF as indicated above. Iso, Keta and MMF ingredients are commonly used in clinical practice and Xyl is widely used in veterinary medicine. MMF applies the most recently recommended management strategy in anesthetic care, namely multimodal general anaesthesia, which requires the simultaneous administration of different drugs to create a state of anaesthesia (Brown, Pavone, and Naranjo 2018). Balanced general anaesthesia uses fewer of each drug than if given alone, thereby increasing the likelihood of its intended effect and reducing the likelihood of its side effects.

Isoflurane

Isoflurane is a volatile anesthetic used for induction and maintenance of general anesthesia, which allows for rapid induction and precise adjustments of the anesthesia levels. To date, many studies have identified a number of targets for its mechanisms of action including GABA, glutamate and glycine receptors (Nishikawa 2011; Grasshoff and Antkowiak 2006; Hung et al. 2020). Isoflurane could relax muscles and reduces pain sensitivity, but for survival surgery, once the animals wake up from Iso, there is no residual analgesic activity. Pre-treatment with intravenous buprenorphine or lidocaine or both is required to reduce complications (Cheong and Khoo 1996; LaTourette et al. 2020; Kolesnikov, Chereshnev, and Pasternak 2000).

Ketamine/Xylazine

Ketamine induces dissociative anesthesia, a state providing pain relief, sedation and amnesia (Davis, Davis, and Hooper 2019). Ketamine acts as an antagonist of NMDA receptors and normally is combined with alpha-2 receptor agonists, xylazine or medetomidine to produce deep sedation. This combination may produce short-term anesthesia with moderate analgesia, and also the recovery can be accelerated by reversing the alpha2-agonist with Atipamezole. It is worth noting that ketamine/alpha2-agonist combinations may cause profound cardiac depression.

At lower subanesthetic doses, ketamine acts as an antidepressant, in which ketamine inhibits only a fraction of NMDARs (likely <50% block for most NMDAR subtypes at steady-state under physiological conditions) (Li et al. 2010; Abdallah et al. 2015; Zhang and Hashimoto 2019). Even at the peak of drug action, a significant proportion of NMDAR remains unblocked. While at anesthetic doses, the antidepressant effects of ketamine are not observed in rodents (Li et al. 2010). There is a study showing that complete blockade of

NMDARs by high concentrations of ketamine further eliminated the complex effects of the drug on neuronal excitability, as well as the delayed metamorphic inhibition of LTP in the hippocampal region of young rats observed at low micromolar concentrations (Izumi and Zorumski 2014).

Medetomidine, midazolam and fentanyl

Medetomidine, an α2 adrenergic agonist, is a synthetic drug used as both a surgical anesthetic and an analgesic (Sinclair 2003). Midazolam is a benzodiazepine, which does not directly activate $GABA_A$ receptors, but enhances the neuroinhibitory effects mediated by GABA (Olkkola and Ahonen 2008). The main effects of benzodiazepines are sedation, hypnosis, anterograde amnesia, and centrally mediated muscle relaxation. Fentanyl is the most commonly used opioid in the care of experimental animals, which is a powerful analgesic with a relatively long duration of action exceeding 1h (Vardanyan and Hruby 2014). The combination of medetomidine, midazolam and fentanyl (MMF) is one type of multimodal general anesthesia administered in veterinary anesthesia, which can be antagonized by the injection of a wake-up cocktail (Flumazenil, Atipamezole and Buprenorphine, FAB) (Albrecht et al. 2014; Fleischmann et al. 2016).

1.4 Imaging hippocampal neurons and synapses

Real-time large-scale recording of neural activity in the living brain to resolve the neural circuits and activity patterns involved in specific behavioral paradigms is an important objective of neuroscience. The combination of light microscopy and genetically encoded fluorescent indicators has become a popular means of recording neural activity in the nervous system of model animals. In this thesis, part I combines two-photon imaging with GCaMP6f, a genetically encoded calcium indicator (GECI), or Thy1-GFP transgenic mouse line, to respectively observe neural activity or spine dynamics in the hippocampal dCA1

region under three states of general anesthesia, wakefulness, and sleep. in part II I study the application of postSynTagMA, a photoconvertible GECI, in living mice.

1.4.1 Two-photon excitation fluorescence laser scanning microscopy

Traditionally, single-photon microscopes have been used to study biological tissues and cells. This requires tissue extraction and preparation to obtain optical access to the region of interest because single-photon microscopy is limited to a maximum depth of 100 μm. Due to the scattering effect of light, conventional light microscopes cannot be used to image deeper tissues, such as the mammalian brain. The invention of two-photon excitation fluorescence laser scanning microscopy using long, near-infrared wavelengths allows deeper light penetration of tissue with less scattering (Denk, Strickler, and Webb 1990). Also, phototoxicity is reduced because the photons are concentrated in one focal point. By using this microscopy technique, in combination with fluorescent dyes that label cells, led to the possibility to study deep tissues in vivo to a depth of up to 1 mm (Theer, Hasan, and Denk 2003). Using two-photon excitation of the fluorophore, two photons need to reach the fluorophore almost simultaneously within 0.5 fs to combine their energies and only then allow the fluorophore to reach its excited state. In order to generate sufficient signal using two-photon excitation, the light needs to be focused spatially and temporally. The use of a high numerical aperture (NA) objective leads to a spatial concentration of photons at a focal point and efficient light collection of the emitted photons. A powerful laser delivering ~100 fs pulses at a MHz repetition rate is required to achieve temporal concentration of photons.

In summary, two-photon fluorescence microscopy has three main advantages over confocal fluorescence microscopy.

1) Optical sectioning. Due to the nonlinearity of two-photon excitation, the absorption rate depends on the laser intensity. The excitation of fluorescence is restricted to the region near the focal point. This is advantageous when imaging thick samples because the optical sectioning can provide an ultra-high signal to background ratio.

2) Deeper imaging depth. Due to the inhomogeneity of the refractive index of biological samples, scattering of light can reduce the signal-to-noise ratio. Two-photon excitation uses a longer excitation light wavelength than single-photon, resulting in less scattering of light by biological tissues.

3) Lower phototoxicity. In some biological applications, especially in vivo applications, the most prominent advantages of two-photon imaging over confocal single-photon imaging are safer excitation wavelengths and lower phototoxicity, making it the best choice for long-duration in vivo observation of biological tissues.

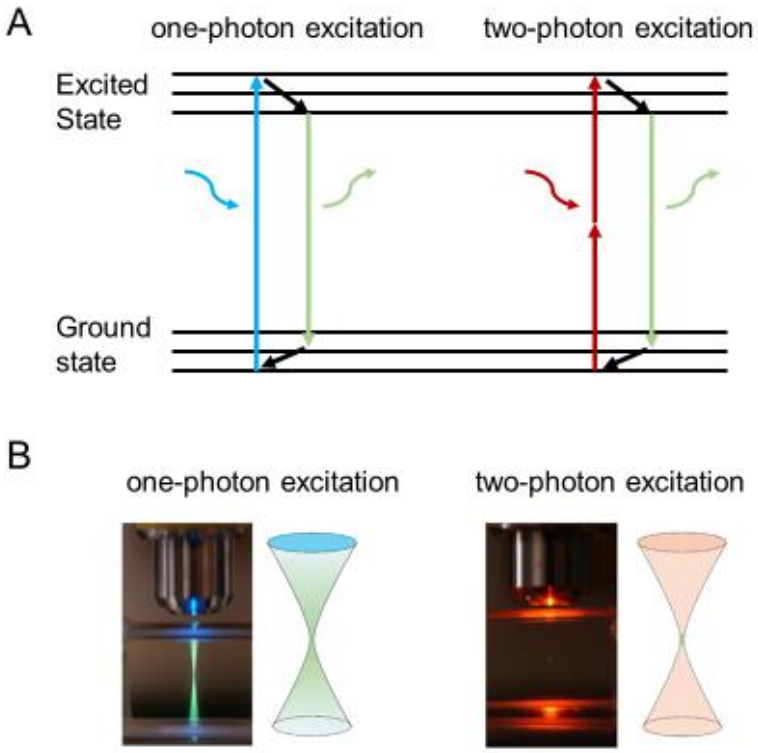

Figure 5. The mechanism of two-photon excitation. (A) Jablonsky diagram, illustrating one-photon excitation on the left and two-photon excitation on the right. One photon of high-energy blue light is needed to bring the green fluorescent molecule to its excited state before it emits green fluorescence. On the other hand, two photons of half the energy or double the wavelength arriving simultaneously (0.5 fs) sum their energy to lift the green fluorescent molecule to its excited state before it emits green fluorescence. **(B)** Differences in the focal point of one- and two-photon excitation. Although the focal plane is the same, in one-photon microscopy an entire cone of fluorescence light (green) is generated, whereas in two-photon microscopy signal production is localized to the vicinity of the focal spot, where sufficient photon density is reached for near-simultaneous absorption of thw photons by a fluorophore molecule. Photos by Steve Ruzin and Holly Aaron, UC Berkeley.

1.4.2 Genetically encoded calcium indicators: GCaMP6f

Genetically encoded calcium indicators (GECI) are classified into two types depending on the fluorescent protein, Förster resonance energy transfer (FRET) based GECIs and single fluorophore based GECIs (Grienberger and Konnerth 2012).

FRET refers to a form of non-radiative energy transfer between the excited donor fluorophore and the acceptor fluorophore. In order to act as a FRET pair, their distance must be less than 10 nm apart to achieve FRET and the emission spectrum of the donor needs to overlap with the excitation spectrum of the acceptor. Cameleon is the first GECI and is composed of an enhanced cyan fluorescent protein, acting as donor fluorophore, calmodulin, calmodulin-binding peptide M13 and an enhanced yellow fluorescent protein, acting as acceptor fluorophore (Miyawaki et al. 1997). In the absence of calcium, its emission is dominated by ECFP fluorescence. Binding of Ca^{2+} makes calmodulin wrap around the M13 domain, the change in molecular conformation leads to a decrease in the spatial distance between the two fluorescent proteins, and increase the fluorescence resonance energy transfer (FRET) between the flanking GFPs. As FRET occurs, the blue fluorescence is reduced and the yellow fluorescence is increased.

Compared to FRET-based GECIs, where the change in fluorescence after calcium binding is the FRET ratio, the change in fluorescence of single fluorophore-based GECIs after calcium binding is calculated based on baseline fluorescence ($F-F_0/F_0$) (Yasuda et al. 2004). The most commonly used single fluorophore GECI is the GCaMP family, which is increasingly used for in vivo calcium imaging (Dombeck et al. 2010; Akerboom et al. 2013; Broussard et al. 2018). GCaMP consists of circularly permuted enhanced green fluorescent proteins (EGFP) with calcium-binding proteins on one side and calmodulin M13 on the other (Grienberger and Konnerth 2012). In the presence of calcium, the interaction between calmodulin and M13 induces a conformational change, which leads to an increase in the emitted fluorescence (Nakai, Ohkura, and Imoto 2001). To date, the GCaMP family of GECIs

has evolved through multiple iterations of mutagenesis and selection (Chen et al. 2013; Dana et al. 2019).

The advantages of FRET-based biosensors include an inherent ratiometric fluorescence response that is more suitable for calibration for quantitative imaging. One disadvantage is that two emission bands are required (limiting the possibility of multicolor, multiparametric imaging) (Carlson and Campbell 2009). Another disadvantage is that different wavelengths of light are absorbed and scattered differently within the tissue, so the observed emissivity may vary with tissue depth (Nasu et al. 2021). Compared to FRET-based biosensors, single FP-based biosensors, in contrast, are easier to use because they require only a single chromophore for excitation and emission. Also, they are well suited for multiparametric imaging (Mehta et al. 2018) and avoid the problem of differences in absorbance and scattering at different wavelengths as a function of tissue depth.

GCaMP6f was used in the project I, which was shown to report single action potentials (APs) in mouse cortex with ΔF/F of 20%, which is superior to organic dyes, and a half-life of 142 ms (Chen et al. 2013). Calcium imaging via GCaMP6f in combination with two-photon microscopy makes it possible to measure the cellular activity of deep neuronal populations in vivo, such as pyramidal neurons in the hippocampus. Aside from the previously mentioned advantages, in two-photon scanning microscopy, the sample is excited and the signal is collected point by point. This overcomes the pixel cross-talk in wide-field imaging of scattered tissue. Although two-photon microscopy can deeply penetrate into brain tissue, the hippocampal CA1 region is more than one millimeter below the cortical surface and therefore cannot be imaged directly. To overcome this limitation, a chronic hippocampal window is made by removing the overlying cortex by aspiration and implanting a customized brain window (see Methods section).

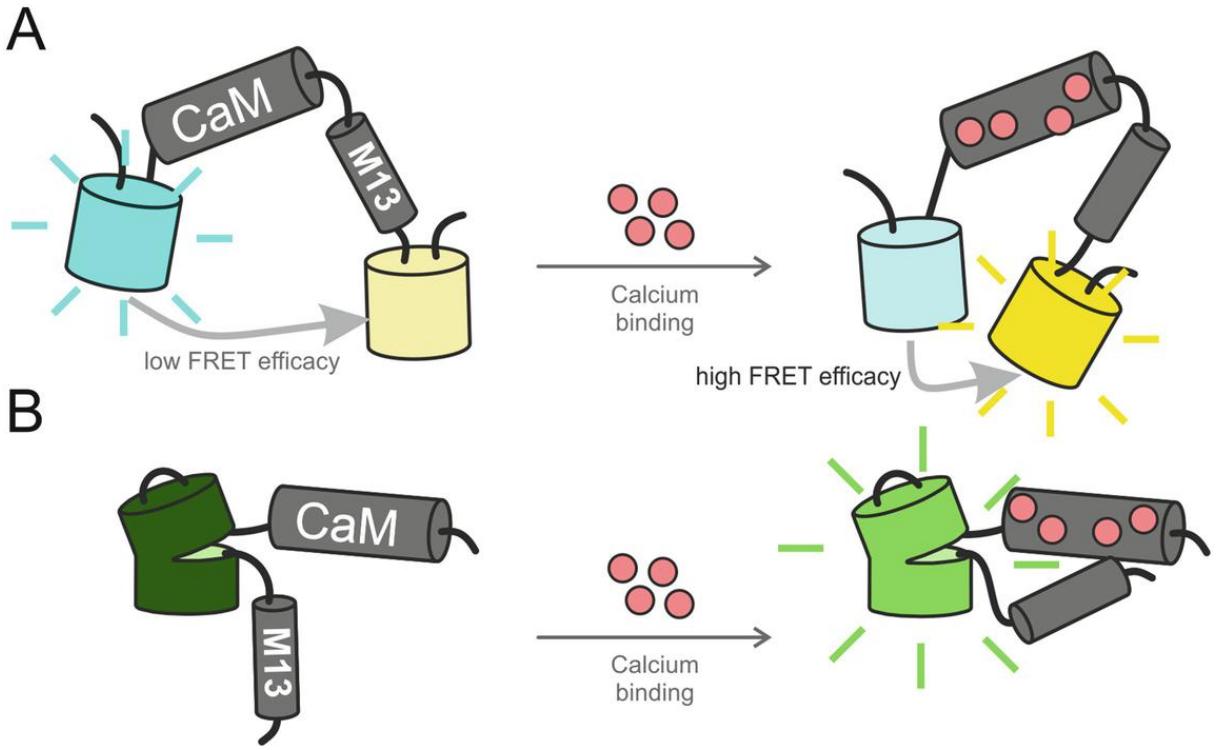

Figure 6. Schematic depiction of genetically encoded calcium indicators. (A) Förster resonance energy transfer (FRET)-based calcium indicators use two fluorescent proteins (e.g. a cyan fluorescent protein, CFP, depicted in cyan color, and a yellow fluorescent protein, YFP, depicted in yellow color). Excitation of CFP results in cyan and (via FRET) yellow fluorescence. Binding of Ca^{2+} (red circles) to a calcium-binding domain (such as the calmodulin (CaM)– M13 complex shown here) increases the efficacy of FRET between CFP and YFP and therefore decreases cyan fluorescence and increases yellow fluorescence. **(B)** Single fluorescent protein indicators of the GCaMP type incorporate a circularly permuted fluorescent protein (cpFP, depicted in green hue). Binding of Ca^{2+} to CaM–M13 increases the cpFP fluorescence. adapted from ref (Mollinedo-Gajate, Song, and Knopfel 2019).

1.4.3 CAMPARI and SynTagMA

When calcium imaging is performed with two-photon microscopy, it can be used to image neuronal activity in behaving mice at the sub-cellular resolution including dendrites and axons. Despite these advances, we are still limited by the nature of the indicators and the instruments. The trade-off between spatial and temporal resolution makes it challenging to simultaneously measure the fluorescence of thousands of synapses in even one single pyramidal neuron. Therefore, most functional imaging experiments are limited to the cell body, or to monitor the activity of several synapses within a limited field of view. In general,

the need to choose between high temporal resolution or high spatial resolution limits our ability to extract information from the brain using optical methods.

A GECI suitable for studying active neuronal ensembles is called CaMPARI (calcium-modulated photoactivatable ratiometric integrator), which allows a temporally precise “activity snapshot” of a large tissue volume (Fosque et al. 2015). CaMPARI undergoes efficient and irreversible green-to-red conversion only in the presence of both elevated intracellular calcium and violet light illumination. By pairing violet illumination with neuronal activity, for example during a behavior, active cells become red, while inactive cells remain green. The red and green components of CaMPARI still retain their normal calcium indicator characteristics, although their fluorescence decreases after calcium binding, rather than the more common increase in fluorescence. Compared with other genetically encoded calcium indicators (GECIs) (Pologruto, Yasuda, and Svoboda 2004), the main advantage of CaMPARI is the photoconvertible feature enables optical selection and post-hoc analysis of an active network in a large field of view during the specific time period of interest. Also, the CaMPARI signal is ratiometric, which allows correcting for expression-level differences. The protein engineering principles it uses could be extended to allow permanent marking of cell states. Improvements to the original CaMPARI lead to CaMPARI2 with brighter green and red fluorescence, faster calcium unbinding kinetics, decreased photoconversion in low calcium conditions (Moeyaert et al. 2018). Based on this, SynTagMA, Synaptic Tag for Mapping Activity, was created by anchoring CaMPARI2 to either pre- or post-synaptic compartments, including preSynTagMA and postSynTagMA.

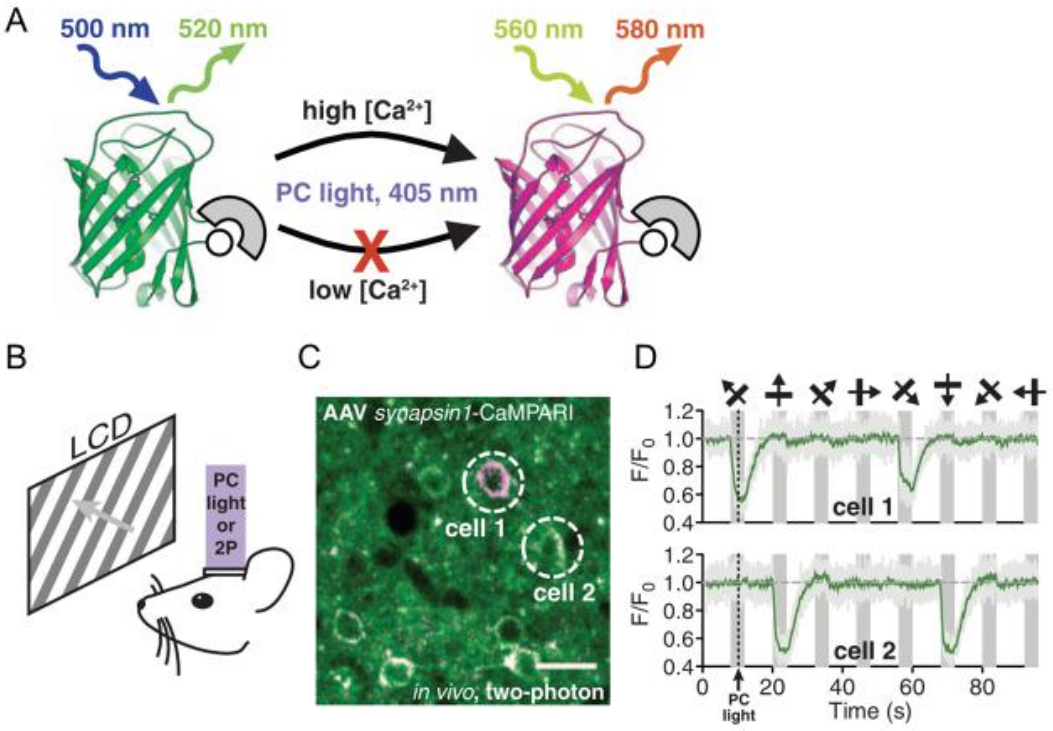

Figure 7. Labeling of active neural circuits in vivo with CaMPARI. (A) Schematic of CaMPARI function. Only in the condition of both high calcium and violet light (395-405 nm) is CaMPARI irreversibly photoconverted from green to red. **(B)** Example use of CaMPARI in vivo. **(C)** Two-photon fluorescence from cortical layer 2/3 of V1 after visual stimulus and PC light pulses. Two cells are circled and labeled for reference. **(D)** Calcium imaging fluorescence traces of the same two cells in response to different directions of drifting gratings (arrows and lines above traces). Neurons responsive to the grating direction shown will photoconvert when the grating presentation is combined with violet light. Adapted from ref (Fosque et al. 2015).

1.4.4 Spine imaging in vivo

Dendritic spines form the postsynaptic components of most excitatory synapses, and their structure is closely related to synaptic function. In vitro, the formation of new spines is induced by long-term potentiation, while long-term depression leads to the elimination of dendritic spines (Engert and Bonhoeffer 1999; Wiegert and Oertner 2013; Wiegert et al. 2018). The formation and elimination of dendritic spine underlies the rewiring of neural circuits and is considered to be one mechanism underlying learning and memory formation (Nimchinsky, Sabatini, and Svoboda 2002). Dendritic spines are further thought to be the

subcellular substrate for memory storage (Kasai et al. 2010). Notably, it has been shown that newly acquired motor skills depend on the formation of task-specific dense synaptic assemblies, while optically induced shrinkage of the potentiated spine will disrupt newly acquired motor skills, which indicates a causal relationship between spinal plasticity and memory (Hayashi-Takagi et al. 2015).

Indeed, long-term in vivo two-photon imaging studies have begun to reveal the structural dynamics of cortical neurons in normal and injured adult brains, which indicating experience-dependent structural synaptic plasticity under different stimuli in mammalian cortex (Holtmaat and Svoboda 2009). In contrast to the extensive in vivo spine imaging studies in cortex, studies of hippocampus are just beginning, which are challenging as hippocampus locates more than 1 mm below the mouse brain surface. Currently, in order to identify hippocampal synaptic structural plasticity, multiple studies applied chronic in vivo two-photon hippocampal spine imaging using permanently implanted hippocampal brain windows (Gu et al. 2014a; Pfeiffer et al. 2018) or microendoscopic methods (Attardo, Fitzgerald, and Schnitzer 2015). To this end, transgenic mice sparsely expressing fluorescent proteins under the control of neuron-specific elements from the *thy1* gene are commonly used (Feng et al. 2000). Spines can be divided into two kinetic groups: persistent and transient (Richards and Frankland 2017). Persistent spines are formed and stabilized in the short and medium term. Transient spines, however, are formed and are removed within a few days.

Data from the first long-term in vivo two-photon hippocampal spine imaging studies on radial oblique dendrites, using Keta/Xyl anesthesia found that spine density in stratum radiatum (1.1 per micrometer) remained stable over weeks (Gu et al. 2014a). Also, the majority of the dendritic spines (~96%) imaged at the first time point survived 16 days. Besides, the actual turnover rate of dendritic spines was very low (~ 4%) at 4-day intervals. Another study investigating basal dendrites under Iso anesthesia came to a contradictory conclusion. Although spine density in stratum oriens (1 per micrometer) remained stable, fewer dendritic spines imaged at the first time point (~80%) survived for 21 days, and the actual turnover

rate of dendritic spines was higher at a 3-day interval (~12%) (Attardo, Fitzgerald, and Schnitzer 2015). The main differences between these studies may come from the imaging techniques, the identity of selected dendrites and the general anesthetic used during imaging. Yet another study observed higher spine density (2 per micrometer) and higher spine turnover (40%) than the previous studies using superresolution two-photon imaging (Pfeiffer et al. 2018). Since the current imaging studies were performed under general anesthesia, the extent to which the use of general anesthetics affects the spine dynamics remains to be investigated.

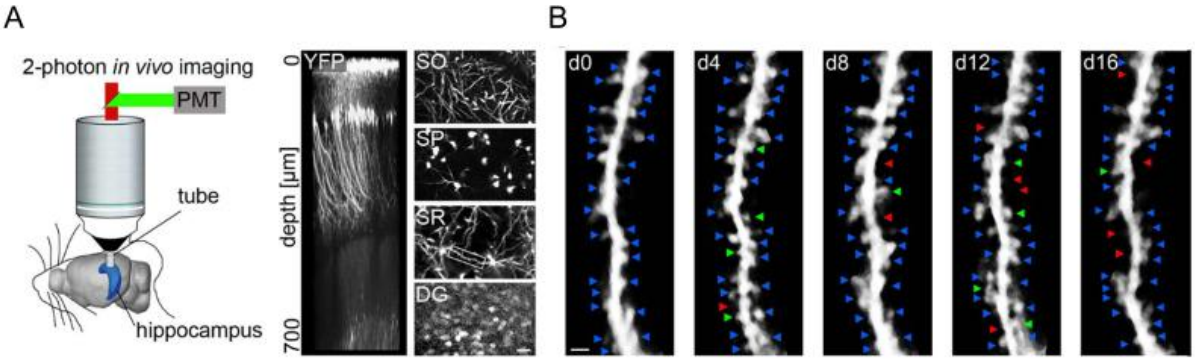

Figure 8. Dendritic spine imaging in the hippocampus. (A) Left, Schematic illustrating two-photon in vivo imaging in the hippocampus. Right, Side projection of a z-stack acquired up to a depth of 700 µm below the hippocampal surface and maximum intensity projections from different depths in stratum oriens (SO), stratum pyramidale (SP), stratum radiatum (SR), and dentate gyrus (DG). **(B)** Example use of time-lapse images of a radial oblique dendrite over a period of 16 d. Note labeled stable spines (blue arrowheads), gained spines (green arrowheads), and lost spines (red arrowheads). Adapted from ref (Gu et al. 2014b).

1.5 Aims of this study

Project 1: The effects of general anesthetics on memory consolidation, hippocampal network activity, and spine dynamics

General anesthesia is characterized by a reversible loss of consciousness accompanied by anterograde and/or retrograde amnesia. However, long-term memory impairment is an undesirable side effect. It is still poorly understood how different types of general anesthesia

affect network activity and dendritic structure of the hippocampus and how this relates to memory formation.

In this project I addressed the following questions:

1) What is the effect of general anesthesia on episodic memory consolidation?
2) How are the neuronal population dynamics affected by general anesthesia measured with calcium imaging?
3) Are the results of calcium imaging consistent with the electrically recorded neuronal population dynamics under general anesthesia?
4) How long does the effect of general anesthesia last at the network level?
5) What is the effect of general anesthesia on spine dynamics acutely and chronically?
6) How do neuronal population dynamics under general anesthesia compare to natural sleep?

Project 2: Labeling active neurons and synapses with postSynTagMA

SynTagMA is a labeling tool generated by anchoring CaMPARI2 to pre- or postsynaptic compartments, including preSynTagMA and postSynTagMA. It has been proven, in vitro, that it allows to capture all synapses that were active within a defined time window under 395-405 nm light.

In this project, I specifically worked on the following aims for postSynTagMA:

1) Can postSynTagMA be used to identify active neurons in vivo, using the nuclear fraction of SynTagMA?
2) Can SynTagMA label active synapses under general anesthesia and during wakefulness?
3) Is SynTagMA suitable to label active neurons during a defined behavioral paradigm?

2 Results

Project I

In this project, I investigated the effects of three different general anesthetics (GAs), isoflurane (Iso), medetomidine/midazolam/fentanyl (MMF), and ketamine/xylazine (Keta/Xyl) on memory consolidation, hippocampal network activity and spine dynamic. First, I investigated whether a single exposure to the GAs causes postanesthetic memory deficits in mice using Morris Water Maze, I found that anesthesia with MMF or Keta/Xyl, but not Iso, impaired memory consolidation. Next, to determine how the cellular activities were affected, I did in vivo two-photon calcium imaging in the same field of view of CA1 of each individual mouse under different anesthetics to compare the population dynamics and recovery timeline for each condition. I found that different GAs induced distinct cellular network states. Iso induced 0.1 Hz oscillations, Keta/Xyl had the strongest reduction in calcium dynamics, and MMF strongly impaired population dynamics for many hours. Next, I showed extracellular recording results from our collaborators to further confirm and complement the calcium imaging results. To determine whether dendritic spines dynamics were modulated, I did in vivo two-photon spine imaging to record the formation and elimination of dendritic spines under each condition. I found different long-term effects on dendritic spine dynamics, with Keta/Xyl having the strongest effect. Finally, to compare general anesthesia with sleep, I performed calcium imaging under NREM and REM sleep states and found that sleep modifies CA1 activity to a much lower degree than anesthesia. Taken together, this study revealed distinct effects of Iso, MMF and Keta/Xyl on network activity and structural spine dynamics in the hippocampal CA1 of adult mice.

2.1 The effect of general anesthesia on episodic memory consolidation

Many patients undergoing general anesthesia and surgery experience cognitive deficits and the duration of general anesthesia has been shown to be a predictive factor in postoperative cognitive dysfunction. The underlying mechanisms in the adult brain in the hippocampus, a

brain region involved in memory formation and consolidation, remain poorly understood. Here, I test the effects of Iso, MMF, and Keta/Xyl on episodic memory consolidation.

2.1.1 Episodic memory consolidation is impaired by MMF and Keta/Xyl, but not by Iso

First, I tested whether a single exposure to the three commonly used general anesthetics respectively leads to postanesthetic memory deficits in mice using the classic Morris Water Maze (Morris 1984). Mice were handled for at least one week before the start of the experiment. Handling was followed by one day of training in a small water tank to reduce their anxiety and allow them to learn to find the hidden platform after entering the water. After this habituation period, the water maze experiment was done, which lasted of 4 days.

On days 1 and 2, the animals were trained to find the platform in position 1 (Figure 1A). On day 3 reversal learning was performed, by moving the hidden platform to the quadrant opposite to the initial target position, and the animals had to learn to go to position 2 to find the platform (Figure 1A). 30 minutes after the end of training, each group underwent one of the four designated treatments: Iso, MMF, Keta/Xyl and no anesthesia (Figure 1A). Mice were anesthetized with Iso or MMF for one hour, while Keta/Xyl anesthesia was left to recede spontaneously. On day 4, mice were tested for memory consolidation for the new platform at position 2 (Figure 1A). I compared the performance of the mice during the probe trial done on day 3 immediately after the reversal learning protocol, with the performance during the probe trial on day 4, twenty-four hours after anesthesia. During the probe trial on day 3, animals of all four groups spent significantly more time in the new target quadrant compared to chance (25 %), which indicates that they learned the new platform position successfully (Figure 1B, C). On day 4, control animals that did not undergo anesthesia showed the same performance as on day 3, suggesting that they had retained the memory of the new platform location (Figure 1B-D). However, animals that were anesthetized with Keta/Xyl or MMF spent significantly less time in the new target quadrant and showed a significantly larger mean distance to the target platform position compared to the probe trial

on day 3. In the Iso group, no significant difference compared to day 3 was detectable (Figure 1B-D).

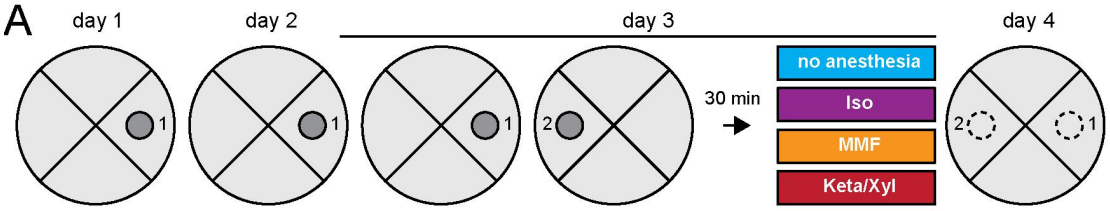
A
day 1
day 2
day 3
day 4
1
1
1
2
30 min
no anesthesia
Iso
MMF
Keta/Xyl
2
1

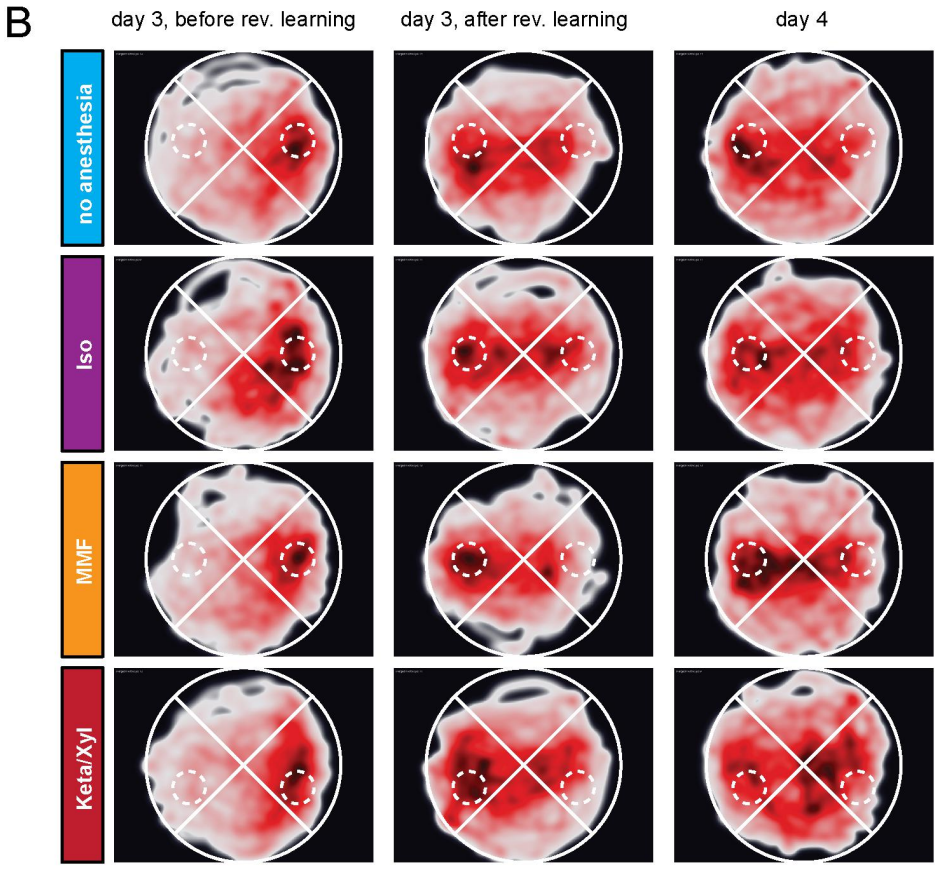
B
day 3, before rev. learning
day 3, after rev. learning
day 4
no anesthesia
Iso
MMF
Keta/Xyl

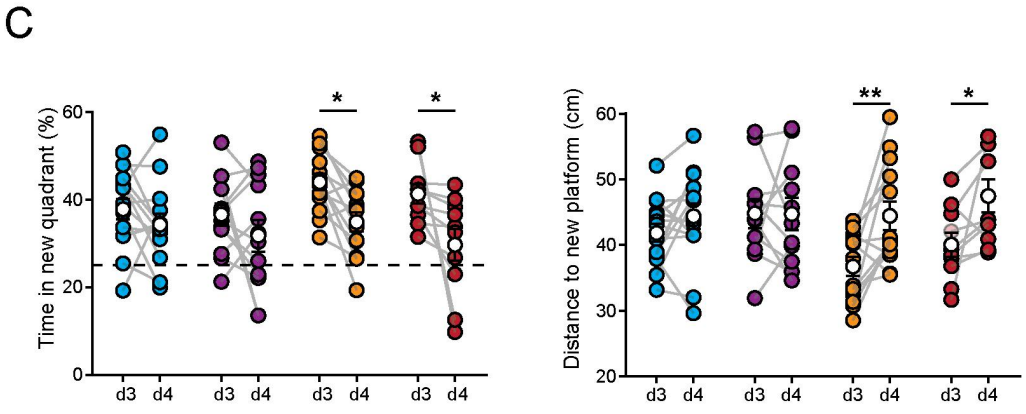
C
Time in new quadrant (%)
60
40
20
0
*
*
d3
d4
d3
d4
d3
d4
d3
d4
Distance to new platform (cm)
60
50
40
30
20
**
*
d3
d4
d3
d4
d3
d4
d3
d4

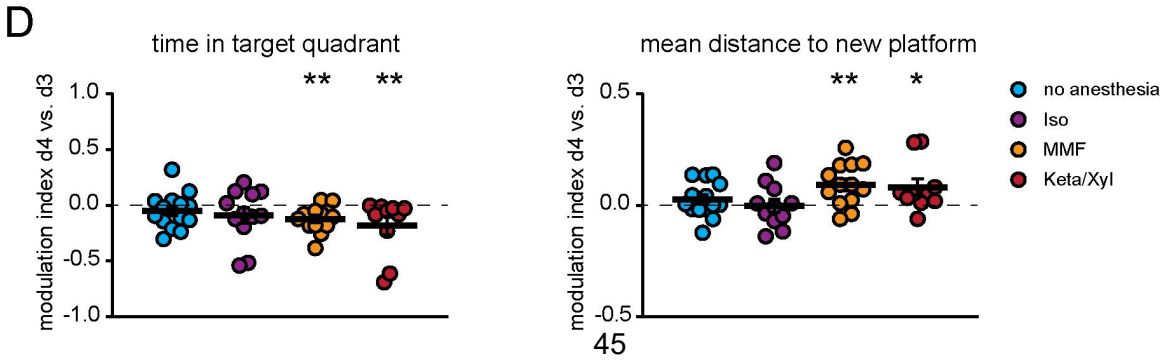
D
time in target quadrant
modulation index d4 vs. d3
1.0
0.5
0.0
-0.5
-1.0
**
**
mean distance to new platform
modulation index d4 vs. d3
0.5
0.0
-0.5
**
*
no anesthesia
Iso
MMF
Keta/Xyl

Figure 1. Episodic-like memory consolidation is impaired by MMF and Keta/Xyl, but not by Iso. (A) Experimental design for testing episodic-like memory in a Morris water maze. On days 1 and 2, animals were trained to find the platform in position 1. Reversal learning was performed on day 3 where animals had to learn the new platform in position 2. 30 mins after the training, each group was given one of the 4 indicated treatments for 1 hour. On day 4, memory consolidation for the new platform in position 2 was tested. **(B)** Heat maps showing trajectories of all mice during the first probe trial before reversal learning on day 3 (left column), after reversal learning on day 3 (middle column), and after treatment on day 4 (right column). The position of the target zone is indicated by dashed circles. **(C)** Scatter plots showing quantification of time spent in the new target quadrant (top) and distance to the new platform (bottom) after reversal learning on day 3 and on day 4. **(D)** Scatter plots showing quantification of change in the time spent in the new target quadrant (left) and distance to the new platform (right) on day 4 after 1 h of indicated anesthesia or no treatment compared to day 3. Filled, colored circles indicate individual animals, and white circles indicate mean ± SEM. Asterisks in **(C)** indicate significant differences between days and asterisks in **(D)** indicate significant deviation from 0. * $p < 0.05$, ** $p < 0.01$.

2.1.2 The impairment of memory consolidation was not explained by the longer duration of recovery after Keta/Xyl or MMF compared to Iso

Since Keta/Xyl cannot be antagonized and shows the strongest effect, it is necessary to test whether the duration of anesthesia is the key factor in impairing memory consolidation. Therefore, I tested whether prolonging the duration of Iso anesthesia also leads to the impairment of memory consolidation. I extended the Iso anesthesia to 2 and 4 hours to test the effect of long duration of Iso anesthesia on memory consolidation. On day 4, mice treated with different duration of iso anesthesia showed the same performance as on day 3, indicating that the prolonged recovery time after Iso anesthesia did not explain the impairment of memory consolidation (Figure 2A, B).

Therefore, it is not the duration of the induced loss of consciousness, but rather the type of anesthetic that may explain the impaired memory consolidation. It is worth noting that the effect is relatively mild, and there is no significant difference in performance on day 4 between the treatment groups. In summary, Keta/Xyl and MMF will impair episodic-like memory consolidation, and on the contrary, Iso has little effect.

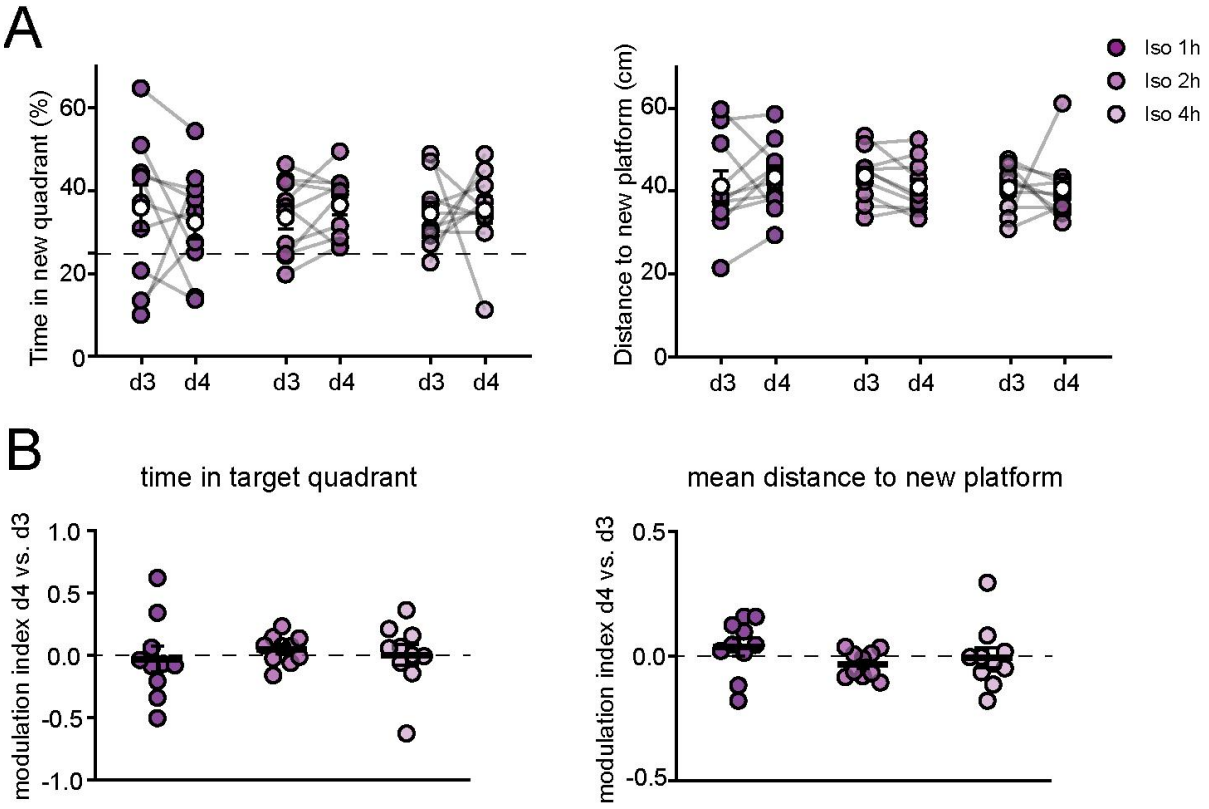

Figure 2. Comparison of the effect of Iso, MMF and Keta/Xyl on episodic memory consolidation. (A) Scatter plots showing quantification of time spent in the new target quadrant (left) and distance to the new platform (right) after reversal learning on day 3 and day 4 after 1, 2, and 4 h of Iso anesthesia. Filled, colored circles indicate individual animals, White circles indicate mean ± SEM. **(B)** Scatter plots showing quantification of change in the time spent in the new target quadrant (left) and distance to the new platform (right) on day 4 after 1, 2, and 4 h of Iso anesthesia compared to day 3. * $p < 0.05$, ** $p < 0.01$. Note, significant differences between groups were not evident.

2.2 Iso, MMF and Keta/Xyl reduce number, amplitude, and duration of calcium transients

Next, to determine how hippocampal neuronal activity, a cellular correlate of memory, was affected during and after anesthesia, I investigated the population dynamics of CA1 neurons in the presence of different anesthetics. I imaged the same field of view (FOV) using the genetically encoded indicator GCaMP6f (Chen et al. 2013) and systematically compared the activity of identified neurons during quiet wakefulness and in the presence of different general anesthetics considering all active neurons and a unique group of neurons active during all conditions respectively.

2.2.1 Chronic two-photon calcium imaging in dCA1

I first monitored the activity of neuronal populations by calcium imaging in the hippocampal dCA1 area in head-restrained mice. They were trained to stay quiet on a treadmill prior to imaging. To compare the modulation of neuronal activity by different anesthetics using the same field of view of the same mouse and to get rid of the effects of other anesthetics, I did calcium imaging once a week in a randomized sequence with the same mouse (Figure 3A). There was a large number of active CA1 pyramidal neurons in the presence of all three GAs. Using extraction parameters that restricted the number of ROIs but maximized signal quality (see Methods), there were many neurons detected with a median of 311 (min-max of 16-817) active neurons per FOV, for a total of 189 five-minutes recordings. All GAs significantly altered calcium dynamics in CA1 neurons (Figure 3B-C).

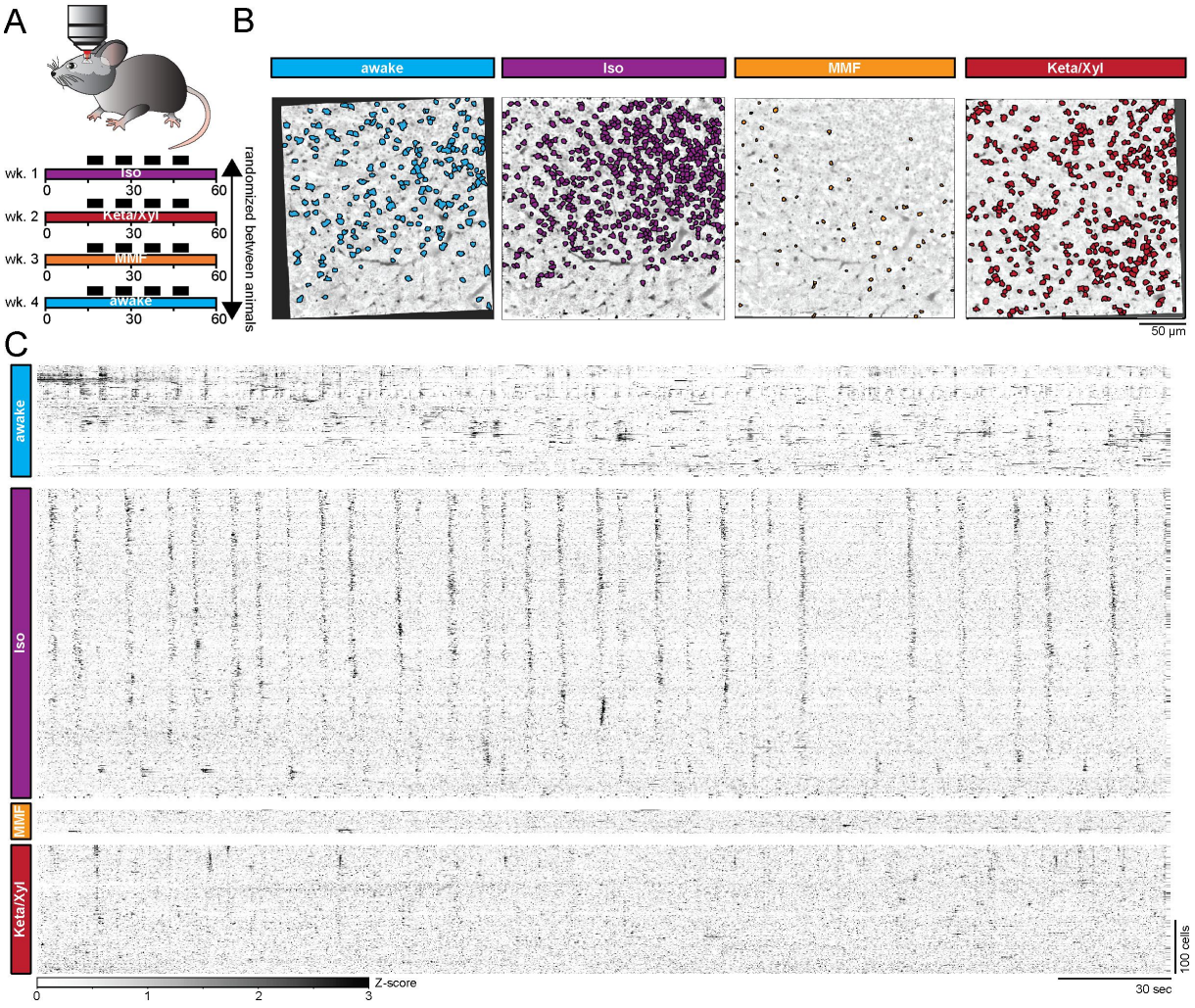

Figure 3. Repeated calcium imaging in dorsal CA1 reveals distinct activity profiles for Iso, MMF and Keta/Xyl. (A) Experimental strategy for chronic calcium imaging of cellular activity in dorsal CA1. For each condition, seven mice were imaged four times for five minutes, as indicated by black fields in the scheme. The order of imaging conditions was pseudo-randomized. **(B)** Time-averaged, two-photon images of the same FOV in CA1 aligned to the Iso condition. ROIs of automatically extracted, active neurons are overlaid for each condition. **(C)** Raster plots of z-scored calcium transients in the same animal under different conditions. Traces are sorted by similarity.

2.2.2 Iso, MMF and Keta/Xyl reduce number, amplitude, and duration of calcium transients

Each condition was characterized by a specific signature in their calcium dynamics. Iso yielded a moderate decrease of rate and amplitude, but a strong reduction of duration of calcium transients. In contrast to Iso, MMF did not significantly affect the duration of transients but reduced their rate and amplitude when compared to wakefulness. Keta/Xyl-anesthesia had the strongest effect on calcium dynamics, leading to a reduction of all three parameters compared to wakefulness (Figure 4A-C). Considering all parameters, the four groups tended to segregate into clusters. One group is mainly composed of recordings under Keta/Xyl, and another one is composed of awake and Iso recordings. Most recordings under MMF clustered between these two groups (Figure 4D). Importantly, these findings were robust to changes in the signal extraction pipeline. Varying the threshold for calcium transient detection across a wide range of values did not affect the reported effects on rate and height of transients (Figure 4E, F).

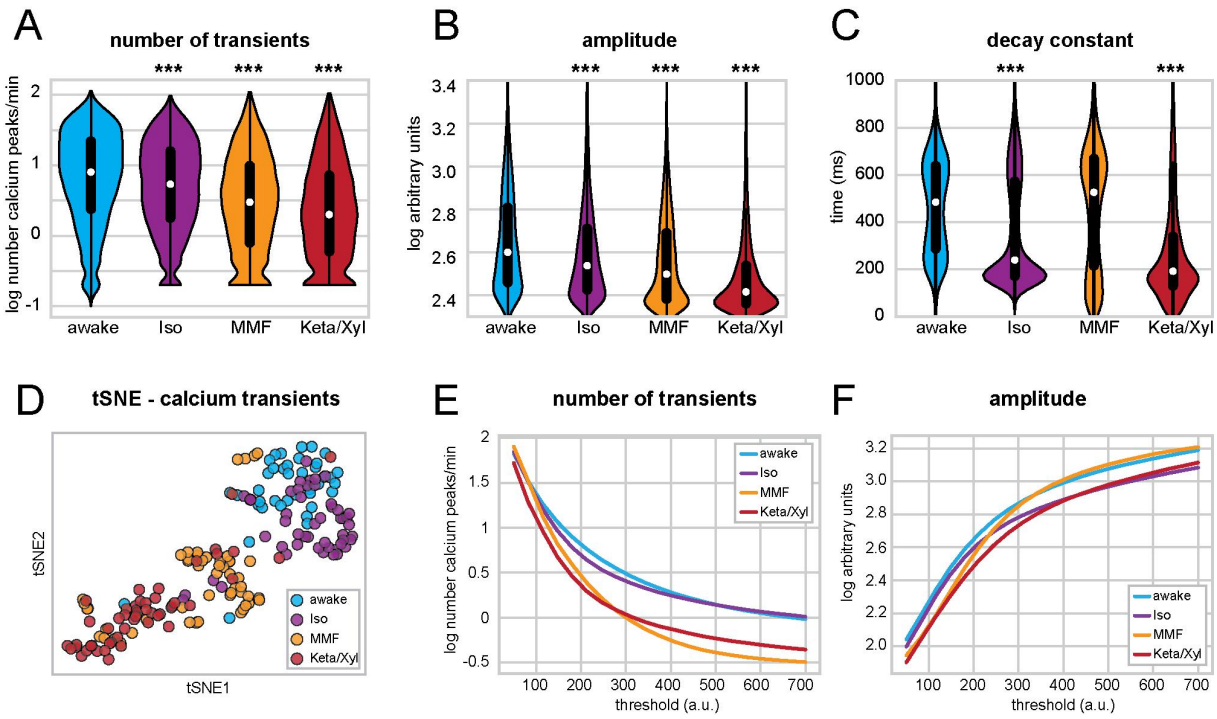

Figure 4. Iso, Keta/Xyl and MMF reduce number, amplitude, and duration of calcium transients. (A-C) Violin plots quantifying the number (left), amplitude (middle), and decay (right) of detected calcium transients. White dots indicate median, vertical thick and thin lines indicate 1st-3rd quartile and interquartile range, respectively. **(D)** tSNE plot summarizing the average calcium transients properties. Each data point represents one recording session. **(E-F)** Line plot of the number in **(E)** and amplitude in **(F)** of detected calcium transients across varying threshold values used for transient detection. *** $p < 0.001$. Note, to facilitate readability, only differences to wakefulness are indicated. Data analysis carried out by Mattia Chini.

2.2.3 Power spectra of calcium transients are distinctly altered by Iso, MMF and Keta/Xyl

Due to the intrinsic nature of the calcium signal, GECI is not ideal for monitoring sub-second neural dynamics, e.g., GCaMP6f with a 1 AP having the rise time-to-peak of ~50 ms and a decay time ($\tau_{½}$ after 1 AP) of ~140 ms. Due to the limitation of temporal resolution of the calcium indicator, only the slow oscillation ranging from 0.1-4 Hz were analyzed. The results showed that calcium transients under Iso displayed a spectral peak between 0.1 and 0.2 Hz for both calcium traces and deconvolved spikes (Figure 5).

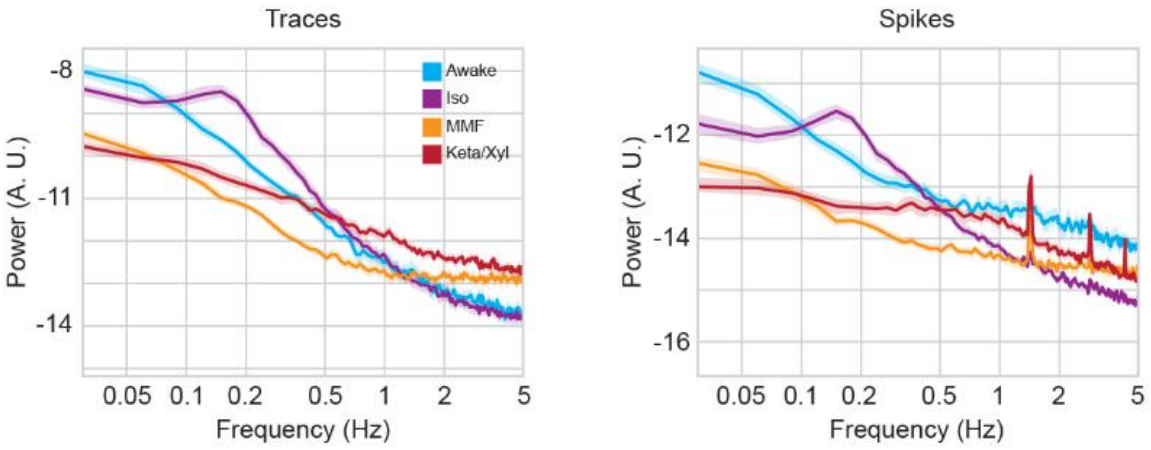

Figure 5. Oscillations of calcium transients are distinctly altered by Iso, MMF and Keta/Xyl. Line plot displaying the spectrograms for population activity power, for raw calcium transients **(left)** and deconvolved spikes **(right)** during wakefulness and three different anesthetic conditions. Data analysis carried out by Mattia Chini.

2.3.4 Iso, MMF and Keta/Xyl distinctly modulate cellular calcium dynamics in individual neurons

One possible explanation for these distinct patterns of calcium activity could be that each anesthetic condition recruits a unique set of neurons characterized by particular spiking properties. To test this possibility, the calcium transients in neurons that were active during all conditions were considered for analysis (Figure 6A). When considering only neurons that were active in all four conditions, rate and amplitude of calcium peaks were generally reduced under anesthesia, being lowest in the Keta/Xyl condition (Figure 6B). While differences in decay constant were less pronounced. Under awake and MMF conditions, the median decay constant was strongly reduced, while it increased for Iso and Keta/Xyl. These results indicate that both the between- as well as the within-condition variance strongly decreased when considering only neurons active under all conditions.

The number of neurons active in all four conditions was relatively small (335 neurons), which limited the statistical analysis. Therefore, neurons active in any combination of two conditions were analyzed (Figure 6C). The rate, amplitude, and duration of calcium transients were most similar between the awake state and Iso compared to the other GAs. In contrast, neurons active in the awake state and Keta/Xyl or MMF showed a decrease in rate, amplitude, and duration in the anesthetized state, with Keta/Xyl resulting in the strongest phenotype (Figure 6C). Altogether, this suggests that anesthetics affect the firing properties of hippocampal neurons, but the magnitude and direction of these effects varied considerably. Iso anesthesia has the mildest effect, and it most likely arises from distinct neuronal populations being active in the two conditions (awake vs. Iso anesthesia), as the firing properties of cells that are active in both were barely affected (Figure 6B, C). On the other hand, the strong effects of MMF and Keta/Xyl on all calcium parameters in the same cells indicate that different anesthetics directly alter the firing properties of individual neurons. Thus, alterations in firing properties of neuronal populations are not solely explainable by different subpopulations of neurons being active between awake and anesthesia.

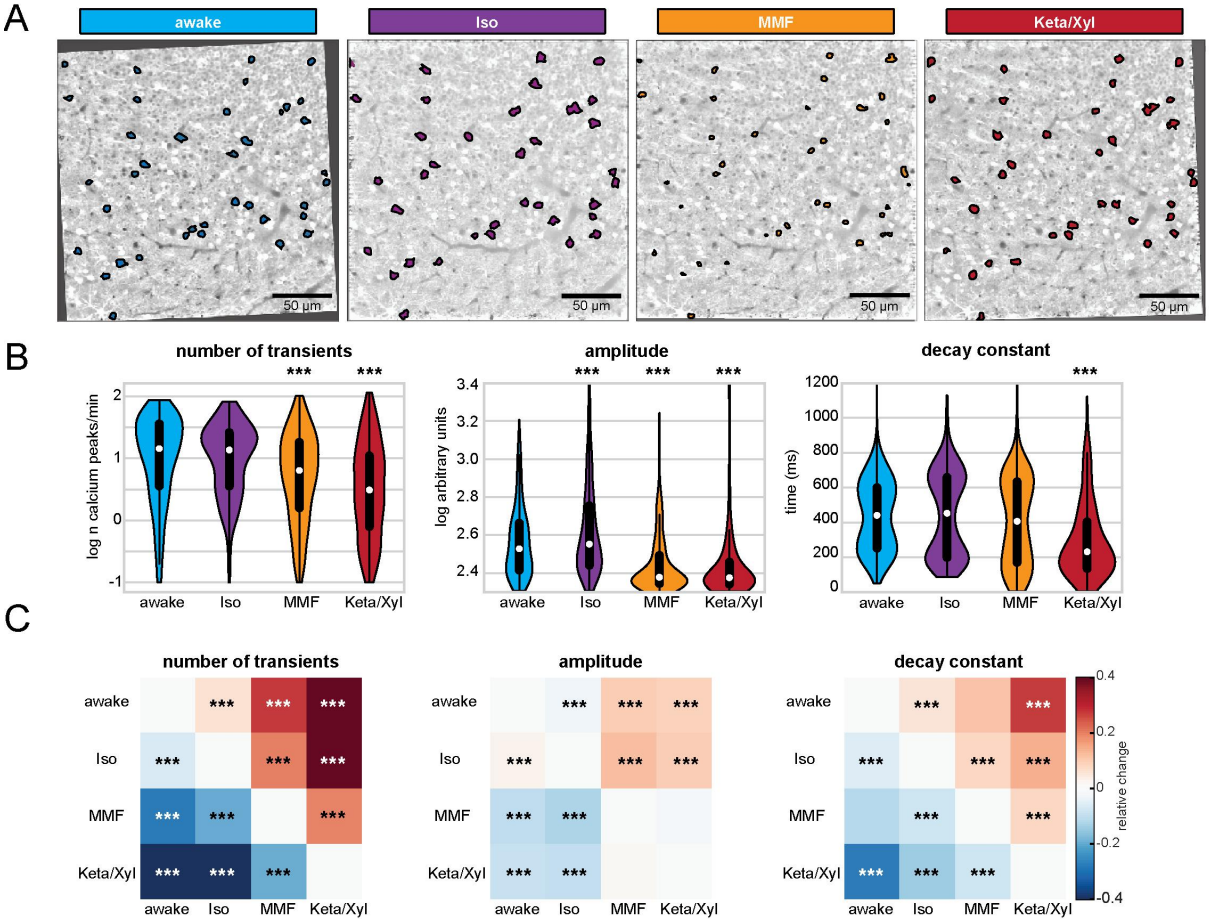

Figure 6. Calcium activity profiles in neurons active during all conditions are similar between wakefulness and Iso. (A) Two-photon time-averaged images of the same FOV in CA1, aligned to the Iso condition (same images as in figures. 3). ROIs show neurons active in each condition, allowing direct comparison of calcium transients in the same cells under different conditions. **(B)** Violin plots quantifying the number **(left)**, amplitude **(middle)**, and decay **(right)** of detected calcium transients. White dots indicate median, vertical thick and thin lines indicate 1st-3rd quartile and interquartile range, respectively. **(C)** Heat maps displaying the relative change in the number **(left)**, amplitude **(middle)**, and decay **(right)** of calcium transients between neurons active in pairs of conditions. Data analysis carried out by Mattia Chini and Andrey Formozov.

2.3 LFP recordings in dorsal CA1 reveal neuronal population dynamics induced by Iso, Keta/Xyl and MMF: a comparison with calcium imaging

To date, electrophysiology and imaging have been considered complementary techniques for solving the same experimental problems, and each has its own advantages (Wei et al. 2020). Electrodes record the direct consequences of ions flowing back and forth across the neuronal membrane via individual action potentials or local field potentials; in contrast,

calcium imaging shows intracellular calcium levels, which are representative of cumulative neural activity, leading to biases in the detection of spike bursts because its relationship with the number of spikes fired is nonlinear. Compared to electrophysiological recordings, functional imaging allows for the simultaneous recording of more neurons and provides information about the anatomical location of each recorded cell. However, due to the slow temporal dynamics of calcium signals, they do not provide precise information about the timing of spikes in neurons. In the following section, I will briefly describe our collaborators' efforts on studying the effects of Iso, Keta/Xyl and MMF anesthetics on hippocampal dorsal CA1 by local field potential (LFP) recordings, in comparison with the imaging experiments above.

2.3.1 LFP recording in dCA1 during wakefulness and anesthesia

To investigate the effects of Iso, Keta/Xyl and MMF anesthetics on hippocampus dorsal CA1, extracellular recordings of local field potentials and firing of individual neurons (single-unit activity, SUA) were performed during wakefulness, followed by 45 min of anesthesia and 45 min of recovery (Figure 7A). The results have shown that the anesthetics have different effects on population activity across various frequency bands (Figure 7B). During wakefulness, LFP power in CA1 was highest in the theta (4-12 Hz) and low-gamma (40-60 Hz) frequency bands (Figure 7C). When the mice were exposed to 2-2.5% Iso, LFP power > 4 Hz was strongly reduced within the first 2 minutes, which was accompanied by the loss of animal mobility (Figure 7C). Similarly, MMF injection rapidly decreased LFP power in the same frequency bands. Iso- and MMF-anesthesia can be efficiently antagonized by removing the face mask or injecting a wake-up cocktail (Flumazenil, Atipamezole and Buprenorphine, FAB), respectively (Albrecht et al. 2014; Fleischmann et al. 2016). Up to 20 min after Iso withdrawal, animals regained motility and LFP power gradually recovered in theta and low-gamma frequency bands (Figure 7C). In contrast to post-Iso, LFP power could not be fully recovered after FAB for the entire 45 min-post anesthesia recording period (Figure 7C). Contrary to Iso and MMF, Keta/Xyl increased LFP power across all frequencies within the

first 10 minutes after injection, with the most prominent effect apparent at 5-30 Hz. As there is no antagonization of Keta/Xyl, the elevated LFP remained throughout the entire recording period (Figure 7C).

As GAs favor slow oscillations at the expense of faster oscillations, to fit the oscillation from imaging, the analysis focuses on how the anesthetic affects the slow oscillations. Consistent with the imaging results, Iso strongly enhanced LFP power below 0.5 Hz, peaking at 0.1 to 0.2 Hz (Figure 7D, E). In contrast, Keta/Xyl strongly enhanced LFP power at 0.5-4 Hz throughout the recording period, but suppressed frequencies below 0.5 Hz (Figure 7D, E). While MMF caused no significant increase in the low-frequency system. However, similar to Keta/Xyl, there was a significant decrease below 0.5 Hz, which persisted throughout the recording period (Figure 7D, E).

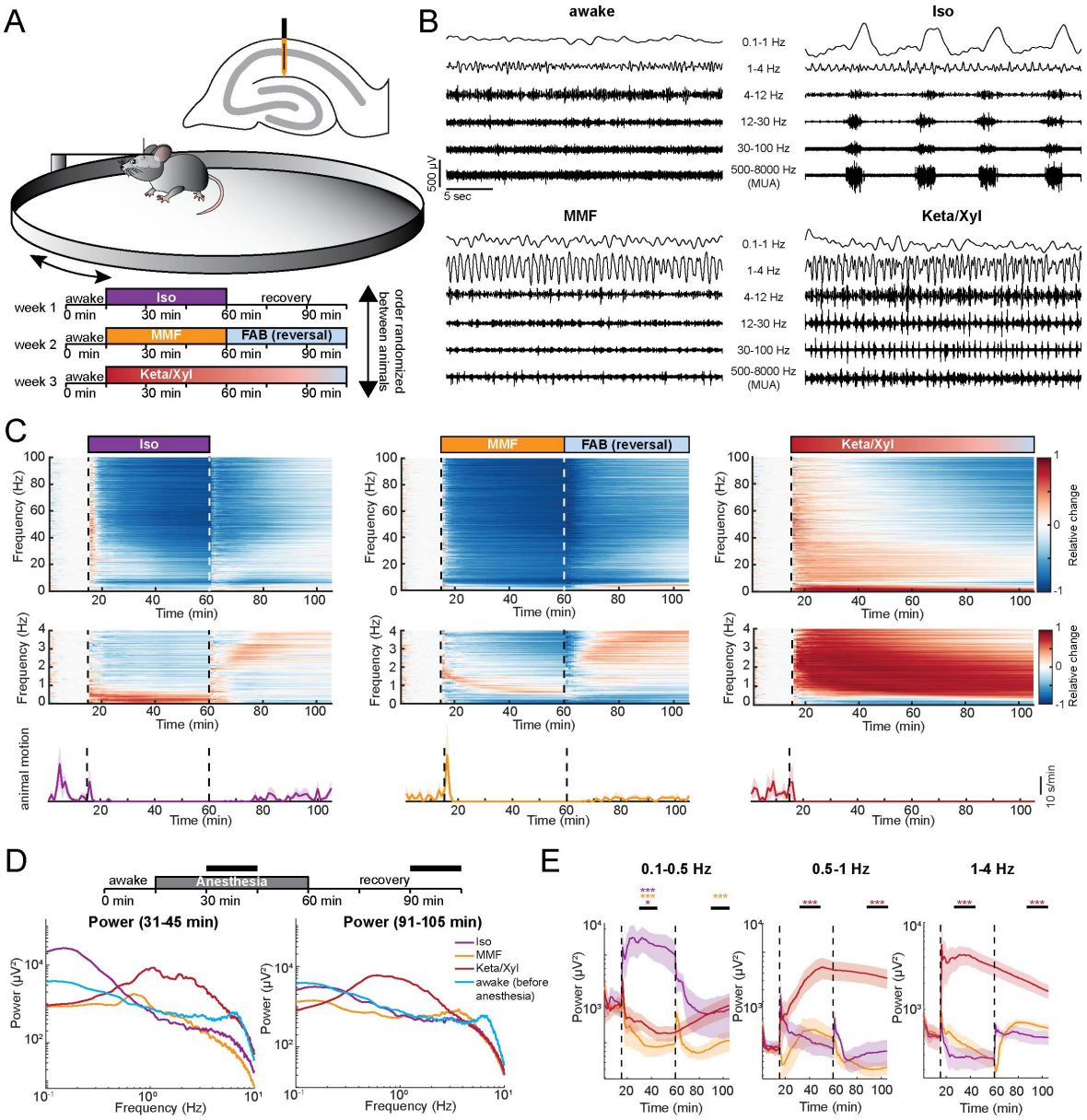

Figure 7. LFP recordings in dorsal CA1 during wakefulness and anesthesia reveal distinct and complex alterations by Iso, MMF and Keta/Xyl. (A) Experimental setup. Extracellular electrical recordings in dorsal CA1 were performed in 4 head-fixed mice for 105 minutes, continuously. Each animal was recorded under all anesthetics as indicated in the scheme. Order of anesthetics was pseudo-randomized. **(B)** Characteristic LFP recordings during wakefulness and under 3 different anesthetics. **(C)** Color-coded heat maps depicting relative change (upper and middle panels) for LFP power and motion profiles (lower panels) for the 3 different anesthetic conditions. Upper panels display LFP power for 0–100 Hz frequency range, lower panels for 0–4 Hz. **(D)** Line plot displaying LFP power spectra for the 2 time periods indicated by horizontal black bars. For comparison, the 15-minute spectrum of the awake period before anesthesia induction is plotted in both graphs. Statistical differences are indicated in S1C Fig. **(E)** Average LFP power over time in different frequency bands. Vertical dashed lines in all panels indicate time points of anesthesia induction (Iso, MMF, Keta/Xyl) and reversal (Iso & MMF only). Lines display mean ± SEM. Asterisks indicate significance of time periods indicated by black horizontal line compared to 15-min period

before anesthesia. Anesthetic conditions are color-coded. * $p < 0.05$, ** $p < 0.01$, *** $p < 0.001$. Data were acquired and analyzed by Jastyn A. Pöpplau.

2.3.2 SUA in dCA1 strongly reduced during anesthesia

Next, to assess the effect of GA on CA1 neurons, analysis was performed on the spiking of single units (56-72 units per animal, n = 4 mice) before, during and after each state of anesthesia. All anesthetics significantly and rapidly (<1 minute) reduced the spiking activity of CA1 neurons (Figure 8A), of which MMF had the strongest inhibitory effect, followed by Iso and Keta/Xyl. To study whether the rhythm of a single neuron firing is similar to LFP, the spectral properties of 1 ms-binned SUA firing were analyzed. At higher frequencies, Iso led to a peak in the theta frequency range, similar to wakefulness, yet it reduced the SUA power in the beta/gamma range. Keta/Xyl and MMF caused an overall reduction in SUA power at frequencies >5 Hz (Figure 8B). At lower frequencies, in the presence of Iso, the SUA power continued to increase in the range of 0.1 to 0.5 Hz (Figure 8C), which is consistent with the strong modulation of LFP at 0.1-0.2 Hz. Of note, this effect did not vanish after Iso removal, which suggests that Iso has a long-lasting impact on firing rhythmicity. In contrast, MMF generally reduced, albeit not significantly, SUA power in the range between 0.1 and 4 Hz and a significant reduction of SUA power was present 45 min after antagonization in the 0.1-0.5 Hz band (Figure 8C). On the other hand, Keta/Xyl only showed a tendency towards reduced SUA power in the frequency band below 0.5 Hz but increased SUA power significantly in the range between 0.5 and 4 Hz (Figure 8C). Strikingly, SUA power did not fully recover for any of the tested anesthetics. Thus, GAs differentially impair spiking rhythmicity. These changes appeared to follow similar dynamics to those in the LFP.

Taken together, these results show that all investigated GAs caused a persistent and robust reduction of CA1 firing. Moreover, analysis of dCA1 recording data under different anesthesia for single unit and population activity properties revealed comparable effects to those observed with calcium imaging.

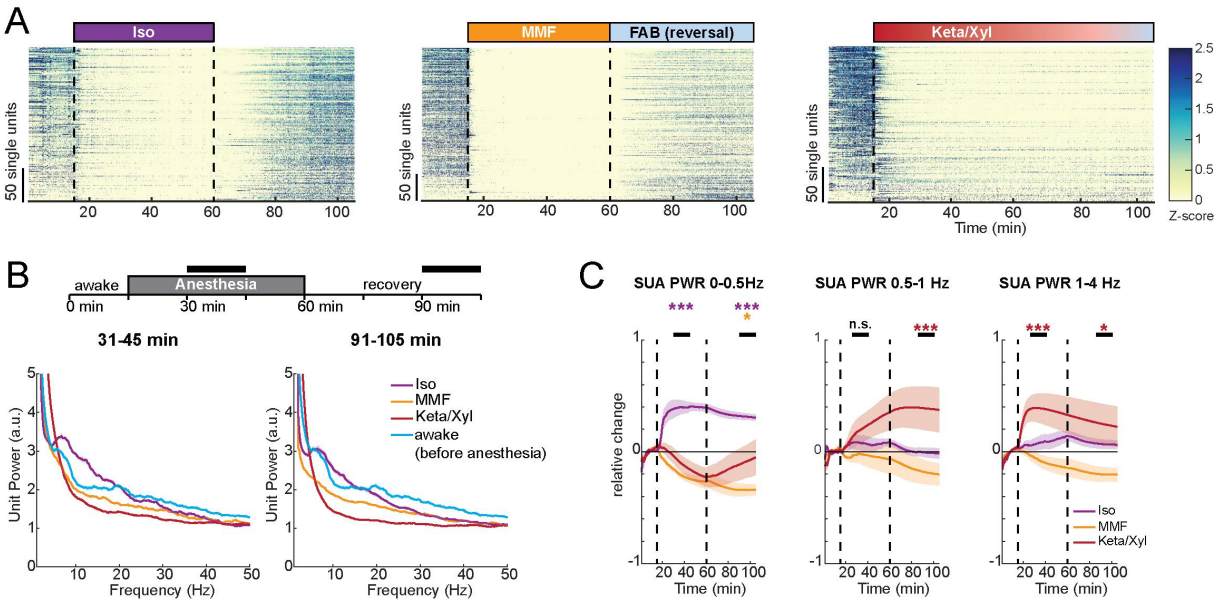

Figure 8. Single unit activity in dorsal CA1 is strongly reduced during anesthesia, and remains significantly altered long after its termination. (A) Raster plots of z-scored single-unit activity (SUA) for the three different anesthetic strategies in four mice. Units are sorted according to initial activity during wakefulness. **(B)** Line plot displaying the normalized power spectra of population firing rate for the two time periods indicated by horizontal black bars. **(C)** Relative change of population firing rate power in the 0.1-0.5, 0.5-1 and 1-4 Hz frequency band. SUA PWR = power of SUA spike trains. Colored lines in **(C)** display mean ± SEM. The vertical dashed lines in panels **(A)** and **(C)** indicate time points of anesthesia induction (Iso, MMF, Keta/Xyl) and reversal (Iso & MMF only). Asterisks in **(C)** indicate significance of periods indicated by black horizontal line compared to period before anesthesia. Anesthetic conditions are color-coded. * $p < 0.05$, ** $p < 0.01$, 261 *** $p < 0.001$, n = 4 mice. Data analysis carried out by Jastyn A. Pöpplau.

2.4 Population activity recovers with different temporal dynamics after Iso, MMF and Keta/Xyl

The LFP recordings showed that even 1.5 h after Keta/Xyl injection, network activity remained altered, and a similar effect was maintained after antagonization of MMF, while most aspects returned to pre-anesthetic conditions during 45 min after Iso removal. To evaluate network effects of the different anesthetics on a longer time scale, I repeated calcium imaging during 6 hours after the onset of anesthesia and 5 hours after Iso termination and MMF antagonization (Figure 9A). In line with the previous results, the number of calcium transients was strongly reduced 30 min after MMF or Keta/Xyl injection,

while the reduction had a lower magnitude for Iso. Similarly, MMF and Keta/Xyl most strongly reduced the amplitude and duration of calcium transients, while Iso mildly increased amplitude without affecting the decay constant (Figure 9B). Confirming the action dynamics monitored by LFP recordings in vivo, recovery from Iso anesthesia was fast and only the rate mildly changed during the hours after removing the mask. In contrast, after Keta/Xyl injection, amplitude and duration of transients were altered throughout the following 6 hours, while the reduction of the calcium transients rate was not reverted until up to 4 hours later. Recovery to the pre-anesthetic state was even slower after MMF/FAB. Despite antagonization of MMF anesthesia with FAB, calcium transients remained disturbed for up to 6 hours. Thus, the different anesthetics not only induced unique alterations of CA1 network dynamics but also showed different recovery profiles (Figure 9C).

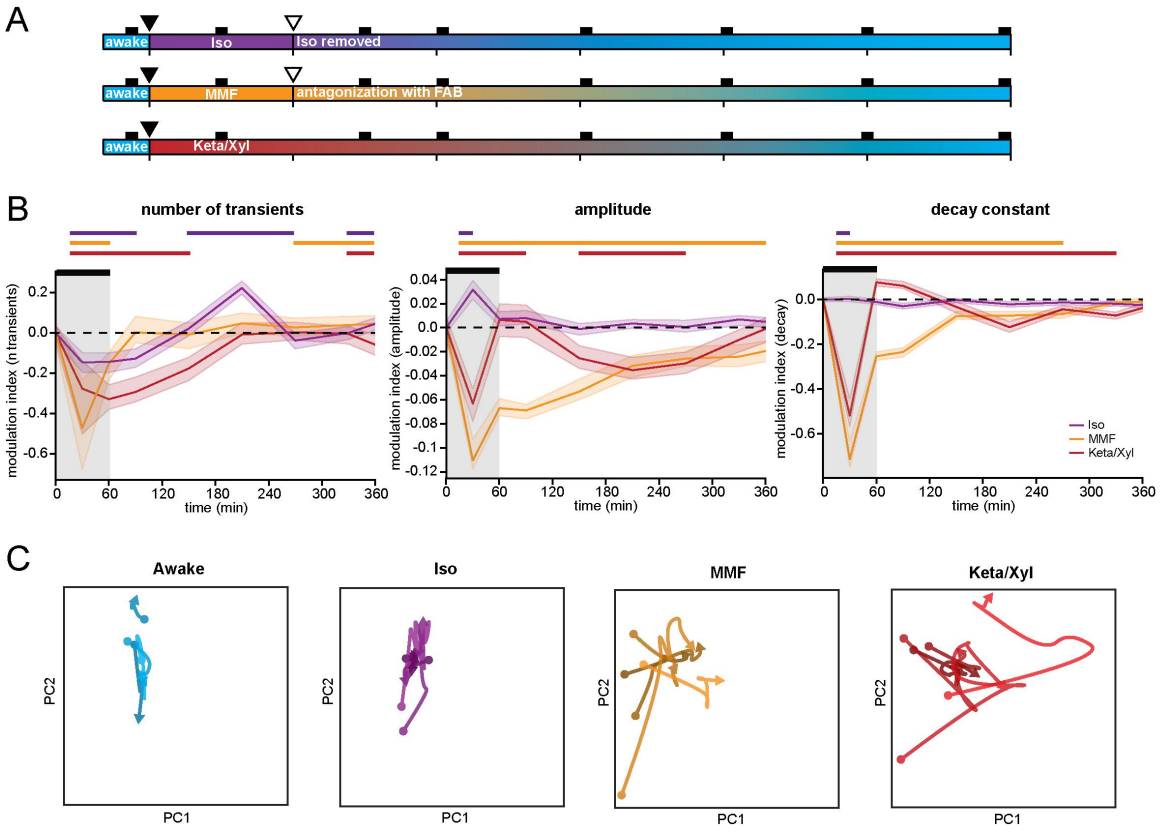

Figure 9. Calcium activity profiles in neurons active during all conditions are similar between wakefulness and Iso. (A) Schematic representation of long-term calcium imaging experiments to assess recovery from anesthesia. Black rectangles indicate imaging time points (up to 10 min duration each). Filled and open triangles indicate the start and end of the anesthesia period. **(B)** Line diagrams showing the relative change (modulation index) of the median number of calcium transients **(left)**, their amplitude **(middle)**, and decay constant

(right) during anesthesia and recovery relative to the awake state before anesthesia induction. The black bar indicates the anesthesia period. Shaded, colored lines indicate 95% confidence interval. The horizontal, colored lines indicate significant difference ($p < 0.05$) to awake time point ($t = 0$) for the respective condition. **(C)** Recovery of CA1 pyramidal neurons from anesthesia. The dots at the beginning of each trajectory represent median values of two principal components (PC1, PC2) calculated on the number, height and decay of the calcium transients during anesthesia in **(B)**. The arrowheads represent the state 6 hours later. Blue dots correspond to awake states in the control group. Every trajectory connects anesthesia and post-anesthesia (recovery) states during the following 6 hours for a given animal. The trajectories were obtained using 3rd-degree B-splines. Data analysis carried out by Andrey Formozov.

2.5 Repeated anesthesia alters spine dynamics in CA1

The impact of Iso, MMF, and Keta/Xyl on CA1 activity might alter spine dynamics at CA1 pyramidal neurons. This issue is of critical relevance since GAs disrupt activity patterns during development (Chini et al. 2019) also involving alteration of synaptic connectivity (Briner et al. 2010; Briner et al. 2011), but less is known about the impact of GAs on hippocampal synaptic structure during adulthood. So far, spine dynamics in hippocampus were only investigated under anesthesia, lacking comparison to the awake state. Moreover, the reported turnover rates varied strongly between studies (Gu et al. 2014a; Attardo, Fitzgerald, and Schnitzer 2015; Pfeiffer et al. 2018). Thus, it is unknown how repeated anesthesia in itself affects spine stability.

2.5.1 Chronic imaging of spine dynamics during four different conditions

I repeatedly imaged the same basal, oblique, and tuft dendritic segments of CA1 pyramidal neurons under all four conditions (five times per condition, every four days), interrupted by a 30-day recovery period between conditions (Figure 10A, B). To rule out time effects, a pseudo-randomized order of anesthetics was used (Figure 10A, B). The first characteristic that I analyzed was the spine turnover ratio. The turnover rate was defined as the sum of all spines gained and lost between two consecutive imaging sections divided by the number of present spines. During wakefulness, without any anesthesia in between, the turnover ratio of spines on all dendrites was on average 18.6 - 20.5 % per four days. This turnover ratio was

stable and did not change systematically over successive imaging sessions (Figure 10C). Notably, all anesthetics affected spine turnover. Both MMF and Iso anesthesia mildly increased the turnover ratio compared to wakefulness (21.1 – 23.8 % for MMF, 24.0 – 24.7 % for Iso). To understand which component, either the gain or the loss, would contribute most to the effect observed in the turnover ratio, I split the data into gained and lost spines (Figure 10D). The spine gain was defined as the number of newborn spines divided by the total amount of spines on that day, whereas the spine loss was defined as the number of lost spines divided by the total amount of spines on that day. In the awake group, the total spine gains and spine losses were balanced. In the Iso group, both gains and losses were significantly increased, and in the MMF group losses were significantly increased (Figure 10D). In contrast, in the Keta/Xyl group, both total gain and loss significantly decreased (Figure 10D). I next analyzed the surviving spine fraction. The surviving fraction of spines was calculated as the percentage of remaining spines compared with the first imaging time point. Iso did not alter the surviving fraction of spines compared to wakefulness (Figure 10E) while it slightly decreased with MMF. In contrast, Keta/Xyl showed strong stabilization of existing spines. The last parameter analyzed was the spine density, which was calculated as the number of spines per µm. During awake imaging and MMF spine density did not change over time, while Iso and Keta/Xyl slightly and gradually increased spine density (Figure 10F). Altogether, these results exhibited the different regulatory characteristics of different GAs on dendritic spine dynamics. Iso significantly increased spine density over time without altering the surviving fraction of spines. Together with high gains and losses, these results indicate that the elevated turnover ratio was due to a rise in the gained fraction of spines.

For MMF, as mentioned, spine density did not change over time. However, the surviving fraction was slightly decreased compared to wakefulness, which, together with slight increase in the fraction of lost spines, indicates that the increased turnover ratio may come from the destabilization of spines. Keta/Xyl anesthesia showed the strongest effect on spine turnover (13.4 - 15.7 %), which was opposite to MMF and Iso, and therefore significantly

lower rather than higher compared to the awake condition. This lower turnover ratio was accompanied by a higher surviving fraction and an increase in density with time. Consistently, the fraction of lost spines was most strongly reduced. Thus, Keta/Xyl anesthesia resulted in marked stabilization of existing spines and a reduction in the formation of new spines, indicative of a significant effect on structural plasticity.

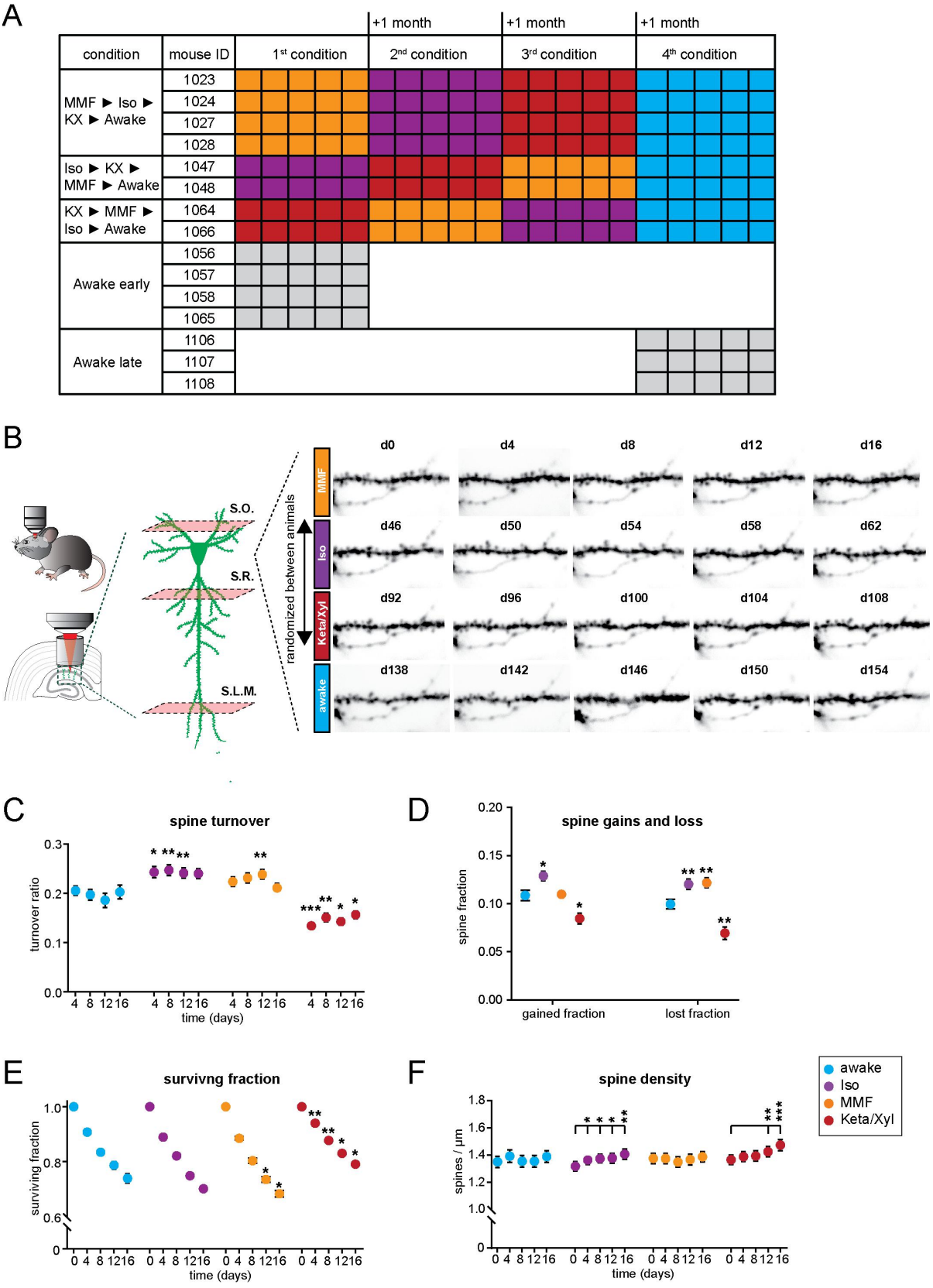

Figure 10. Spine turnover at CA1 pyramidal neurons is distinctly altered by repeated application of Iso, MMF and Keta/Xyl. (A) Experimental scheme for chronic spine turnover

measurements. Spine imaging was performed in a pseudo-randomized order for the different anesthetics followed by imaging during wakefulness. Each colored box indicates one imaging session. For each condition, imaging was done five times every four days, followed by a one-month break. To control for long-term effects of anesthesia and age on the awake condition, we performed imaging only during wakefulness in additional mice as indicated. **(B)** Left: Schematic illustration of in vivo spine imaging strategy. In each animal, spines were imaged on basal dendrites located in stratum oriens (S.O.), oblique dendrites in stratum radiatum (S.R.) and tuft dendrites in stratum lacunosum moleculare (S.L.M.). Right: Example showing an oblique dendrite in S.R. imaged chronically during all conditions. The order of anesthetic treatments was pseudo-randomized between mice. **(C-F)** Dot plots showing quantification of spine turnover in **(C)**, overall gain and loss of spines in **(D)**, spine survival in **(E)** and spine density in **(F)** during chronic imaging under the four different treatments. Dots indicate mean ± SEM. Asterisks indicate significant differences to wakefulness in the left and middle panels. In the right panel, asterisks denote significant changes within each treatment compared to day 0. * $p < 0.05$, ** $p < 0.01$, *** $p < 0.001$.

2.5.2 The effects of age and imaging-time on spine survival

To rule out that the age of the animal influenced spine dynamics in the awake condition, I measured spine turnover in a group of age-matched animals to the first anesthesia group (Figure 11). Moreover, to rule out that the chronic imaging procedure per se and anesthesia, in general, had a long-lasting effect on the awake imaging condition, I also added another awake-imaging control group with naive, age-matched animals to the awake imaging time point in the experimental group (Figure 11). In all three groups, spine turnover was indistinguishable, indicating that neither age nor previous imaging under anesthesia impacted spine dynamics in the awake-imaging group (Figure 11).

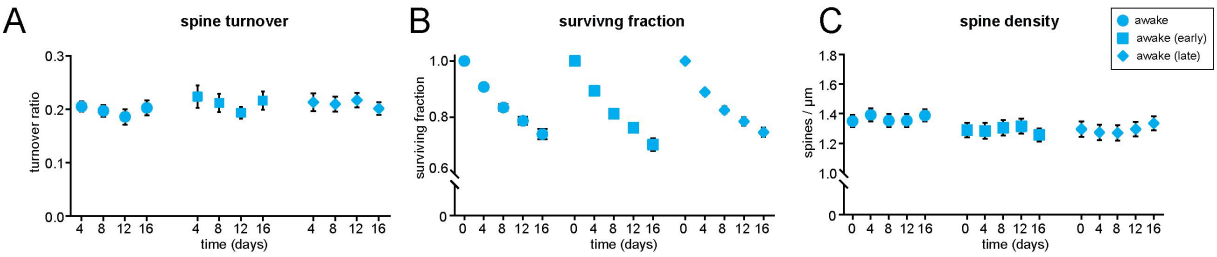

Figure 11. Spine turnover at CA1 pyramidal neurons is awake control condition. (A-C) Dot plots showing quantification of spine turnover in **(A)**, spine survival in **(B)** and spine density in **(C)** during chronic imaging under awake condition. Blue symbols indicate mean ± SEM.

2.5.3 Imaging of acute spine dynamics

Next, I asked whether the modulation of spine turnover by GAs was due to acute remodeling of spines during the time of anesthesia. Alternatively, spine turnover might be driven by long-lasting changes in network activity imposed by the slow reversal of all GAs. To capture fast events such as filopodia formation, I acquired image stacks every 10 min (Figure 12A). Spine turnover, surviving fraction, or spine density were not significantly altered during the one hour of imaging (Figure 12B). Thus, spines were stable during the one hour irrespective of the treatment. While mature spines typically show low elimination/formation rates over one hour, filopodia are more dynamic (Portera-Cailliau, Pan, and Yuste 2003; Lendvai et al. 2000; Dailey and Smith 1996). Unlike other reports, that observed an acute selective formation of filopodia under Keta/Xyl, but not Iso (Yang et al. 2011), I did not detect any acute effects of GAs on filopodia turnover of CA1 pyramidal cell dendrites. Thus, chronic exposure to all GAs consistently impacted spine dynamics, whereas acute effects were lacking. Keta/Xyl caused a strong decrease in spine turnover, accompanied by a higher surviving fraction and an increased density over time.

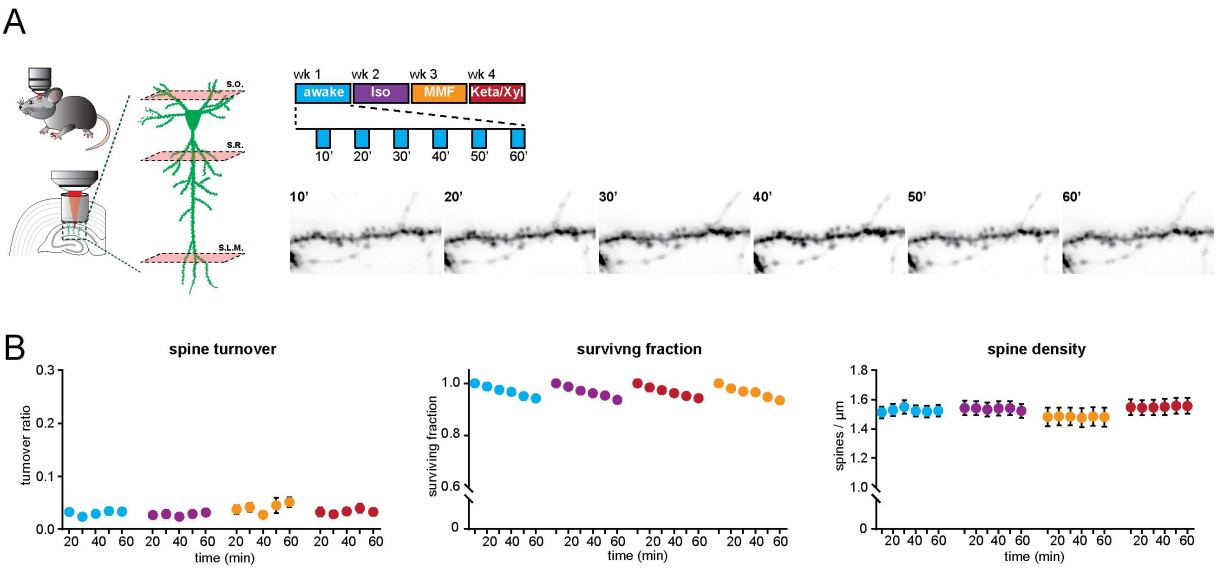

Figure 12. Imaging of acute spine dynamics under awake, Iso, MMF and Keta/Xyl. (A) Imaging of acute spine dynamics during four different conditions. Left: schematic of the experimental timeline. Right: example of dendrite imaged during wakefulness in 10 min intervals (same dendrite as in A). **(B)** Dot plots showing quantification of acute spine turnover **(left)**, spine survival **(middle)** and spine density **(right)** under the four indicated treatments. Dots indicate mean ± SEM.

2.5.4 Different effects on BD, OD and TD

Although Thy-1-GFP labels neurons randomly, it is still of interest to test whether the dynamic changes in dendritic spines under different anesthetics are input specific. I did the above analysis based on basal dendrites of stratum oriens (S.O.), oblique dendrites in stratum radiatum (S.R.) and tuft dendrites in stratum lacunosum moleculare (S.L.M.) (Figure 13 A-C). These effects were present on basal dendrites, oblique dendrites and tuft dendrites, albeit with different magnitude. Under Keta/Xyl the strongest impact on spine density was present in S.R. and S.L.M., while turnover was most strongly reduced in S.O. Also, the increased spine turnover seen under Iso and MMF was most pronounced in S.O. (Figure 13 A-C).

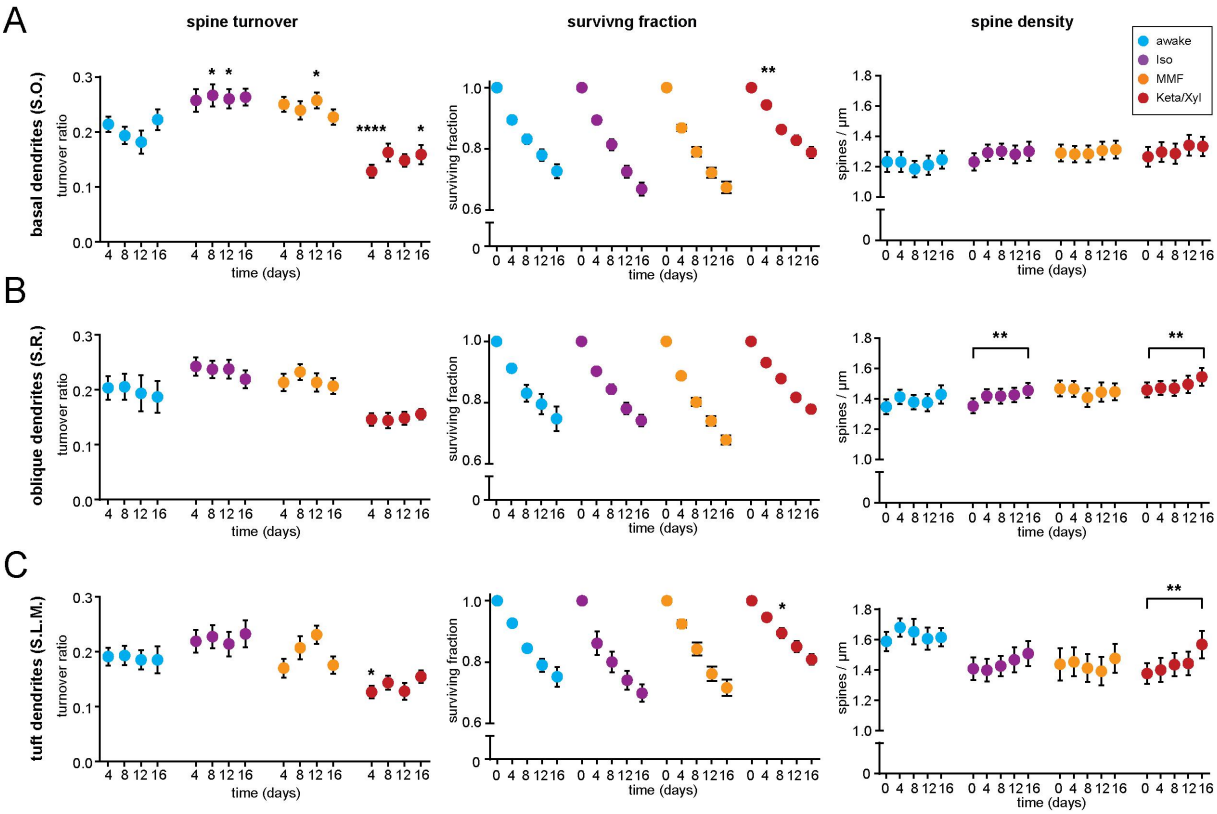

Figure 13. Dendrite-specific changes of spine dynamics. (A-C) Dot plots showing quantification of spine turnover (left column), spine survival (middle column) and spine density (right column) separately for basal **(A)**, oblique **(B)** and tuft dendrites **(C)**. Asterisks indicate significant differences to wakefulness. * $p < 0.05$, ** $p < 0.01$.

2.6 Network alterations during sleep are less pronounced compared to anesthesia

Altered CA1 activity under anesthesia may affect synaptic function and memory processing. A naturally occurring form of unconsciousness is sleep, which is required for network processes involved in memory consolidation (Diekelmann and Born 2010; Klinzing, Niethard, and Born 2019).

To determine whether the above network perturbations are similar to those that occur naturally during sleep, it is important to compare the modulation of neuronal networks under anesthesia with that under natural sleep. It has been reported that pupil size can be used as a reliable indicator of sleep state and that cortical activity is closely linked to pupil size fluctuations during non-rapid eye movement sleep (Yuzgec et al. 2018). This suggests that reliable classification of wakefulness, rapid eye movement (REM) and non-rapid eye

movement (NREM) sleep can be obtained by recording the LFP and spiking together with animal motion, pupil size and electromyography (EMG) of neck muscles in head-fixed mice. The results from our collaborators show that the state of the animal can be classified into 30-second-long time periods of wakefulness, REM and NREM sleep. Notably, a certain percentage of epochs, termed uncertain, could not be reliably assigned to any of the first three categories. Given that the behavioral attribution of these time periods is uncertain and difficult to interpret, these data were excluded from further analysis. Next, my colleague used the electrophysiology recordings to train a machine-learning algorithm to classify wakefulness, NREM and REM sleep from eye videography images alone. It was feasible to reliably distinguish wakefulness and NREM sleep (4-fold cross-validation accuracy >85%), whereas REM classification was less precise (4-fold cross-validation accuracy ~30%). This classifier was then used to predict the physiological state of mice from which I recorded calcium transients in CA1 neurons together with eye videos (Figure 14A-C).

In the experimental environment, it took 10 to 15 days for the mice to gradually get used to sleeping in the light-isolated box. Imaging sessions normally lasted up to 6 hours. Recordings were manually started when the mouse showed indications of sleep and continued for about 5 min per session. In the calcium imaging dataset, sleep periods were dominated by the NREM phase and only 17 min of REM sleep could be detected in a total of 864 min (Figure 14D, E). Given the limited amount of detected REM sleep, its effects on hippocampal calcium activity should be interpreted with caution. In the calcium imaging dataset, both NREM and REM sleep caused a small reduction in transient amplitude (Figure 14F). Further, there was no effect of the sleep state on absolute pairwise correlations (Figure 14G).

In conclusion, the magnitude of effects was much smaller for sleep than for GAs. Both NREM and REM states were more similar to wakefulness than to the anesthetic state. Compared to the three different anesthetics, sleep had the closest resemblance to Iso. Thus, among the

three different anesthetics, network alterations under Iso deviate the least from natural states such as wakefulness and sleep.

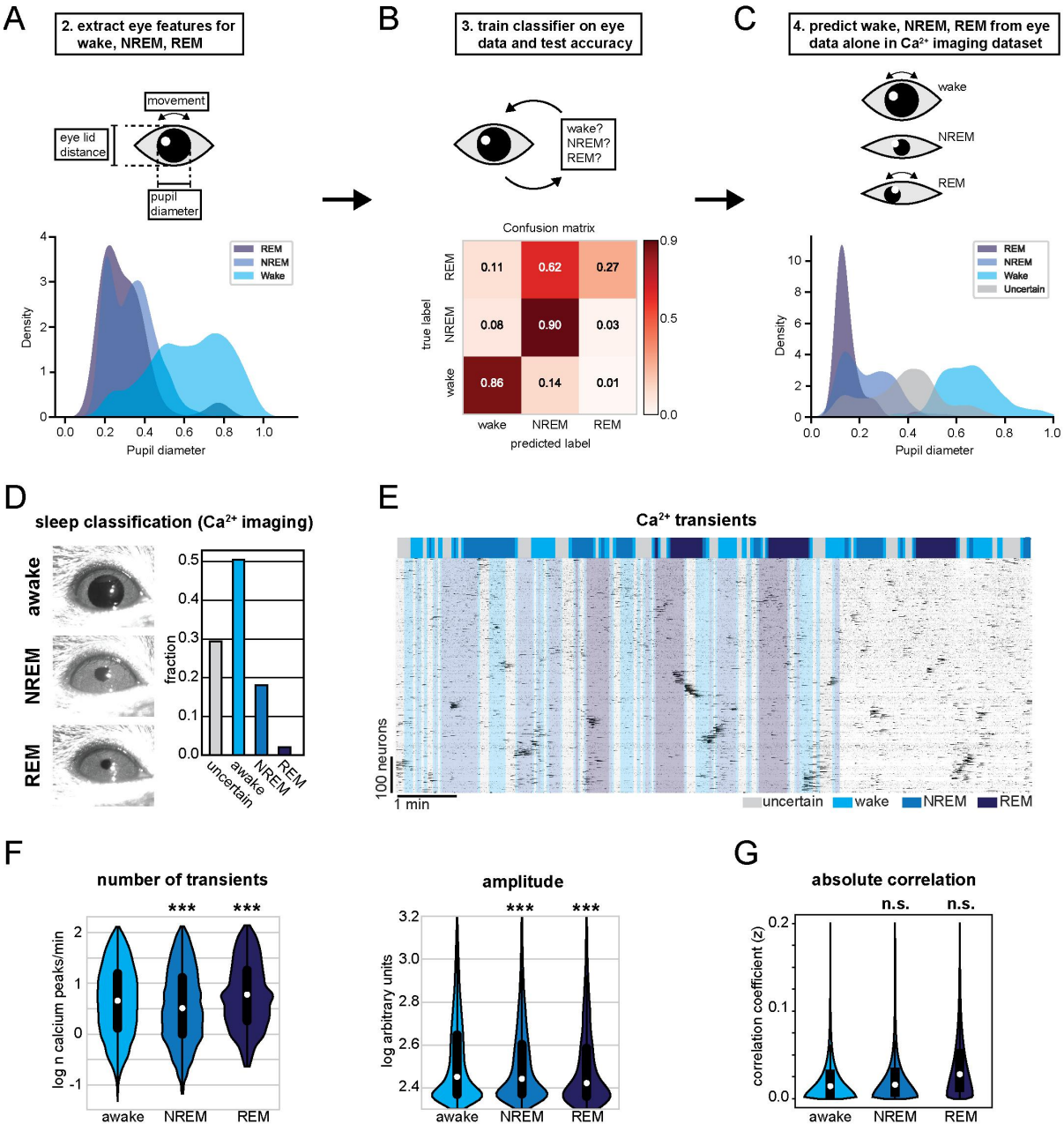

Figure 14. Sleep alters CA1 activity in a similar way to anesthesia but with a lower magnitude. (A) Using the electrophysiology-based classification, the following pupil/eyelid features were extracted to classify sleep: maximum and minimum pupil diameter, standard deviation of pupil diameter, pupil area, pupil motion and eyelid distance. **(B)** Confusion matrix and prediction accuracy for the classification of sleep periods based on eye imaging alone. **(C)** Probability distribution of pupil diameter for predicted awake, NREM and REM periods in the calcium imaging dataset. **(D)** Classification of activity states during CA1 calcium imaging based on eye videography. **(E)** Raster plots of z-scored calcium transients in an example recording of one animal transiting between wakefulness and sleep. Traces are sorted by similarity. **(F)** Violin plots quantifying the number **(left)**, and amplitude **(right)** of detected

calcium transients. **(G)** Violin plots quantifying absolute pairwise correlation of all recorded neurons. White dots indicate median, vertical thick and thin lines indicate 1st-3rd quartile and interquartile range, respectively. * $p < 0.05$, ** $p < 0.01$, *** $p < 0.001$ w.r.t. to wake state, n = 3-7 mice. Data analysis carried out by Alexander Dieter.

Project II

2.7 PostSynTagMA maps active neurons in vivo

SynTagMA (Synaptic Tag for Mapping Activity) is a genetically encoded calcium indicator targeted to synapses, which allows to rapidly ‘freeze’ activity in a user-defined time window with violet light illumination (Perez-Alvarez et al. 2020). Spine-localized postSynTagMA is engineered by targeting CaMPARI2 to the postsynaptic density via fusion to an intrabody against PSD95 (Son et al. 2016). In addition, cytoplasmic expression is reduced by an additional KRAB zinc finger binding domain (Margolin et al. 1994).

Since a fraction of postSynTagMA is sequestered to the nucleoplasm, I tested whether this nuclear fraction of SynTagMA could be used to identify active neurons in vivo. Based on project 1, which investigated neuronal activity in the hippocampal dCA1 region under different anesthetics and during wakefulness, I first compared SynTagMA labeling during wakefulness and under isoflurane or ketamine-xylazine anesthesia. As shown with GCaMP6f imaging, these three different states, are accompanied by very different levels of neuronal activity. After injection with rAAV2/9-hSyn-postSynTagMA in the mouse hippocampus dorsal CA1 and implantation of a chronic hippocampal window, head-fixed mice were habituated to head-fixation on a linear treadmill (Figure 15A). In voluntarily moving animals the hippocampus was illuminated with 405 nm light through the window, which lead to a small percentage of photoconverted CA1 neuronal nuclei (Figure 15B). In the same mouse, there was no photoconversion during ketamine-xylazine induced anesthesia (Figure 15C), which is consistent with the strongly reduced activity observed using GCaMP6f.

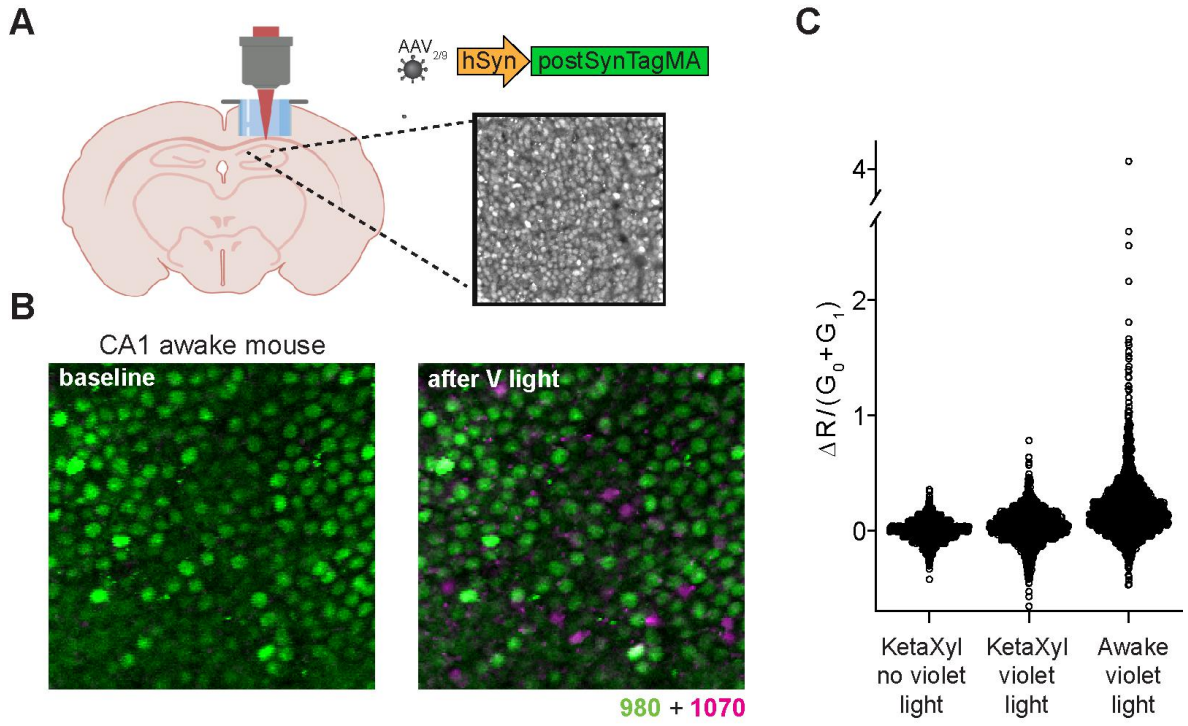

Figure 15. Using postSynTagMA to map active neurons in vivo. (A) Nuclei of CA1 neurons expressing AAV2/9-hSyn-postSynTagMA imaged in vivo through a chronic cranial window. **(B)** Representative images before and after violet light illumination (Ten 2 s, 405 nm, 12.1 mWmm−2 light pulses were applied). A small percentage of nuclei became photoconverted (magenta) after the violet light. 980 nm and 1070 nm were used to excite green and red SynTagMA fluorescence, respectively. **(C)** Photoconversion relative to baseline under ketamine-xylazine only anesthesia, after violet light and under awake conditions.

Next, to explore the application of postSynTagMA further, I demonstrated the performance during goal-directed navigation, a condition for which it has been shown that there is a dedicated population for reward coding in the hippocampus even the hippocampal maps are relatively randomized (Gauthier and Tank 2018). I trained mice to decelerate and receive a water reward at a particular location and started the imaging when the mice reached the specific criterion (Figure 16A). During the task, I imaged green fluorescence continuously for four laps (Figure 16B-D), followed by 15 laps with 405 nm light illumination triggered by reward (sans imaging). I observed that the neurons displayed dimming (i.e. increased [calcium]) just prior to each reward (Figure 16E, magenta), were photoconverted in the

following rounds, while a matched number of randomly selected non-converted neurons did not show photoconversion (Figure 16E, green). As a result, postSynTagMA photoconversion in active behaving animals could selectively map behaviorally relevant neurons with high calcium transients.

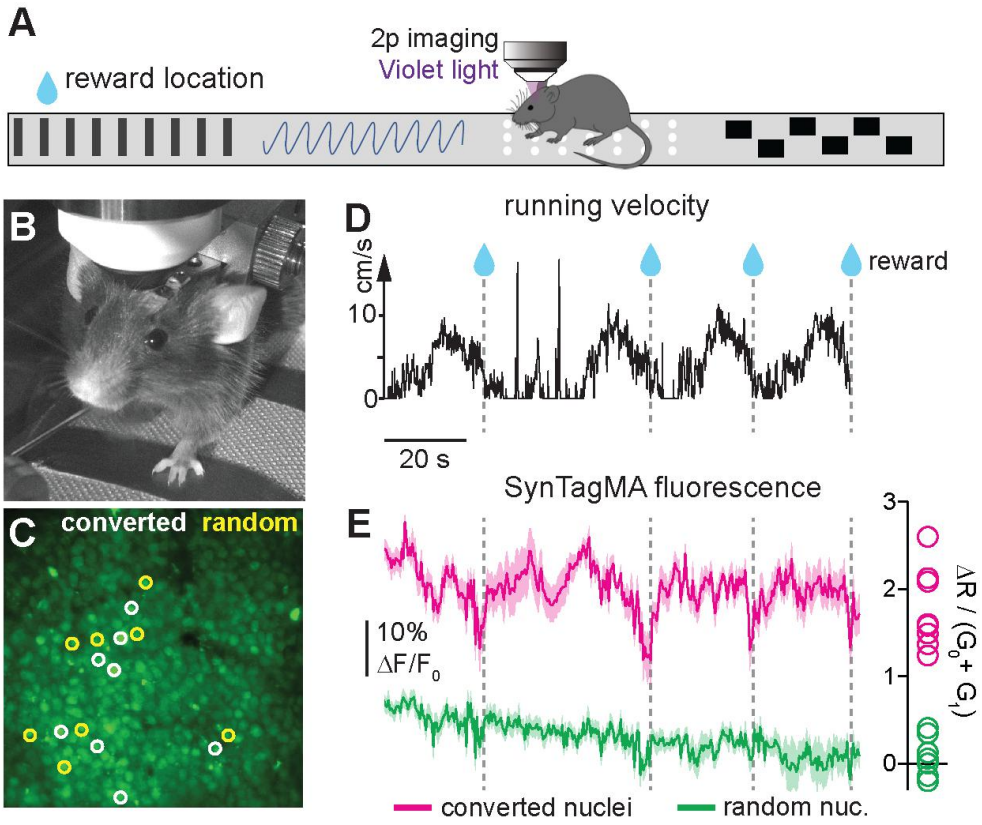

Figure 16. Using postSynTagMA to map active neurons in behaving mice. (A) Closed-loop paradigm: a head-fixed mouse was trained to stop at a certain position on the running belt to receive a water reward (teardrop). Nuclear fluorescence in CA1 was continuously monitored during 4 laps, followed by 15 laps where 405 nm, 12.1mWmm−2, 2 s light pulses were triggered during water reward. **(B)** Mouse engaged in the task. Note spout for water delivery. **(C)** 2P image of CA1 cell body layer during running. Eight nuclei that later became photoconverted are marked by white circles. Yellow circles are eight randomly selected non-converted nuclei used for comparison of calcium signals. **(D)** Black trace is running speed during the first 4 laps with times of reward delivery (teardrop/dashed line). **(E)** Magenta and green traces are the average green SynTagMA fluorescence of the 8 photoconverted nuclei and the 8 non-converted nuclei indicated in C, respectively. Photoconversion of the individual nuclei shown on the right. Note the consistent dips in the magenta trace (i.e., high calcium) just before the water reward/photoconversion light would be triggered.

2.8 PostSynTagMA maps active synapses in vivo

In order to test whether postSynTagMA could be used to identify individual active synapses/dendrites in vivo, I expressed postSynTagMA in interneurons under the mDlx promoter to achieve sparse labeling and avoid dense neuropil labeling from pyramidal neurons. I photoconverted sparsely labeled interneurons in stratum oriens of the CA1 region under isoflurane anesthesia, which keeps neuronal activity closely to awake condition but reduces motion artifacts (Figure 17). Photoconversion of clusters of synapses was observed, which was consistent with local dendritic calcium activity that has been described in hippocampal oriens interneurons in awake mice during locomotion and immobility (Francavilla et al. 2019). Therefore, under conditions of sparse postSynTagMA expression, it is possible to resolve individual photoconverted synapses in vivo.

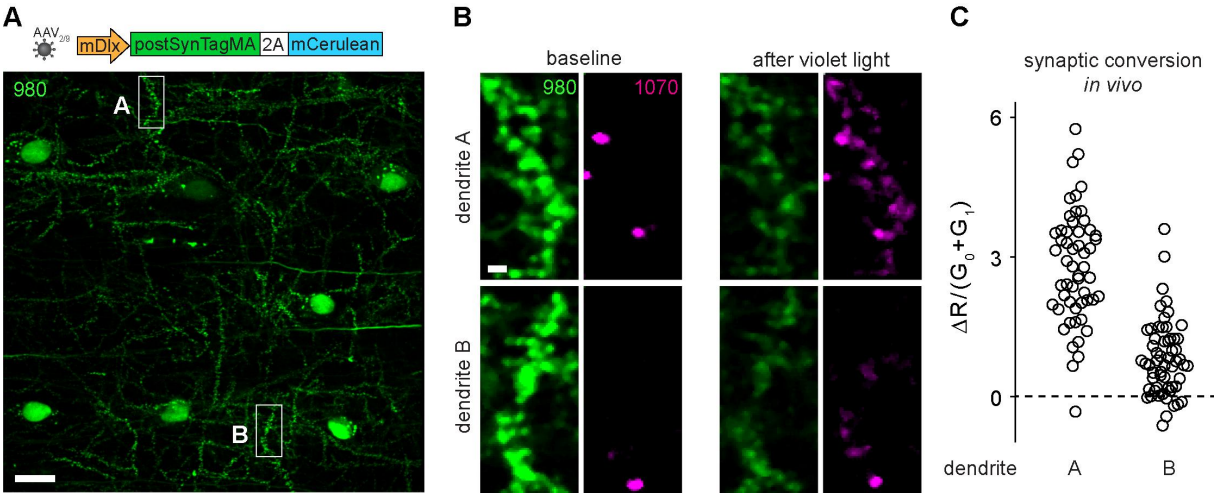

Figure 17. Using postSynTagMA to map active dendrites in anesthetized mice. (A) Interneurons expressing rAAV2/9-mDlx-postSynTagMA-2A-mCerulean imaged through a chronic cranial window under isoflurane anesthesia (mCerulean fluorescence not shown). **(B)** At high magnification, green fluorescence reveals PSD spots on the dendrite. Red spots at baseline are autofluorescent material, unrelated to SynTagMA. Violet light (20 flashes, 0.2 Hz, 3 s duration, 0.42mWmm−2) was applied to photoconvert postSynTagMA. **(C)** Photoconversion of synapses on dendrite A (n = 54 synapses) and B (n = 58 synapses) indicates higher activity levels in dendrite A. Scale bars: 20 µm (A) and 2 µm (B). All experiments were performed in at least two mice and found to be reproducible.

3 Discussion

In this dissertation, I investigated and systematically compared the pre-, intra- and post-anesthetic effects of three different commonly used general anesthetic strategies on the mouse hippocampus involving multiple levels of analysis. Despite sharing some common traits, brain and cellular network states vary considerably under the influence of various types of anesthetics (Steriade, Nunez, and Amzica 1993; Clark and Rosner 1973; Sarasso et al. 2015). At the neuronal level, all three anesthetics showed reduced spike activity in individual neurons, reduced power in the high oscillatory band compared to the awake state and natural sleep. However, the three anesthetic conditions induced distinct network states in CA1. Iso led to prominent network oscillations at around 0.1 Hz, which timed the spiking activity of single units and neuronal calcium transients. Keta/Xyl caused significant oscillations between 0.5 and 4 Hz and the strongest reduction in calcium dynamics. In contrast, MMF most strongly reduced LFP and SUA and impaired population dynamics over many hours as assessed with calcium imaging. Long-term effects on spine dynamics were present as well, with Keta/Xyl stabilizing spines, leading to a decrease in turnover ratio and an increase in density. On the other hand, MMF slightly increased spine dynamics. Keta/Xyl cannot be antagonized and therefore changes of the CA1 network mediated by this anesthetic were present hours after the injection, which is consistent with long-lasting overall changes of animal physiology (Albrecht et al. 2014). More unexpectedly, and in contrast to overall effects on physiology (Albrecht et al. 2014), CA1 network dynamics were still disturbed for at least 6 hours after antagonization of MMF anesthesia. These long-lasting alterations were associated with impairment of episodic-like memory consolidation after exposure to Keta/Xyl- or MMF, but not Iso. Thus, despite all anesthetic strategies fulfilling the same hallmarks of general anesthesia, different GAs distinctly alter hippocampal network dynamics, synaptic connectivity, and memory consolidation.

3.1 Iso, MMF and Keta/Xyl have different molecular targets and distinctly modulate functional and structural features of CA1

The GAs used here represent three different strategies based on the large repertoire of currently available anesthetics. Isoflurane represents the class of halogenated diethyl ether analogues, which are volatile and therefore administered by inhalation. The use of fentanyl in combination with the analgesic medetomidine and the sedative midazolam, represents an anesthetic approach based on the injection of a combination of drugs with sedative, analgesic and anxiolytic properties. Finally, ketamine can be used both as an anesthetic and, at a lower dosage, as a treatment against depression. For anesthesia, it is generally combined with xylazine, which acts as a sedative, analgesic and muscle relaxant.

All three strategies differ markedly in their molecular targets. Thus, they have unique modulatory effects on general physiology (Albrecht et al. 2014) and brain activity (Sarasso et al. 2015). Isoflurane is a potent GABA- and glycine receptor agonist. In addition, it activates two-pore potassium channels and acts as α-amino-3-hydroxy-5-methyl-4-isoxazolepropionic acid receptor (AMPAR) inhibitor (Alkire, Hudetz, and Tononi 2008). Similar to Iso, midazolam, the hypnotic component of the MMF mix, mainly acts as a GABAR agonist with little effect on NMDARs. In contrast, ketamine is a potent, use-dependent NMDAR blocker with less pronounced effects on potassium channels, GABA, glycine and other glutamate receptors such as AMPA or kainite receptors (Alkire, Hudetz, and Tononi 2008). Moreover, while most anesthetics reduce the activity of thalamic nuclei, ketamine increases thalamic drive (Langsjo et al. 2005), leading to enhanced rather than reduced oscillations in mid-to-high frequency bands such as theta and gamma (Soltesz and Deschenes 1993; Lee et al. 2013). In accordance with this, this study reveals major differences in the action of the different anesthetics on functional and structural features of CA1. With both electrical recordings and calcium imaging, results suggest that anesthetics affect the firing properties of hippocampal neurons and cause persistent and robust reduction of CA1 firing. Notably, effects on electrical activity and calcium activity were well in line for both Iso and MMF, despite the

different recording methods. However, there was some divergence for Keta/Xyl. With spine imaging, both Iso and MMF significantly increased the turnover ratio; however, the increased turnover ratio under Iso was likely due to an increase in the gained fraction of dendritic spines, while, under MMF, it was due to a loss of existing spine. In contrast, Keta/Xyl anesthesia had the strongest effect on spine turnover, but was significantly lower rather than higher, accompanied by a higher surviving fraction and an increase in density with time, which suggests that Keta/Xyl could stabilize existing spines.

3.2 Comparison of calcium imaging and electrophysiological recordings

In vivo calcium imaging and electrophysiological are powerful methods for recording the activity in large neuronal populations. They share many common features and have their own strengths that can complement each other.

First, the difference between electrophysiological recordings and calcium imaging data may result from the location of the detected signal. In the calcium imaging experiments, the signal was sampled in a horizontal plane located inside and parallel to stratum pyramidale of CA1. Therefore, somatic, action-potential driven calcium transients mainly from pyramidal neurons dominate the signal. In contrast, the electrodes on linear probes are arranged orthogonally to the strata of CA1 and parallel to the dendrites of CA1 cells. Thus, synaptic potentials mainly constitute the LFP across all layers and spikes are picked up from both pyramidal cells (in stratum pyramidale) and GABAergic neurons in all layers.

The second difference comes from the temporal-spatial accuracy. Due to the kinetic and calcium binding properties of GCaMP6f, action potentials can only be resolved below approximately 5 Hz and are reported nonlinearly (Chen et al. 2013; Wei et al. 2020) . However, imaging allows intensive sampling of neural activity over a large area, revealing spatial relationships between neurons with specific correlations. Although electrophysiological recordings report neural activity with high temporal precision, they had their own limitations. Electrophysiological recordings are biased toward large neurons with

high spike rates that are in close proximity of the electrode. Besides, the process of converting raw recordings into spike times associated with individual isolated units, like spike sorting, can introduce artifacts such as merging spikes from different neurons.

Third, calcium imaging can be used in cell type-specific patterns to sample rare neuronal populations that are difficult to target by electrophysiology. In addition, calcium imaging is also possible to record the activity of neuronal microcomponents that are beyond the reach of electrophysiology (Jia et al. 2010).

In this thesis, there was a contradiction found when comparing calcium imaging and electrophysiological results. More specifically, under Keta/Xyl, the overall firing rate of single units showed the smallest reduction of all three anesthetics. At the same time, calcium imaging revealed the most substantial reduction in rate, amplitude and duration of calcium transients. One reason for this discrepancy may be the inhibitory action of ketamine on NMDARs. CA1 pyramidal cells display large, NMDAR-driven dendritic plateau potentials and calcium spikes (Katz et al. 2009). Moreover, ketamine likely inhibits L-type voltage-gated calcium channels (Yamakage, Hirshman, and Croxton 1995) and reduces burst firing (Yang et al. 2018), leading to calcium transients with reduced amplitude and a faster decay constant. In contrast, ketamine has little influence on sodium spikes and AMPAR-mediated synaptic potentials, which are detected in electrical recordings as SUA and LFP, respectively. In accordance with electrical recordings, calcium transients showed increased power at 0.1-0.2 Hz under Iso. However, we did not detect a clear peak at 1-4 Hz in the presence of Keta/Xyl, as seen in LFP and SUA, probably due to its strongly dampening effect on calcium transients. The (low-pass) filtering of neuronal activity imposed by calcium indicators might also play a role (Wei et al. 2020).

Notably, the differences between electrical recordings and calcium imaging under Keta/Xyl are relevant. Calcium is a second messenger central to neuronal plasticity and metabolism (West, Griffith, and Greenberg 2002; Wiegert and Bading 2011). NMDARs are a major source for activity-dependent calcium entry into the cell, involved in regulating synaptic

plasticity, metabolism, and pathology (Hardingham and Bading 2010). The present findings suggest that Keta/Xyl has a particularly strong effect on neuronal calcium activity, uncoupling action potential firing from associated cytosolic calcium transients, leading to reduced intracellular calcium signaling. In contrast, calcium transients under MMF and Iso anesthesia closely matched the electrical activity profile of neurons. Therefore, aside from overall effects on network activity, Keta/Xyl may selectively alter neuronal plasticity by suppressing NMDAR-dependent postsynaptic calcium signals.

3.3 Iso, MMF and Keta/Xyl distinctly alter spine dynamics in CA1

There is a large body of literature showing various effects of general anesthesia on spine dynamics, depending on the brain region, preparation, age of the animal and anesthetic strategy. For example, enhanced synaptogenesis has been reported with different types of anesthetics on cortical and hippocampal neurons during development (Briner et al. 2010; De Roo et al. 2009). In contrast, one study indicated no change in spine dynamics on cortical neurons in adult mice with Keta/Xyl or Iso (Yang et al. 2011), while another study demonstrated an increase in spine density in somatosensory cortex with ketamine (Pryazhnikov et al. 2018). Also, fentanyl-mediated, concentration-dependent bidirectional modulations of spine dynamics were reported in hippocampal cultures (Lin et al. 2009). Most such studies have been conducted ex vivo or on cultured neurons, and only a few have examined spine dynamics in vivo. One study indicated that permanent memory is stored in stably connected synaptic networks in living animals (Yang, Pan, and Gan 2009). It is therefore essential to study the effects of different anesthesia on dendritic spine dynamics in vivo.

To systematically compare spine dynamics in CA1 in vivo under different anesthetic treatments, I imaged spines at basal, oblique and tuft dendrites in a large set of dendrites and compared the anesthetized state with the awake state. I found that the spine density and turnover ratio were stable through time in the awake group, but small and robust chronic effects under repeated anesthesia were present. This suggests that anesthetics may remain

in the organism longer than expected and that repeated imaging at every four days may help detecting cumulative effects of anesthetics on synaptic connectivity.

Keta/Xyl decreased spine turnover leading to a mild increase in spine density over time by stabilizing existing spines. This observation agrees with recent studies that showed a stabilizing effect of ketamine in the somatosensory cortex, resulting in increased spine density (Pryazhnikov et al. 2018). Thus, repeated anesthetic doses of Keta/Xyl may limit overall synaptic plasticity and thus spine turnover. It was further shown that sub-anesthetic, antidepressant doses of ketamine enhance spine density in the prefrontal cortex (Li et al. 2010; Phoumthipphavong et al. 2016), similar to our study of CA1 neurons. Iso and MMF had contrasting effects on spine dynamics compared to Keta/Xyl, mildly enhancing spine turnover, which might be explained by their different pharmacology compared to ketamine. A second aspect that distinguishes Keta/Xyl from Iso and MMF is its irreversibility, which might lead to longer-lasting alterations of synaptic transmission and E/I ratios leading to differential spine dynamics. This idea is supported by the observation that during the anesthesia period itself, spine turnover was not altered, suggesting that long-lasting and repeated disturbances are required to leave a mark in synaptic connectivity.

Moreover, alterations of spine stability were present in all strata of CA1. It is worth investigating whether the dendritic structures of the different layers of CA neurons have layer-specific dynamic changes as they are receiving different input from both excitatory and inhibitory presynaptic neurons. The main excitatory inputs arrive form the entorhinal cortex and CA3 pyramidal neurons. Inputs from layer III pyramidal neurons in the EC project to CA1 neurons via the perforant path and selectively innervate the distal apical dendrites in the stratum lacunosum-moleculare. Inputs from CA3 pyramidal neurons through Schaffer collateral form synapses on the apical dendrites in the stratum radiatum and on the basal dendrites in the stratum oriens.

3.4 MMF and Keta/Xyl, but not Iso, retrogradely affect episodic-like memory formation

The state of anesthesia is characterized by an altered level of consciousness, reduced responsiveness to external stimuli, amnesia, decreased muscle tone, and altered function of autonomic nerves. The degree to which these effects are achieved depends on the anesthetic and its dose. Sleep is a natural form of unconsciousness and is required for memory consolidation, including hippocampus-dependent memories (Diekelmann and Born 2010; Klinzing, Niethard, and Born 2019). Recent work suggested that sleep- and anesthesia-promoting circuits differ (Eikermann, Akeju, and Chamberlin 2020; Vanini et al. 2020) while others identified circuit elements shared between sleep and general anesthesia (Jiang-Xie et al. 2019), especially during development (Chini et al. 2019). Therefore, it is worth investigating how the diverse alterations of CA1 network dynamics imposed by the different anesthetics impact memory consolidation. In this study Iso resembled most closely network states during wakefulness and natural sleep, while Keta/Xyl and MMF caused strong, lasting alterations of LFP, SUA and calcium dynamics.

Notably, a single dose of anesthesia with Keta/Xyl and MMF, but not Iso disrupted memory consolidation using a water maze assay in adult mice. Keta/Xyl and MMF most strongly decorrelated CA1 network activity and reverted only slowly. Extending the duration of Iso anesthesia up to 4 h, to match the slow recovery after MMF and Keta/Xyl, did not affect memory consolidation. Retrograde amnesia appeared to be more sensitive to the magnitude than the duration of CA1 network disturbance imposed by the various anesthetics. This observation indicates that the slow recovery of network activity after Keta/Xyl and MMF alone cannot explain anesthesia-mediated disruptions of memory consolidation. Instead, specific aspects of the different anesthetics may selectively impact hippocampus-dependent memory formation. For example, ketamine is an NMDAR blocker that has been shown to be necessary for the long-term stabilization of place fields in CA1 (Kentros et al. 1998), encoding of temporal information of episodes (Hayashi 2019), and formation of episodic-like memory (de Souza et al. 2019).

These results appear at odds with a report (Zurek, Bridgwater, and Orser 2012), where a single, 1-h treatment with Iso caused deficits in the formation of contextual fear memory, object recognition memory and performance in the Morris water maze in the following 48 h. However, that study investigated memory acquisition after anesthesia (i.e., anterograde amnesia), while in my I study asked whether anesthesia affects the consolidation of a memory formed shortly before the treatment (i.e., retrograde amnesia).

Changes in synaptic connections are considered essential for memory formation and storage (Segal 2005; Kasai et al. 2010; Frey and Morris 1997; Yang, Pan, and Gan 2009). Despite a small effect on spine dynamics, the strong and lasting disturbance of hippocampal network activity in CA1 (and most likely other brain areas) by Keta/Xyl and MMF was sufficient to interfere with memory consolidation. The chronic alterations of spine turnover, especially by Keta/Xyl, may therefore indicate that repeated anesthesia can impact long-lasting hippocampus-dependent memories.

To establish a direct link between spine dynamics, network disruptions and memory, future studies are required that investigate both spine turnover and changes in population coupling at hippocampal neurons causally involved in memory formation and maintenance.

3.5 Labeling active neurons: IEG-based genetic switches, CaMPARI2 and nuclear postSynTagMA

Mapping active neurons can be based on activity-driven expression of immediate early genes (IEGs) or transient increases in intracellular calcium concentration. IEGs, like *c-fos* and *Arc*, are genes being transiently and rapidly activated in response to cellular stimuli. A very popular transgenic system based on IEG, the TetTag system, was developed by the Mayford laboratory in 2007, which allows persistent tagging of neurons active during a specific time window (Reijmers et al. 2007). This system uses inducible tetracycline-controlled trans-activator (tTA) and Cre recombinase (Cre) under the control of an IEG promoter, combined with the expression of a transgene (e.g., GFP, lacZ) regulated by time-

specific administration of drugs, such as doxycycline (Dox) (Ohkawa et al. 2015; Tanaka et al. 2014; Tayler et al. 2013). Further, a combination of the TetTag system with optogenetic or chemogenetic tools has advanced the application in various behavioral paradigms with the manipulation of activated neuron ensembles (Liu et al. 2012; Garner et al. 2012; Ramirez et al. 2013). However, the use of IEG expression has several drawbacks, including its relatively slow temporal resolution (hours to days) and low signal relative to baseline expression. In addition, certain cell types and brain regions rarely show IEG expression, limiting the utility of these techniques.

CaMPARI2 could provide precise labeling of active neurons, which enables acquisitions of snapshots of calcium activity around 30 seconds. The postSynTagMA was created by anchoring CaMPARI2 to post-synaptic compartments by using PSD95.FingR and its expression is regulated by a zinc-finger-KRAB sequence. This zinc-finger-KRAB sequence promotes the sequestration of redundant proteins in the nucleus and inhibits further transcription (Wang et al. 2014).

Using recombinant AAVs for delivery, postSynTagMA under different promoters can label pyramidal neurons and interneurons in dCA1, and efficiently map active neurons. To further apply this tool, goal-directed behavior was chosen, which, according to previous articles, showed that this behavior was engaged by a very low percentage of hippocampal CA1 pyramidal neurons. I observed that neurons that were light-converted showed dimming before each reward, whereas a corresponding number of randomly selected non-converted neurons did not. Thus, in behaviorally active animals, posSynTagMA photoconversion can selectively map behaviorally relevant neurons with high calcium transients after photoconversion.

3.6 Mapping active synapses with postSynTagMA

There are some pioneer tools developed to visualize synaptic events in vitro or in vivo, such as the GFP reconstitution across synaptic partners (GRASP) technique. Synapses are bilateral microstructures involving both the presynaptic terminal and postsynaptic density, so

dual-component labeling can provide more information about active circuitry. GRASP is based on functional complementation between two nonfluorescent GFP fragments across the synaptic cleft (Feinberg et al. 2008). When these complementary GFP fragments are fused to ubiquitous transmembrane proteins, GFP fluorescence appears uniformly along with membrane contacts across the synaptic cleft. When one or both GFP fragments are fused to synaptic transmembrane proteins, GFP fluorescence is tightly localized to synapses. In an optimized version, mGRASP, optimizing transmembrane split-GFP carriers for mammalian synapses, split GFP fragments are specifically targeted to pre-and post-synaptic compartments (Kim et al. 2011). I tested this tool early in my PhD and did not succeed in reproducing the results. The GRASP signal intensity was too weak to do in vivo imaging. Even for ex vivo confocal imaging it had only very faint expression and was challenging to be distinguished from background noise. Another GRASP-based tool was developed recently by combining GRASP with the IEG promoter-based expression system (Choi et al. 2018). This enhanced version of GRASP (eGRASP) has some improvements of the GRASP signal intensity by introducing a weakly interacting domain that facilitates GFP reconstitution and a single mutation commonly found on most advanced GFP variants. This improvement has the potential to facilitate the application of the tool and warrants further replicate validation in different labs.

The postSynTagMA is another potential active synapse labeling tool. I tested its basic imaging and photoconversion in anesthetized mice. I found the photoconversion of synaptic clusters in this experiment. So, it is possible to resolve individual photoconverted synapses in vivo under conditions of sparse postSynTagMA expression. Furthermore, brain motion during light is not a problem because imaging is asynchronous and postSynTagMA can be used to label the behavior of active neurons and synapses. The biggest challenge for me came from imaging at the individual synapse level in vivo before and after illumination. In this experiments, Iso anesthesia was chosen based on the previous project about general anesthesia, which more closely approximates neural activity at awake state while minimizing

brain motion. However, this was a compromise between imaging quality and practical application. For future experiments, the tool is very useful if used only for in vivo labeling of active dendrites while detecting ex vivo.

In summary, in the first project of the thesis, I investigated the effects of three different general anesthetics on memory consolidation, hippocampal network activity and spinal dynamics. First, I showed that anaesthesia with MMF or Keta/Xyl, but not Iso, impaired memory consolidation. Subsequently, investigating the short- and long-term effects of different anesthesia on changes in hippocampal neuronal activity and spine structure during and after anesthesia, I found that different GAs induced highly different network statesthat iso induced oscillations at 0.1 Hz, Keta/Xyl had the strongest reduction in calcium dynamics, while MMF strongly impaired population dynamics for several hours. By imaging the formation and elimination of dendritic spines in each condition, I found different long-term effects on dendritic spine dynamics, with Keta/Xyl having the strongest effect. Finally, to compare general anaesthesia and sleep, I found that sleep modified CA1 activity to a much lesser extent than anesthesia. For Project 2, I focused on in vivo application of post SynTagMA working as a photoconvertible fluorescent probe. First, I verified the in vivo expression of hSyn-postSynTagMA or mDlx-postSynTagMA and showed that postSynTagMA possessed photoconverted functions. I then further applied this tool at the behavioral level and found that it could selectively map behaviorally relevant neurons and synapses with high calcium transients in behaviouring mice.

4 Materials & methods

4.1 Materials

4.1.1 Mouse strains

Strain	Characteristic
C57BL/6J	wild-type
Thy1-GFP line M	Enhanced green fluorescent protein (eGFP) expression under the control of a modified Thy1 promoter region (containing the sequences required for neuronal expression but lacking the sequences required for expression in non-neural cells). EGFP expression in a sparse subset of neurons within specific populations (Feng et al. 2000). (stock No:007788)

4.1.2 Virus

virus	source
AAV2/7-syn-GCaMP6f	In house
AAV2/9-hSyn-postSynTagMA	In house
AAV2/9-mDlx-SynTagMA-2A-mCerulean	In house

4.1.3 General Anesthesia

drug	dose	Manufacturer
Isoflurane	100%	Baxter
Ketamine	130 mg/kg	Richter Pharma AG
Xylazine	10 mg/kg	Bayer
Midazolam	5.0 mg/kg	Roche
Medetomidine	0.2 mg/kg	Zoetis
Fentanyl	0.05 mg/kg	Piramal Critical Care Deutschland
Flumazenil	0.5 mg/kg	Cheplapharm Arzneimittel
Atipamezole	2.5 mg/kg	Zoetis
Buprenorphine	0.1 mg/kg	Indivior Europe limited

4.2 Methods

4.2.1 Mice

Adult C57BL/6J mice and transgenic Thy1-GFP-M mice of both sexes were housed and bred in pathogen-free conditions at the University Medical Center Hamburg-Eppendorf. The light/dark cycle was 12/12 h and the humidity and temperature were kept constant (40% relative humidity; 22°C). Food and water were available ad libitum. Experiments were conducted during the 12-hour light period. All procedures were performed in compliance with

German law according and the guidelines of Directive 2010/63/EU. Protocols were approved by the Behörde für Gesundheit und Verbraucherschutz of the City of Hamburg.

4.2.2 Morris Water Maze

I used a protocol for reversal learning in Morris water maze to assess the possible effects of the different anesthetics on episodic-like memory in mice (Chen et al. 2000; Morellini 2013). The water maze consisted of a circular tank (145 cm in diameter) circled by dark curtains and walls. The water was made opaque by the addition of non-toxic white paint such that the white platform (14 cm diameter, 9 cm high, 1 cm below the water surface) was not visible. Four landmarks (35 X 35 cm) differing in shape and grey gradient were positioned on the wall of the maze. Four white spotlights on the floor around the swimming pool provided homogeneous indirect illumination of 60 lux on the water surface. Mice were first familiarized for one day to swim and climb onto a platform (diameter of 10 cm) placed in a small rectangular maze (42.5 x 26.5 cm and 15.5 cm high). During familiarization, the position of the platform was unpredictable since its location was randomized, and training was performed in darkness. After familiarization, mice underwent three learning days, during which they had to learn the location of a hidden platform. The starting position and the side of the maze from which mice were taken out of the maze were randomized. On day 1, mice underwent four learning trials (maximum duration of 90 seconds, inter-trial interval of 10 minutes). After staying on the platform for 15 s, mice were returned to their home cage and warmed up under red light. On day 2, mice underwent two training trials before they performed a 60 seconds-long probe trial to assess their searching strategy. Afterwards, one additional training trial was used to re-consolidate the memory of the platform position, and mice were distributed into four groups with a similar distribution of performance. On day 3, the long-term memory of the platform position was tested with a 45-seconds long probe trial, followed by another training trial with the platform in place to avoid extinction. Then mice underwent four reversal learning trials with the platform located in the quadrant opposite the one in which the platform was during the previous training trials. To assess whether the mice

learned the new platform position, mice underwent a 60-seconds long probe trial followed by one more training trial to consolidate the memory of the new location. One hour after the last reversal learning trial, mice were anesthetized to analyze the effects of the anesthesia on the consolidation of the memory of the new platform position. Mice were assigned to four groups with an equal average performance during the probe trial on day 2. Each group was subjected to different conditions: one-hour Iso anesthesia, one-hour MMF anesthesia, Keta/Xyl anesthesia (which was not antagonized), and one group was left untreated. On day 4, mice underwent a 60-seconds long probe trial to evaluate their searching strategies; namely, the “episodic-like memory” of the reversal learning trials performed one hour before having been anesthetized on day 3.

4.2.3 Stereotaxic virus injection

C57BL/6J wild-type mice were anesthetized via intraperitoneal injection of MMF and placed on a heating blanket to maintain the body temperature. Eyes were covered with eye ointment (Vidisic, Bausch + Lomb) to prevent drying. Prior to surgery, the depth of anesthesia and analgesia was evaluated with a toe-pinch to test the paw-withdrawal reflex. Subsequently, mice were fixed in a stereotactic frame, the fur was removed with a fine trimmer and the skin of the head was disinfected with Betaisodona. The skin was removed by a midline scalp incision (1-3 cm), the skull was cleaned using a bone scraper (Fine Science Tools) and a small hole was drilled with a dental drill (Foredom) above the injection site. Virus (AAV2/7-syn-GCaMP6f or AAV2/9-hSyn-postSynTagMA or AAV2/9-mDlx-SynTagMA-2A-mCerulean) was targeted unilaterally to the dorsal CA1 area (− 2.0 mm AP, ± 1.3 mm ML, − 1.5 mm DV relative to Bregma). 0.6 µl of virus suspension was injected. All injections were done at 100 nl*min^{-1} using a glass micropipette. After the injection, the pipette stayed in place for at least 5 min before it was withdrawn and the scalp was closed with sutures. For complete reversal of anesthesia, mice received a subcutaneous dose of Flumazenil, Atipamezole and Buprenorphine (FAB). During the two days following surgery, animals were provided with Meloxicam mixed into soft food.

4.2.4 Hippocampal window surgery

Two weeks after virus injection, mice were anesthetized as described above to implant the hippocampal window. After fur removal, skin above the frontal and parietal bones of the skull was removed by one horizontal cut along basis of skull and two rostral cuts. The skull was cleaned after removal of the periosteum, roughened with a bone scraper and covered with a thin layer of cyanoacrylate glue (Pattex). After polymerization a 3-mm circle was marked on the right parietal bone (anteroposterior, −2.2 mm; mediolateral, +1.8 mm relative to bregma) with a biopsy punch and the bone was removed with a dental drill (Foredom). The dura and somatosensory cortex above the hippocampus were carefully aspirated until the white matter tracts of the corpus callosum became visible. The craniotomy was washed with sterile PBS and a custom-built imaging window was inserted over the dorsal hippocampus. The window consisted of a hollow glass cylinder (diameter: 3 mm, wall thickness: 0.1 mm, height: 1.8 mm) glued to a No. 1 coverslip (diameter: 3mm, thickness: 0.17 mm) on the bottom and to a stainless-steel rim on the top with UV-curable glass glue (Norland NOA61). The steel rim and a head holder plate (Luigs & Neumann) were fixed to the skull with cyanoacrylate gel (Pattex). After polymerization, cranial window and head holder plate were covered with dental cement (Super Bond C&B, Sun Medical) to provide strong bonding to the skull bone. Following the surgery, animals were provided with Meloxicam mixed into soft food for 3 days. The position of the hippocampal window was confirmed in brain slices postmortem.

4.2.5 Mouse handling for awake imaging on treadmill

At the start of water restriction, 2 ml was initially provided to each mouse. When a mouse reaches 85% of the initially measured free weight (reference weight) of the target weight, I would start training and give water to the mice manually. For the first 3-5 days, I would extend my hand into the cage and provide water for approximately 30 minutes per cage at the same time each day. When the mice were free to explore my hand and began to explore the arm, it was the time to enter the running belt training phase. The mice were placed on a

treadmill and allowed to move freely on it. Next, I would hold their tails or the brain window fixation bar and allowed them to move forward. This training usually takes 3-5 days. And then the mice can be head-fixed to the treadmill. I would provide rewards at random locations. The fixation time starts from 10 minutes and is gradually extended to the desired time in 15-minute increments. For in vivo awake imaging, it usually takes 3-5 days to extend to 1 hour, while for sleep calcium imaging, I will train for at least 10 days to extend the time to 4 hours.

4.2.6 Two-photon calcium imaging in anesthetized and awake mice

The same animals were sequentially imaged under Keta/Xyl, MMF or Iso in a pseudo-randomized order during the dark phase of the dark/light cycle. The following drug combinations were administered: 2.0 % isoflurane in 100% O_2; 130 mg/kg ketamine, 10 mg/kg xylazine s.c.; 5.0 mg/kg midazolam, 0.2 mg/kg medetomidine and 0.05 mg/kg fentanyl s.c.; and for complete reversal of anesthesia, 0.5 mg/kg flumazenil, 2.5 mg/kg atipamezole and 0.1 mg/kg buprenorphine s.c. After losing the righting reflex, generally 5–10 min after application of the anesthetics, the animals were positioned on a heating-pad to maintain body temperature at approximately 37°C during anesthesia. The intensity of anesthesia and evaluation of the different stages of anesthesia were assessed by recording the presence or absence of distinct reflex responses: righting reflex, palpebral reflex, toe-pinch reflex. Between each imaging session, mice were allowed to recover for one week.

Anesthetized mice were head-fixed under the microscope on a heated blanket to maintain body temperature. Eyes were covered with eye ointment (Vidisic, Bausch + Lomb) to prevent drying. The window was centered under the two-photon microscope (MOM-scope, Sutter Instruments, modified by Rapp Optoelectronics) and GCaMP6f expression was verified in the hippocampus using epi fluorescence. Images were acquired with a 16x water immersion objective (Nikon CFI75 LWD 16X W, 0.80 NA, 3.0 mm WD).

For awake imaging I used a linear treadmill, which allowed imaging during quiet and running states. 5-min-timelapse images were acquired every 10 minutes for a period of 50 minutes.

Only quiet periods were considered for analysis in this study. Image acquisition was carried out with a Ti:Sa laser (Chameleon Vision-S, Coherent) tuned to 980 nm to excite GCaMP6f. Single planes (512x512 pixels) were acquired at 30 Hz with a resonant-galvanometric scanner at 29-60 mW (980 nm) using ScanImage 2017b (Vidrio). Emitted photons were detected by a pair of photomultiplier tubes (H7422P-40, Hamamatsu). A 560 DXCR dichroic mirror and a 525/50 emission filter (Chroma Technology) was used to detect green fluorescence. Excitation light was blocked by short-pass filters (ET700SP-2P, Chroma). For the repetitive imaging, the position of the FOV was registered in the first imaging session with the help of vascular landmarks and cell bodies of CA1 pyramidal neurons. This allowed for subsequent retrieval of the FOV for each mouse.

Calcium imaging experiments to measure recovery from anesthesia were done in five additional animals. They were trained to maintain immobile on the treadmill for extended periods. I ensured to measure the same FOV and to maintain overall stability of fluorescence intensity for every recording in each imaging session for a given animal. The time-lapse recordings were extended to up to a maximum of 10 min per time point to have a higher probability of capturing motionless periods continuously, in awake and recovery states. Iso was applied for 60 min. FAB was injected 60 min after the application of MMF. Keta/Xyl was not antagonized. Imaging of calcium activity was performed before, 0.5, 1.5, 2, 3, 4, 5, and 6 hours after induction of anesthesia. For Iso and MMF, the 1.5 h time point represented the first imaging session after reversal. Untreated control animals were imaged every hour for the same amount of time.

To habituate mice to sleep under head-fixation, I still used the linear treadmill. Through the first 4 sessions mice were kept head-fixed for 15 to 30 min. In ten following sessions the fixation period was extended up to 4h with increasing intervals of 30 min. The state of the mouse was continuously monitored with a USB camera and the running speed was recorded with custom-written scripts in the Matlab. After habituation to 4h head-fixation, sleep imaging

sessions were recorded, which were synchronized with recordings of the pupil and running speed. Sleep imaging was performed during the light phase of the dark/light cycle.

4.2.7 Two-Photon calcium imaging Processing

In vivo calcium imaging data were analyzed with custom-written scripts in the Python and Matlab environment available at https://github.com/mchini/Yang_Chini_et_al.

Alignment of multiple recordings.

To track the activity of the same set of neurons in different anesthetic conditions and during wakefulness, we acquired two-photon time series of a defined field of view for each animal and each condition across multiple weeks. Over such long time periods, the field of view was susceptible to geometrical transformations from one recording to another and thus, any two time series were never perfectly aligned. This problem scaled with time that passed between recordings. However, optimal image alignment is critical for the successful identification and calcium analysis of the same neurons across time (Rose et al. 2016; Sheintuch et al. 2017).

To address this problem, we developed an approach based on the pystackreg package, a Python implementation of the ImageJ extension TurboReg/StackReg (Thevenaz, Ruttimann, and Unser 1998). The source code that reproduces the procedure described in this section is available on github (https://pypi.org/project/pystackreg/). The *pystackreg* package is capable of using different combinations of geometrical transformations for the alignment. We considered rigid body (translation + rotation + scaling) and affine (translation + rotation + scaling + shearing) transformation methods, which we applied to mean and enhanced-mean intensity images generated by Suite2p during the registration of each single recording. We performed the alignment using all four combinations (2 transformations x 2 types of images) choosing the one with the best performance according to the following procedure. Squared difference between the central part of a reference and aligned image served as a distance function d to quantify the alignment (since the signal is not always present on the borders of the image they were truncated):

$$d = \sum_{i,j}^{Tranc.\ images} (x_{i,j}^{ref} - x_{i,j}^{aligned})^2,$$

where $x_{i,j}^{ref}$ and $x_{i,j}^{aligned}$ are intensities of the pixel with coordinates i,j of the reference and aligned images. The combination with the smallest score was chosen for the final transformation. In some rare cases, the algorithm of the alignment did not converge for a given transformation method and image type (mean or enhanced-mean), crumbling the aligned image in a way that most of the field of view remained empty. This combination may have the smallest distance function *d* and may be falsely identified as the best one. To overcome this issue, an additional criterion was applied, which requires the central part of the aligned picture to contain more than 90 % of the non-empty pixels. The overall performance of the algorithm was verified by visual inspection. An example of the alignment of two recordings is shown in Fig. S5. The alignment for all recordings of an example mouse is demonstrated in a supplementary video (Supplementary_video_37529_aligned_recordings.avi).

In case of relatively small distortions across recordings, for example, when consecutive acquisitions were done within one imaging session, registration can alternatively be performed simultaneously with ROI detection in Suite2p by concatenating those TIFF-stacks. In this approach, every ROI is automatically labeled with the same identification number across all recordings.

Identification of the same neurons across different recordings & unique neuron ID assignment.

After the alignment procedure, we set out to identify neurons which were active across multiple recordings (and thus, multiple conditions). To achieve this, we developed an algorithm similar to the one described in Sheintuch. et al. 2017 (Sheintuch et al. 2017). The

algorithm processes in series all recordings for a given animal and assigns unique identification (ID) numbers to each ROIs of every recording. Since the recordings under Iso-anesthesia had the largest number of active neurons, we chose the first recording of this condition as reference. We assigned IDs that ranged from 1 to the total amount of neurons to all the ROIs of this recording. For every other recording of each mouse, Neuron ID assignment consisted of: 1. comparison of the properties (details below) of each ROI with each ROI that had already been processed. 2a. If the properties of the ROI matched the properties of an ROI from a previously analyzed recording, the ROI received the same Neuron ID. 2b. If no match was found, a new (in sequential order) Neuron ID was assigned to the ROI. In order to be identified as representing the same neuron in two different recordings, two ROIs had to respect the following criteria: the distance between their centroids had to be below 3 μm, and the overlap between their pixels had to be above 70%. An example of the identification of unique neuron pairs in two recordings is presented in Fig. S6A. The thresholds were chosen based on the distribution of the distances between centroids and percentage of the overlaps. An example for a single mouse is graphically illustrated in Fig. S6B. Both properties have a clearly bimodal distribution (similar to (Sheintuch et al. 2017)) with cutoffs close to the chosen thresholds.

Signal extraction and analysis.

Signal extraction, correlation and spectral analysis for calcium signal was performed using Python (Python Software Foundation, NH, USA) in the Spyder (Pierre Raybaut, The Spyder Development Team) development environment. Calcium imaging data were analyzed with the Suite2p toolbox (Pachitariu et al. 2017) using the parameters given in table 1.

Parameter	**Variable**	**Value**
Sampling rate, frames per second	fs	30

Registration		
Subsampled frames for finding reference image	nimg_init	2000
Number of frames per batch	batch_size	200
Maximum allowed registration shift, as a fraction of frame max(width and height)	maxregshift	0.1
Precision of subpixel registration (1/subpixel steps)	subpixel	10
Smoothing	smooth_sigma	1.15
Bad frames to be excluded	th_badframes	100.0
Non-rigid registration		
Use nonrigid registration	nonrigid	True
Block size to register (** keep this a multiple of 2 **)	block_size	[128,128]
if any nonrigid block is below this threshold, it gets smoothed until above this threshold. 1.0 results in no smoothing	snr_thresh	2.0
maximum pixel shift allowed for nonrigid, relative to rigid	maxregshiftNR	10
Cell detection		
Run ROI extraction	roidetect	True
Run sparse_mode	sparse_mode	False
Diameter for filtering and extracting	diameter	12.0
Keep ROIs fully connected (set to 0 for dendrites)	connected	True

Maximum number of binned frames for cell detection	nbinned	5000
Maximum number of iterations to do cell detection	max_iterations	20
Adjust the automatically determined threshold by this scalar multiplier	threshold_scaling	1.0 or 0.1
Cells with more overlap than this get removed during triage, before refinement	max_overlap	0.75
Running mean subtraction with window of size 'high_pass'	high_pass	100
ROI extraction		
Number of pixels to keep between ROI and neuropil donut	inner_neuropil_radius	2
Minimum number of pixels in the neuropil	min_neuropil_pixels	100
Pixels that are overlapping are thrown out (False) or added to both ROIs (True)	allow_overlap	True
Deconvolution		
Deconvolution time constant, seconds	tau	0.7

The same analytical pipeline was applied to both the raw fluorescence traces as well as the deconvolved (“spikes”) signal, as extracted by the Suite2p toolbox. Generally, the raw fluorescence signal was preferred over the deconvolved one given that its extraction is more straightforward and relies on less assumptions. However, while the reported effects varied in magnitude depending on which of the two signals was considered, the same results were obtained on both datasets. The effects were entirely consistent. For raw signal analysis of

each neuron, previous to any further step, we subtracted 0.7 of the corresponding neuropil fluorescence trace.

The number and height of calcium transients properties were calculated with the scipy function *find_peaks* on the raw calcium traces with the following parameters: height = 200, distance = 10 and prominence = 200. The decay was computed on the 10 best-isolated transients of each neuron, using the *OASIS* toolbox (https://github.com/j-friedrich/OASIS). We used the *deconvolve* function with the following parameters: penalty = 0, optimize_g = 10. Traces with an estimated decay over 2 seconds were considered cases of failed extraction and removed from further analysis.

The choice of the parameter values for transient detection is somewhat arbitrary. Similarly, it is debatable whether and how the calcium traces should best be normalized. Therefore, we tested the robustness of our findings by systematically varying signal extraction choices. We first varied the height and prominence threshold across a wide range of values (50 to 700 arbitrary units). We further computed transients features on normalized ΔF/F calcium traces. To normalize calcium signals, we used the baseline value as extracted by the *deconvolve* function. Also, in this case, we varied the height and prominence threshold across a wide range of values (0.5 to 3 arbitrary units). Finally, we computed two measures of neuronal activity that are independent of calcium transients detection: the average of the trace integral and its standard deviation, with and without normalization. Across all of these scenarios, the reported effects were robustly consistent.

Correlations were computed both as Pearson (numpy function *corrcoeff*) and Spearman (custom written function) coefficient on the z-scored signal. To both sets of coefficients, the Fisher correction (the inverse of the hyperbolic tangent function, numpy function *arctanh*) was applied. For power analysis, we first created a population activity vector by summing all the single neuron z-scored signals, and then estimated the power spectral density by applying the Welch method (sampling frequency = 30 Hz, number of points for fast Fourier transformation = 1024, no overlap, window length = 1 s).

For analysis of recovery from anesthesia, all recordings of the imaging session for a given animal were concatenated in Suite2p. As a consequence, each recording in the imaging session has the same set of reconstructed neurons. A time window of 5000 frames was used for the analysis to ensure continuous motionless periods. To track the neuronal activity changes, the number of fluorescence peaks, their amplitude, and the characteristic decay constant of the transients were considered. Each imaging session's threshold was chosen to match the median activity in the pre-anesthesia (awake) state across all animals. To assess the relative changes of these parameters induced by anesthesia and their subsequent recovery over time, the parameters were normalized to their median value at the pre-anesthesia (awake) state. Notably, we focused our analysis on neurons that maintained some detectable activity during anesthesia, and neurons with no detected peaks were excluded from the distributions. Additionally, we applied the cut *decay constant* > 1/30 [s] (where 30 frames per second is an acquisition rate) to remove the traces where the OASIS algorithm considered a single noise peak to be a calcium transient.

Complexity analysis was performed in the Matlab (MathWorks) environment. For complexity analysis, we limited the number of neurons to the minimum (N_{min}) present in any recording of any condition for each single mouse (median = 265, min = 156, max = 1068). The resulting matrix therefore had the $T_{rec}xN_{min}$ dimensions, where T_{rec} represents the time vector for the recording, with a length of 5 min and a sampling rate of 30 Hz. For recordings that had a number of neurons larger than N_{min} for that mouse, we randomly sampled n = N_{min} neurons and repeated the analysis 5 times. For every extracted parameter, we then considered the median value over the 5 repetitions. For further analysis, the signal was down sampled from the original sampling frequency of 30 Hz to 10 Hz (100 ms bins). The same analytical pipeline was then applied to both the raw fluorescence traces, as well as the deconvolved signal.

tSNE clustering.

tSNE clustering was performed similar to (Wenzel et al. 2019). Briefly, in a range between 5 and 45, the perplexity value that minimized the reconstruction error was selected. The number of PCA components used for this step was limited to 30. For the raw fluorescence signal, Euclidian distance was used, whereas for the deconvolved signal we opted for cosine distance, as it is better suited to a sparse signal. We computed the probability distribution of the resulting embedded matrix ($2xT_{rec}$), that was then convolved with a 2D Gaussian window (standard deviation was set to be equal to 1/40 of the total maximum value). To evaluate the number of clusters in the distribution, we then applied a series of standard steps in image analysis: background subtraction with the rolling ball method, smoothing with a median filter, thresholding, watershedding to avoid undersegmentation, and extended minima transformation. Finally, the exterior boundaries of the objects were traced and counted. This gave the number of clusters.

4.2.8 Two-photon spine imaging in anesthetized and awake mice

3 - 4 weeks after window implantation, chronic spine imaging started in Tg(Thy1-EGFP)MJrs/J mice with the first of a total of four imaging series. Each imaging series was done under one of the three anesthetic conditions (Iso, Keta/Xyl, MMF, see above for details) or during wakefulness. Within one series, mice were imaged 5 times every 4 days. Afterwards, mice were allowed to recover for three to four weeks until the next imaging series under a different anesthetic condition was started. Thus, each experiment lasted approx. 5 months. To avoid time-dependent effects, anesthetic conditions were pseudo-randomized. For imaging sessions under anesthesia mice were head fixed under the microscope on a heated blanket to maintain body temperature. Eyes were covered with eye ointment (Vidisic, Bausch + Lomb) to prevent drying. The window was centered under the two-photon microscope (MOM-scope, Sutter Instruments, modified by Rapp Optoelectronics) and GFP expression was verified in the hippocampus using epi-fluorescence. Image acquisition was carried out with a Ti:Sa laser (Chameleon Vision-S, Coherent) tuned to 980 nm to excite GFP. Images were acquired with a 40x water immersion objective (Nikon CFI APO NIR 40X

W, 0.80 NA, 3.5 mm WD). Single planes (512x512 pixels) were acquired at 30 Hz with a resonant scanner at 10-60 mW (980 nm) using ScanImage 2017b. Before the first imaging session, I registered the field of views with the help of vascular landmarks and cell bodies of CA1 pyramidal neurons and selected several regions for longitudinal monitoring across the duration of the time-lapse experiment. Each of these regions contained between 1 and 2 dendritic segments visibly expressing GFP. The imaging sessions lasted for max 60 min and mice were placed back to their home cages where they woke up.

4.2.9 Two-Photon Spine Image Processing

In each animal, at least one GFP-expressing CA1 pyramidal neuron was selected and 1-3 dendrites of 20–50 µm length of each of the following types were analyzed: basal dendrites, oblique dendrites emerging from the apical trunk and tuft dendrites. Motion artefacts were corrected with a custom-modified Lucas-Kanade-based alignment algorithm written in Matlab. Spines that laterally emanated from the dendrite were counted by manually scrolling through the z-stacks of subsequent imaging time points of the same dendritic element, by an expert examiner blinded to the experimental condition. Protrusions from the dendrite that reached a threshold of 0.2 µm were scored as dendritic spines regardless of shape. If spine neck positions differed 0.5 µm on the subsequent images, the spine was scored as a new spine. Spines were scored as lost if they fell below the threshold of 0.2 µm. Spine density was calculated as the number of spines per µm. The turnover ratio was calculated for every time point by dividing the sum of gained and lost spines by the number of present spines. The survival fraction of spines was calculated as the percentage of remaining spines compared with the first imaging time point.

4.2.10 Intracardial perfusion and brain dissection

The mice were deeply anesthetized with Keta/Xyl and checked for anesthesia with the toe pinch reflex test. Then, I made an incision below the diaphragm and the rib cage rostrally on the lateral edges to expose the heart and fix the Xiphoid with clamp. The needle was inserted

into left ventricle and fixed, then the right atrium is cut to allow flow. The animal was transcardially perfused with 1x PBS wash for 10 ml and then switch to perfuse with 4% Paraformaldehyde (PFA) for 50 ml. Visualize the animal's extremities and tail for evidence of tremors resulting from the aldehyde-crosslinking of nerves and muscle, which was an indication that fixation was taking place. Remove head, trim off skin and store head in small jar of 4% PFA for 24 hours.

4.2.11 Plotting and statistical analysis

In vivo calcium imaging data were analyzed with custom-written scripts in the Python and Matlab environment available at https://github.com/mchini/Yang_Chini_et_al. Statistical analyses were performed using R Statistical Software (Foundation for Statistical Computing, Vienna, Austria) or GraphPad Prism. All R scripts and datasets are available on GitHub https://github.com/mchini/Calcium-Imaging---Anesthesia.

4.2.12 Data and Code Availability

The code generated during this study is available at https://github.com/OpatzLab/HanganuOpatzToolbox and https://github.com/mchini/Calcium-Imaging---Anesthesia

The calcium imaging and electrophysiology data sets generated during this study are available at https://gin.g-node.org/SW_lab/Anesthesia_CA1

5 Appendix

5.1 References

Abdallah, C. G., G. Sanacora, R. S. Duman, and J. H. Krystal. 2015. 'Ketamine and rapid-acting antidepressants: a window into a new neurobiology for mood disorder therapeutics', *Annu Rev Med*, 66: 509-23.

Akerboom, J., N. C. Calderon, L. Tian, S. Wabnig, M. Prigge, J. Tolo, A. Gordus, M. B. Orger, K. E. Severi, J. J. Macklin, R. Patel, S. R. Pulver, T. J. Wardill, E. Fischer, C. Schuler, T. W. Chen, K. S. Sarkisyan, J. S. Marvin, C. I. Bargmann, D. S. Kim, S. Kugler, L. Lagnado, P. Hegemann, A. Gottschalk, E. R. Schreiter, and L. L. Looger. 2013. 'Genetically encoded calcium indicators for multi-color neural activity imaging and combination with optogenetics', *Frontiers in Molecular Neuroscience*, 6.

Albrecht, M., J. Henke, S. Tacke, M. Markert, and B. Guth. 2014. 'Effects of isoflurane, ketamine-xylazine and a combination of medetomidine, midazolam and fentanyl on physiological variables continuously measured by telemetry in Wistar rats', *BMC Vet Res*, 10: 198.

Alkire, M. T., R. J. Haier, S. J. Barker, N. K. Shah, J. C. Wu, and Y. J. Kao. 1995. 'Cerebral metabolism during propofol anesthesia in humans studied with positron emission tomography', *Anesthesiology*, 82: 393-403; discussion 27A.

Alkire, M. T., R. J. Haier, and J. H. Fallon. 2000. 'Toward a unified theory of narcosis: brain imaging evidence for a thalamocortical switch as the neurophysiologic basis of anesthetic-induced unconsciousness', *Conscious Cogn*, 9: 370-86.

Alkire, M. T., A. G. Hudetz, and G. Tononi. 2008. 'Consciousness and anesthesia', *Science*, 322: 876-80.

Attardo, A., J. E. Fitzgerald, and M. J. Schnitzer. 2015. 'Impermanence of dendritic spines in live adult CA1 hippocampus', *Nature*, 523: 592-6.

Bannister, N. J., and A. U. Larkman. 1995. 'Dendritic morphology of CA1 pyramidal neurones from the rat hippocampus: I. Branching patterns', *J Comp Neurol*, 360: 150-60.

Bekker, A., C. Lee, S. de Santi, E. Pirraglia, A. Zaslavsky, S. Farber, M. Haile, and M. J. de Leon. 2010. 'Does mild cognitive impairment increase the risk of developing postoperative cognitive dysfunction?', *Am J Surg*, 199: 782-8.

Betz, H., and B. Laube. 2006. 'Glycine receptors: recent insights into their structural organization and functional diversity', *J Neurochem*, 97: 1600-10.

Bird, C. M., and N. Burgess. 2008. 'The hippocampus and memory: insights from spatial processing', *Nat Rev Neurosci*, 9: 182-94.

Bourne, J. N., and K. M. Harris. 2008. 'Balancing structure and function at hippocampal dendritic spines', *Annu Rev Neurosci*, 31: 47-67.

Boveroux, P., A. Vanhaudenhuyse, M. A. Bruno, Q. Noirhomme, S. Lauwick, A. Luxen, C. Degueldre, A. Plenevaux, C. Schnakers, C. Phillips, J. F. Brichant, V. Bonhomme, P. Maquet, M. D. Greicius, S. Laureys, and M. Boly. 2010. 'Breakdown of within- and between-network resting state

functional magnetic resonance imaging connectivity during propofol-induced loss of consciousness', *Anesthesiology*, 113: 1038-53.

Brackmann, M., C. Zhao, V. Schmieden, and K. H. Braunewell. 2004. 'Cellular and subcellular localization of the inhibitory glycine receptor in hippocampal neurons', *Biochem Biophys Res Commun*, 324: 1137-42.

Briner, A., M. De Roo, A. Dayer, D. Muller, W. Habre, and L. Vutskits. 2010. 'Volatile anesthetics rapidly increase dendritic spine density in the rat medial prefrontal cortex during synaptogenesis', *Anesthesiology*, 112: 546-56.

Briner, A., I. Nikonenko, M. De Roo, A. Dayer, D. Muller, and L. Vutskits. 2011. 'Developmental Stage-dependent persistent impact of propofol anesthesia on dendritic spines in the rat medial prefrontal cortex', *Anesthesiology*, 115: 282-93.

Broussard, G. J., Y. Liang, M. Fridman, E. K. Unger, G. Meng, X. Xiao, N. Ji, L. Petreanu, and L. Tian. 2018. 'In vivo measurement of afferent activity with axon-specific calcium imaging', *Nat Neurosci*, 21: 1272-80.

Brown, E. N., K. J. Pavone, and M. Naranjo. 2018. 'Multimodal General Anesthesia: Theory and Practice', *Anesth Analg*, 127: 1246-58.

Burgess, N., E. A. Maguire, and J. O'Keefe. 2002. 'The human hippocampus and spatial and episodic memory', *Neuron*, 35: 625-41.

Campagna, J. A., K. W. Miller, and S. A. Forman. 2003. 'Mechanisms of actions of inhaled anesthetics', *N Engl J Med*, 348: 2110-24.

Carlson, H. J., and R. E. Campbell. 2009. 'Genetically encoded FRET-based biosensors for multiparameter fluorescence imaging', *Curr Opin Biotechnol*, 20: 19-27.

Carter, M. E., J. Brill, P. Bonnavion, J. R. Huguenard, R. Huerta, and L. de Lecea. 2012. 'Mechanism for Hypocretin-mediated sleep-to-wake transitions', *Proc Natl Acad Sci U S A*, 109: E2635-44.

Carter, M. E., O. Yizhar, S. Chikahisa, H. Nguyen, A. Adamantidis, S. Nishino, K. Deisseroth, and L. de Lecea. 2010. 'Tuning arousal with optogenetic modulation of locus coeruleus neurons', *Nat Neurosci*, 13: 1526-33.

Chandra, D., F. Jia, J. Liang, Z. Peng, A. Suryanarayanan, D. F. Werner, I. Spigelman, C. R. Houser, R. W. Olsen, N. L. Harrison, and G. E. Homanics. 2006. 'GABAA receptor alpha 4 subunits mediate extrasynaptic inhibition in thalamus and dentate gyrus and the action of gaboxadol', *Proc Natl Acad Sci U S A*, 103: 15230-5.

Chemali, J. J., C. J. Van Dort, E. N. Brown, and K. Solt. 2012. 'Active emergence from propofol general anesthesia is induced by methylphenidate', *Anesthesiology*, 116: 998-1005.

Chen, G., K. S. Chen, J. Knox, J. Inglis, A. Bernard, S. J. Martin, A. Justice, L. McConlogue, D. Games, S. B. Freedman, and R. G. Morris. 2000. 'A learning deficit related to age and beta-amyloid plaques in a mouse model of Alzheimer's disease', *Nature*, 408: 975-9.

Chen, T. W., T. J. Wardill, Y. Sun, S. R. Pulver, S. L. Renninger, A. Baohan, E. R. Schreiter, R. A. Kerr, M. B. Orger, V. Jayaraman, L. L. Looger, K. Svoboda, and D. S. Kim. 2013. 'Ultrasensitive fluorescent proteins for imaging neuronal activity', *Nature*, 499: 295-300.

Cheng, V. Y., L. J. Martin, E. M. Elliott, J. H. Kim, H. T. Mount, F. A. Taverna, J. C. Roder, J. F. Macdonald, A. Bhambri, N. Collinson, K. A. Wafford, and B. A. Orser. 2006. 'Alpha5GABAA receptors mediate the amnestic but not sedative-hypnotic effects of the general anesthetic etomidate', *J Neurosci*, 26: 3713-20.

Cheong, K. F., and S. T. Khoo. 1996. 'Inhalational induction with isoflurane: the influence of lidocaine pretreatment', *J Anesth*, 10: 125-28.

Chini, M., S. Gretenkord, J. K. Kostka, J. A. Popplau, L. Cornelissen, C. B. Berde, I. L. Hanganu-Opatz, and S. H. Bitzenhofer. 2019. 'Neural Correlates of Anesthesia in Newborn Mice and Humans', *Front Neural Circuits*, 13: 38.

Choi, J. H., S. E. Sim, J. I. Kim, D. I. Choi, J. Oh, S. Ye, J. Lee, T. Kim, H. G. Ko, C. S. Lim, and B. K. Kaang. 2018. 'Interregional synaptic maps among engram cells underlie memory formation', *Science*, 360: 430-35.

Chung, S., F. Weber, P. Zhong, C. L. Tan, T. N. Nguyen, K. T. Beier, N. Hormann, W. C. Chang, Z. Zhang, J. P. Do, S. Yao, M. J. Krashes, B. Tasic, A. Cetin, H. Zeng, Z. A. Knight, L. Luo, and Y. Dan. 2017. 'Identification of preoptic sleep neurons using retrograde labelling and gene profiling', *Nature*, 545: 477-81.

Clark, D. L., and B. S. Rosner. 1973. 'Neurophysiologic effects of general anesthetics. I. The electroencephalogram and sensory evoked responses in man', *Anesthesiology*, 38: 564-82.

Culley, D. J., M. G. Baxter, C. A. Crosby, R. Yukhananov, and G. Crosby. 2004. 'Impaired acquisition of spatial memory 2 weeks after isoflurane and isoflurane-nitrous oxide anesthesia in aged rats', *Anesth Analg*, 99: 1393-7; table of contents.

Culley, D. J., M. Baxter, R. Yukhananov, and G. Crosby. 2003. 'The memory effects of general anesthesia persist for weeks in young and aged rats', *Anesth Analg*, 96: 1004-9, table of contents.

Dailey, M. E., and S. J. Smith. 1996. 'The dynamics of dendritic structure in developing hippocampal slices', *J Neurosci*, 16: 2983-94.

Dana, H., Y. Sun, B. Mohar, B. K. Hulse, A. M. Kerlin, J. P. Hasseman, G. Tsegaye, A. Tsang, A. Wong, R. Patel, J. J. Macklin, Y. Chen, A. Konnerth, V. Jayaraman, L. L. Looger, E. R. Schreiter, K. Svoboda, and D. S. Kim. 2019. 'High-performance calcium sensors for imaging activity in neuronal populations and microcompartments', *Nat Methods*, 16: 649-57.

Davis, H. P., and L. R. Squire. 1984. 'Protein synthesis and memory: a review', *Psychol Bull*, 96: 518-59.

Davis, W. D., K. A. Davis, and K. Hooper. 2019. 'The Use of Ketamine for the Management of Acute Pain in the Emergency Department', *Adv Emerg Nurs J*, 41: 111-21.

De Roo, M., P. Klauser, A. Briner, I. Nikonenko, P. Mendez, A. Dayer, J. Z. Kiss, D. Muller, and L. Vutskits. 2009. 'Anesthetics rapidly promote synaptogenesis during a critical period of brain development', *PLoS One*, 4: e7043.

de Sousa, S. L., R. Dickinson, W. R. Lieb, and N. P. Franks. 2000. 'Contrasting synaptic actions of the inhalational general anesthetics isoflurane and xenon', *Anesthesiology*, 92: 1055-66.

de Souza, Ibmb, Ydsr Meurer, P. M. Tavares, K. C. Pugliane, R. H. Lima, R. H. Silva, and F. F. Barbosa. 2019. 'Episodic-like memory impairment induced by sub-anaesthetic doses of ketamine', *Behavioural brain research*, 359: 165-71.

Denk, W., J. H. Strickler, and W. W. Webb. 1990. 'Two-photon laser scanning fluorescence microscopy', *Science*, 248: 73-6.

Diekelmann, S., and J. Born. 2010. 'The memory function of sleep', *Nat Rev Neurosci*, 11: 114-26.

Dombeck, D. A., C. D. Harvey, L. Tian, L. L. Looger, and D. W. Tank. 2010. 'Functional imaging of hippocampal place cells at cellular resolution during virtual navigation', *Nature Neuroscience*, 13: 1433-U180.

Downie, D. L., A. C. Hall, W. R. Lieb, and N. P. Franks. 1996. 'Effects of inhalational general anaesthetics on native glycine receptors in rat medullary neurones and recombinant glycine receptors in Xenopus oocytes', *Br J Pharmacol*, 118: 493-502.

Eikermann, M., O. Akeju, and N. L. Chamberlin. 2020. 'Sleep and Anesthesia: The Shared Circuit Hypothesis Has Been Put to Bed', *Curr Biol*, 30: R219-R21.

Engert, F., and T. Bonhoeffer. 1999. 'Dendritic spine changes associated with hippocampal long-term synaptic plasticity', *Nature*, 399: 66-70.

Feinberg, E. H., M. K. Vanhoven, A. Bendesky, G. Wang, R. D. Fetter, K. Shen, and C. I. Bargmann. 2008. 'GFP Reconstitution Across Synaptic Partners (GRASP) defines cell contacts and synapses in living nervous systems', *Neuron*, 57: 353-63.

Feng, G., R. H. Mellor, M. Bernstein, C. Keller-Peck, Q. T. Nguyen, M. Wallace, J. M. Nerbonne, J. W. Lichtman, and J. R. Sanes. 2000. 'Imaging neuronal subsets in transgenic mice expressing multiple spectral variants of GFP', *Neuron*, 28: 41-51.

Ferrarelli, F., M. Massimini, S. Sarasso, A. Casali, B. A. Riedner, G. Angelini, G. Tononi, and R. A. Pearce. 2010. 'Breakdown in cortical effective connectivity during midazolam-induced loss of consciousness', *Proc Natl Acad Sci U S A*, 107: 2681-6.

Fleischmann, T., P. Jirkof, J. Henke, M. Arras, and N. Cesarovic. 2016. 'Injection anaesthesia with fentanyl-midazolam-medetomidine in adult female mice: importance of antagonization and perioperative care', *Lab Anim*, 50: 264-74.

Flint, R. R., T. Chang, R. Lydic, and H. A. Baghdoyan. 2010. 'GABA(A) receptors in the pontine reticular formation of C57BL/6J mouse modulate neurochemical, electrographic, and behavioral phenotypes of wakefulness', *J Neurosci*, 30: 12301-9.

Fosque, B. F., Y. Sun, H. Dana, C. T. Yang, T. Ohyama, M. R. Tadross, R. Patel, M. Zlatic, D. S. Kim, M. B. Ahrens, V. Jayaraman, L. L. Looger, and E. R. Schreiter. 2015. 'Neural circuits. Labeling of active neural circuits in vivo with designed calcium integrators', *Science*, 347: 755-60.

Franks, N. P. 2008. 'General anaesthesia: from molecular targets to neuronal pathways of sleep and arousal', *Nat Rev Neurosci*, 9: 370-86.

Frey, U., and R. G. Morris. 1997. 'Synaptic tagging and long-term potentiation', *Nature*, 385: 533-6.

Garner, A. R., D. C. Rowland, S. Y. Hwang, K. Baumgaertel, B. L. Roth, C. Kentros, and M. Mayford. 2012. 'Generation of a synthetic memory trace', *Science*, 335: 1513-6.

Gauthier, J. L., and D. W. Tank. 2018. 'A Dedicated Population for Reward Coding in the Hippocampus', *Neuron*, 99: 179-93 e7.

Goupil, L., and T. A. Bekinschtein. 2012. 'Cognitive processing during the transition to sleep', *Arch Ital Biol*, 150: 140-54.

Grasshoff, C., and B. Antkowiak. 2006. 'Effects of isoflurane and enflurane on GABAA and glycine receptors contribute equally to depressant actions on spinal ventral horn neurones in rats', *Br J Anaesth*, 97: 687-94.

Grienberger, C., and A. Konnerth. 2012. 'Imaging calcium in neurons', *Neuron*, 73: 862-85.

Gu, L., S. Kleiber, L. Schmid, F. Nebeling, M. Chamoun, J. Steffen, J. Wagner, and M. Fuhrmann. 2014a. 'Long-term in vivo imaging of dendritic spines in the hippocampus reveals structural plasticity', *J Neurosci*, 34: 13948-53.

Gu, Ligang, Stefanie Kleiber, Lena Schmid, Felix Nebeling, Miriam Chamoun, Julia Steffen, Jens Wagner, and Martin Fuhrmann. 2014b. 'Long-Term In Vivo Imaging of Dendritic Spines in the Hippocampus Reveals Structural Plasticity'.

Hardingham, G. E., and H. Bading. 2010. 'Synaptic versus extrasynaptic NMDA receptor signalling: implications for neurodegenerative disorders', *Nat Rev Neurosci*.

Hayashi-Takagi, A., S. Yagishita, M. Nakamura, F. Shirai, Y. I. Wu, A. L. Loshbaugh, B. Kuhlman, K. M. Hahn, and H. Kasai. 2015. 'Labelling and optical erasure of synaptic memory traces in the motor cortex', *Nature*, 525: 333-8.

Hayashi, Y. 2019. 'NMDA Receptor-Dependent Dynamics of Hippocampal Place Cell Ensembles', *J Neurosci*, 39: 5173-82.

Hedenqvist, P., J. V. Roughan, and P. A. Flecknell. 2000. 'Effects of repeated anaesthesia with ketamine/medetomidine and of pre-anaesthetic administration of buprenorphine in rats', *Lab Anim*, 34: 207-11.

Hollmann, M. W., H. T. Liu, C. W. Hoenemann, W. H. Liu, and M. E. Durieux. 2001. 'Modulation of NMDA receptor function by ketamine and magnesium. Part II: interactions with volatile anesthetics', *Anesth Analg*, 92: 1182-91.

Holtmaat, A., and K. Svoboda. 2009. 'Experience-dependent structural synaptic plasticity in the mammalian brain', *Nat Rev Neurosci*, 10: 647-58.

Hung, W. C., Y. L. Chu, M. L. Tsai, S. B. Wong, M. Y. Min, R. F. Chen, and H. W. Yang. 2020. 'GABAB receptor-mediated tonic inhibition of locus coeruleus neurons plays a role in deep anesthesia induced by isoflurane', *Neuroreport*, 31: 557-64.

Izumi, Y., and C. F. Zorumski. 2014. 'Metaplastic effects of subanesthetic ketamine on CA1 hippocampal function', *Neuropharmacology*, 86: 273-81.

Jia, H., N. L. Rochefort, X. Chen, and A. Konnerth. 2010. 'Dendritic organization of sensory input to cortical neurons in vivo', *Nature*, 464: 1307-12.

Jiang-Xie, L. F., L. Yin, S. Zhao, V. Prevosto, B. X. Han, K. Dzirasa, and F. Wang. 2019. 'A Common Neuroendocrine Substrate for Diverse General Anesthetics and Sleep', *Neuron*, 102: 1053-65 e4.

Jurd, R., M. Arras, S. Lambert, B. Drexler, R. Siegwart, F. Crestani, M. Zaugg, K. E. Vogt, B. Ledermann, B. Antkowiak, and U. Rudolph. 2003. 'General anesthetic actions in vivo strongly attenuated by a point mutation in the GABA(A) receptor beta3 subunit', *FASEB J*, 17: 250-2.

Kasai, H., M. Fukuda, S. Watanabe, A. Hayashi-Takagi, and J. Noguchi. 2010. 'Structural dynamics of dendritic spines in memory and cognition', *Trends Neurosci*, 33: 121-9.

Katz, Y., V. Menon, D. A. Nicholson, Y. Geinisman, W. L. Kath, and N. Spruston. 2009. 'Synapse distribution suggests a two-stage model of dendritic integration in CA1 pyramidal neurons', *Neuron*, 63: 171-7.

Kelz, M. B., and G. A. Mashour. 2019. 'The Biology of General Anesthesia from Paramecium to Primate', *Curr Biol*, 29: R1199-R210.

Kentros, C., E. Hargreaves, R. D. Hawkins, E. R. Kandel, M. Shapiro, and R. V. Muller. 1998. 'Abolition of long-term stability of new hippocampal place cell maps by NMDA receptor blockade', *Science*, 280: 2121-6.

Kim, J., T. Zhao, R. S. Petralia, Y. Yu, H. Peng, E. Myers, and J. C. Magee. 2011. 'mGRASP enables mapping mammalian synaptic connectivity with light microscopy', *Nat Methods*, 9: 96-102.

Klinzing, J. G., N. Niethard, and J. Born. 2019. 'Mechanisms of systems memory consolidation during sleep', *Nat Neurosci*, 22: 1598-610.

Kolesnikov, Y. A., I. Chereshnev, and G. W. Pasternak. 2000. 'Analgesic synergy between topical lidocaine and topical opioids', *J Pharmacol Exp Ther*, 295: 546-51.

Krasowski, M. D., and N. L. Harrison. 1999. 'General anaesthetic actions on ligand-gated ion channels', *Cell Mol Life Sci*, 55: 1278-303.

Langsjo, J. W., A. Maksimow, E. Salmi, K. Kaisti, S. Aalto, V. Oikonen, S. Hinkka, R. Aantaa, H. Sipila, T. Viljanen, R. Parkkola, and H. Scheinin. 2005. 'S-ketamine anesthesia increases cerebral blood flow in excess of the metabolic needs in humans', *Anesthesiology*, 103: 258-68.

LaTourette, P. C., E. M. David, C. Pacharinsak, K. Jampachaisri, J. C. Smith, and J. O. Marx. 2020. 'Effects of Standard and Sustained-release Buprenorphine on the Minimum Alveolar Concentration of Isoflurane in C57BL/6 Mice', *J Am Assoc Lab Anim Sci*, 59: 298-304.

Lee, U., S. Ku, G. Noh, S. Baek, B. Choi, and G. A. Mashour. 2013. 'Disruption of frontal-parietal communication by ketamine, propofol, and sevoflurane', *Anesthesiology*, 118: 1264-75.

Lendvai, B., E. A. Stern, B. Chen, and K. Svoboda. 2000. 'Experience-dependent plasticity of dendritic spines in the developing rat barrel cortex in vivo', *Nature*, 404: 876-81.

Li, N., B. Lee, R. J. Liu, M. Banasr, J. M. Dwyer, M. Iwata, X. Y. Li, G. Aghajanian, and R. S. Duman. 2010. 'mTOR-dependent synapse formation underlies the rapid antidepressant effects of NMDA antagonists', *Science*, 329: 959-64.

Lin, D., and Z. Zuo. 2011. 'Isoflurane induces hippocampal cell injury and cognitive impairments in adult rats', *Neuropharmacology*, 61: 1354-9.

Lin, H., P. Higgins, H. H. Loh, P. Y. Law, and D. Liao. 2009. 'Bidirectional effects of fentanyl on dendritic spines and AMPA receptors depend upon the internalization of mu opioid receptors', *Neuropsychopharmacology*, 34: 2097-111.

Lissek, T., H. A. Obenhaus, D. A. Ditzel, T. Nagai, A. Miyawaki, R. Sprengel, and M. T. Hasan. 2016. 'General Anesthetic Conditions Induce Network Synchrony and Disrupt Sensory Processing in the Cortex', *Front Cell Neurosci*, 10: 64.

Liu, H. T., M. W. Hollmann, W. H. Liu, C. W. Hoenemann, and M. E. Durieux. 2001. 'Modulation of NMDA receptor function by ketamine and magnesium: Part I', *Anesth Analg*, 92: 1173-81.

Liu, X., S. Ramirez, P. T. Pang, C. B. Puryear, A. Govindarajan, K. Deisseroth, and S. Tonegawa. 2012. 'Optogenetic stimulation of a hippocampal engram activates fear memory recall', *Nature*, 484: 381-5.

Lydic, R., and H. A. Baghdoyan. 2005. 'Sleep, anesthesiology, and the neurobiology of arousal state control', *Anesthesiology*, 103: 1268-95.

Mashour, G. A., and A. G. Hudetz. 2017. 'Bottom-Up and Top-Down Mechanisms of General Anesthetics Modulate Different Dimensions of Consciousness', *Front Neural Circuits*, 11: 44.

McDonagh, D. L., J. P. Mathew, W. D. White, B. Phillips-Bute, D. T. Laskowitz, M. V. Podgoreanu, M. F. Newman, and Group Neurologic Outcome Research. 2010. 'Cognitive function after major noncardiac surgery, apolipoprotein E4 genotype, and biomarkers of brain injury', *Anesthesiology*, 112: 852-9.

McGaugh, J. L., and H. P. Alpern. 1966. 'Effects of Electroshock on Memory: Amnesia without Convulsions', *Science*, 152: 665-6.

Megias, M., Z. Emri, T. F. Freund, and A. I. Gulyas. 2001. 'Total number and distribution of inhibitory and excitatory synapses on hippocampal CA1 pyramidal cells', *Neuroscience*, 102: 527-40.

Mehta, S., Y. Zhang, R. H. Roth, J. F. Zhang, A. Mo, B. Tenner, R. L. Huganir, and J. Zhang. 2018. 'Single-fluorophore biosensors for sensitive and multiplexed detection of signalling activities', *Nat Cell Biol*, 20: 1215-25.

Miyawaki, A., J. Llopis, R. Heim, J. M. McCaffery, J. A. Adams, M. Ikura, and R. Y. Tsien. 1997. 'Fluorescent indicators for Ca2+ based on green fluorescent proteins and calmodulin', *Nature*, 388: 882-7.

Moeyaert, B., G. Holt, R. Madangopal, A. Perez-Alvarez, B. C. Fearey, N. F. Trojanowski, J. Ledderose, T. A. Zolnik, A. Das, D. Patel, T. A. Brown, R. N. S. Sachdev, B. J. Eickholt, M. E. Larkum, G. G. Turrigiano, H. Dana, C. E. Gee, T. G. Oertner, B. T. Hope, and E. R. Schreiter. 2018. 'Improved methods for marking active neuron populations', *Nat Commun*, 9: 4440.

Moller, J. T., P. Cluitmans, L. S. Rasmussen, P. Houx, H. Rasmussen, J. Canet, P. Rabbitt, J. Jolles, K. Larsen, C. D. Hanning, O. Langeron, T. Johnson, P. M. Lauven, P. A. Kristensen, A. Biedler, H. van Beem, O. Fraidakis, J. H. Silverstein, J. E. Beneken, and J. S. Gravenstein. 1998. 'Long-term postoperative cognitive dysfunction in the elderly ISPOCD1 study. ISPOCD investigators. International Study of Post-Operative Cognitive Dysfunction', *Lancet*, 351: 857-61.

Mollinedo-Gajate, I., C. Song, and T. Knopfel. 2019. 'Genetically Encoded Fluorescent Calcium and Voltage Indicators', *Handb Exp Pharmacol*, 260: 209-29.

Monk, T. G., B. C. Weldon, C. W. Garvan, D. E. Dede, M. T. van der Aa, K. M. Heilman, and J. S. Gravenstein. 2008. 'Predictors of cognitive dysfunction after major noncardiac surgery', *Anesthesiology*, 108: 18-30.

Moore, J. T., J. Chen, B. Han, Q. C. Meng, S. C. Veasey, S. G. Beck, and M. B. Kelz. 2012. 'Direct activation of sleep-promoting VLPO neurons by volatile anesthetics contributes to anesthetic hypnosis', *Curr Biol*, 22: 2008-16.

Morellini, F. 2013. 'Spatial memory tasks in rodents: what do they model?', *Cell Tissue Res*, 354: 273-86.

Morris, R. 1984. 'Developments of a water-maze procedure for studying spatial learning in the rat', *J Neurosci Methods*, 11: 47-60.

Nakai, J., M. Ohkura, and K. Imoto. 2001. 'A high signal-to-noise Ca(2+) probe composed of a single green fluorescent protein', *Nat Biotechnol*, 19: 137-41.

Nasu, Yusuke, Yi Shen, Luke Kramer, and Robert E. Campbell. 2021. 'Structure- and mechanism-guided design of single fluorescent protein-based biosensors', *Nature Chemical Biology*, 17: 509-18.

Nelson, L. E., J. Lu, T. Guo, C. B. Saper, N. P. Franks, and M. Maze. 2003. 'The alpha2-adrenoceptor agonist dexmedetomidine converges on an endogenous sleep-promoting pathway to exert its sedative effects', *Anesthesiology*, 98: 428-36.

Neves, G., S. F. Cooke, and T. V. Bliss. 2008. 'Synaptic plasticity, memory and the hippocampus: a neural network approach to causality', *Nat Rev Neurosci*, 9: 65-75.

Nicoll, R. A. 1978. 'Pentobarbital: differential postsynaptic actions on sympathetic ganglion cells', *Science*, 199: 451-2.

Nimchinsky, E. A., B. L. Sabatini, and K. Svoboda. 2002. 'Structure and function of dendritic spines', *Annu Rev Physiol*, 64: 313-53.

Nishikawa, K. 2011. '[Roles of glutamatergic and GABAergic nervous system in hypnotic and analgesic actions of general anesthetics]', *Masui*, 60: 534-43.

Ogata, J., M. Shiraishi, T. Namba, C. T. Smothers, J. J. Woodward, and R. A. Harris. 2006. 'Effects of anesthetics on mutant N-methyl-D-aspartate receptors expressed in Xenopus oocytes', *J Pharmacol Exp Ther*, 318: 434-43.

Ohkawa, N., Y. Saitoh, A. Suzuki, S. Tsujimura, E. Murayama, S. Kosugi, H. Nishizono, M. Matsuo, Y. Takahashi, M. Nagase, Y. K. Sugimura, A. M. Watabe, F. Kato, and K. Inokuchi. 2015. 'Artificial association of pre-stored information to generate a qualitatively new memory', *Cell Rep*, 11: 261-9.

Olkkola, K. T., and J. Ahonen. 2008. 'Midazolam and other benzodiazepines', *Handb Exp Pharmacol*: 335-60.

Patel, A. J., E. Honore, F. Lesage, M. Fink, G. Romey, and M. Lazdunski. 1999. 'Inhalational anesthetics activate two-pore-domain background K+ channels', *Nat Neurosci*, 2: 422-6.

Petrenko, A. B., T. Yamakura, K. Sakimura, and H. Baba. 2014. 'Defining the role of NMDA receptors in anesthesia: are we there yet?', *Eur J Pharmacol*, 723: 29-37.

Pfeiffer, T., S. Poll, S. Bancelin, J. Angibaud, V. K. Inavalli, K. Keppler, M. Mittag, M. Fuhrmann, and U. V. Nagerl. 2018. 'Chronic 2P-STED imaging reveals high turnover of dendritic spines in the hippocampus in vivo', *Elife*, 7.

Phoumthipphavong, V., F. Barthas, S. Hassett, and A. C. Kwan. 2016. 'Longitudinal Effects of Ketamine on Dendritic Architecture In Vivo in the Mouse Medial Frontal Cortex', *eNeuro*, 3.

Pologruto, T. A., R. Yasuda, and K. Svoboda. 2004. 'Monitoring neural activity and [Ca2+] with genetically encoded Ca2+ indicators', *J Neurosci*, 24: 9572-9.

Portera-Cailliau, C., D. T. Pan, and R. Yuste. 2003. 'Activity-regulated dynamic behavior of early dendritic protrusions: evidence for different types of dendritic filopodia', *J Neurosci*, 23: 7129-42.

Pryazhnikov, E., E. Mugantseva, P. Casarotto, J. Kolikova, S. M. Fred, D. Toptunov, R. Afzalov, P. Hotulainen, V. Voikar, R. Terry-Lorenzo, S. Engel, S. Kirov, E. Castren, and L. Khiroug. 2018. 'Longitudinal two-photon imaging in somatosensory cortex of behaving mice reveals dendritic spine formation enhancement by subchronic administration of low-dose ketamine', *Sci Rep*, 8: 6464.

Purdon, P. L., E. T. Pierce, G. Bonmassar, J. Walsh, P. G. Harrell, J. Kwo, D. Deschler, M. Barlow, R. C. Merhar, C. Lamus, C. M. Mullaly, M. Sullivan, S. Maginnis, D. Skoniecki, H. A. Higgins, and E. N. Brown. 2009. 'Simultaneous electroencephalography and functional magnetic resonance imaging of general anesthesia', *Ann N Y Acad Sci*, 1157: 61-70.

Ramirez, S., X. Liu, P. A. Lin, J. Suh, M. Pignatelli, R. L. Redondo, T. J. Ryan, and S. Tonegawa. 2013. 'Creating a false memory in the hippocampus', *Science*, 341: 387-91.

Redinbaugh, M. J., J. M. Phillips, N. A. Kambi, S. Mohanta, S. Andryk, G. L. Dooley, M. Afrasiabi, A. Raz, and Y. B. Saalmann. 2020. 'Thalamus Modulates Consciousness via Layer-Specific Control of Cortex', *Neuron*, 106: 66-75 e12.

Reijmers, L. G., B. L. Perkins, N. Matsuo, and M. Mayford. 2007. 'Localization of a stable neural correlate of associative memory', *Science*, 317: 1230-3.

Richards, B. A., and P. W. Frankland. 2017. 'The Persistence and Transience of Memory', *Neuron*, 94: 1071-84.

Ries, C. R., and E. Puil. 1999. 'Mechanism of anesthesia revealed by shunting actions of isoflurane on thalamocortical neurons', *J Neurophysiol*, 81: 1795-801.

Rudolph, U., and B. Antkowiak. 2004. 'Molecular and neuronal substrates for general anaesthetics', *Nat Rev Neurosci*, 5: 709-20.

Salussolia, C. L., M. L. Prodromou, P. Borker, and L. P. Wollmuth. 2011. 'Arrangement of subunits in functional NMDA receptors', *J Neurosci*, 31: 11295-304.

Sara, S. J. 2009. 'The locus coeruleus and noradrenergic modulation of cognition', *Nat Rev Neurosci*, 10: 211-23.

Sarasso, S., M. Boly, M. Napolitani, O. Gosseries, V. Charland-Verville, S. Casarotto, M. Rosanova, A. G. Casali, J. F. Brichant, P. Boveroux, S. Rex, G. Tononi, S. Laureys, and M. Massimini. 2015. 'Consciousness and Complexity during Unresponsiveness Induced by Propofol, Xenon, and Ketamine', *Curr Biol*, 25: 3099-105.

Scoville, W. B., and B. Milner. 1957. 'Loss of recent memory after bilateral hippocampal lesions', *J Neurol Neurosurg Psychiatry*, 20: 11-21.

Segal, M. 2005. 'Dendritic spines and long-term plasticity', *Nat Rev Neurosci*, 6: 277-84.

Sherin, J. E., P. J. Shiromani, R. W. McCarley, and C. B. Saper. 1996. 'Activation of ventrolateral preoptic neurons during sleep', *Science*, 271: 216-9.

Sinclair, M. D. 2003. 'A review of the physiological effects of alpha2-agonists related to the clinical use of medetomidine in small animal practice', *Can Vet J*, 44: 885-97.

Solt, K., J. F. Cotten, A. Cimenser, K. F. Wong, J. J. Chemali, and E. N. Brown. 2011. 'Methylphenidate actively induces emergence from general anesthesia', *Anesthesiology*, 115: 791-803.

Solt, K., C. J. Van Dort, J. J. Chemali, N. E. Taylor, J. D. Kenny, and E. N. Brown. 2014. 'Electrical stimulation of the ventral tegmental area induces reanimation from general anesthesia', *Anesthesiology*, 121: 311-9.

Soltesz, I., and M. Deschenes. 1993. 'Low- and high-frequency membrane potential oscillations during theta activity in CA1 and CA3 pyramidal neurons of the rat hippocampus under ketamine-xylazine anesthesia', *J Neurophysiol*, 70: 97-116.

Soltesz, I., and A. Losonczy. 2018. 'CA1 pyramidal cell diversity enabling parallel information processing in the hippocampus', *Nat Neurosci*, 21: 484-93.

Sonner, J. M., D. F. Werner, F. P. Elsen, Y. Xing, M. Liao, R. A. Harris, N. L. Harrison, M. S. Fanselow, E. I. Eger, 2nd, and G. E. Homanics. 2007. 'Effect of isoflurane and other potent inhaled anesthetics on minimum alveolar concentration, learning, and the righting reflex in mice engineered to express alpha1 gamma-aminobutyric acid type A receptors unresponsive to isoflurane', *Anesthesiology*, 106: 107-13.

Squire, L. R. 1992. 'Memory and the hippocampus: a synthesis from findings with rats, monkeys, and humans', *Psychol Rev*, 99: 195-231.

Squire, L. R., C. E. Stark, and R. E. Clark. 2004. 'The medial temporal lobe', *Annu Rev Neurosci*, 27: 279-306.

Steinberg, E. A., K. A. Wafford, S. G. Brickley, N. P. Franks, and W. Wisden. 2015. 'The role of K(2)p channels in anaesthesia and sleep', *Pflugers Arch*, 467: 907-16.

Steriade, M., A. Nunez, and F. Amzica. 1993. 'A novel slow (< 1 Hz) oscillation of neocortical neurons in vivo: depolarizing and hyperpolarizing components', *J Neurosci*, 13: 3252-65.

Suzuki, M., and M. E. Larkum. 2020. 'General Anesthesia Decouples Cortical Pyramidal Neurons', *Cell*, 180: 666-76 e13.

Szymusiak, R., and D. McGinty. 2008. 'Hypothalamic regulation of sleep and arousal', *Ann N Y Acad Sci*, 1129: 275-86.

Tanaka, K. Z., A. Pevzner, A. B. Hamidi, Y. Nakazawa, J. Graham, and B. J. Wiltgen. 2014. 'Cortical representations are reinstated by the hippocampus during memory retrieval', *Neuron*, 84: 347-54.

Tayler, K. K., K. Z. Tanaka, L. G. Reijmers, and B. J. Wiltgen. 2013. 'Reactivation of neural ensembles during the retrieval of recent and remote memory', *Curr Biol*, 23: 99-106.

Theer, P., M. T. Hasan, and W. Denk. 2003. 'Two-photon imaging to a depth of 1000 microm in living brains by use of a Ti:Al2O3 regenerative amplifier', *Opt Lett*, 28: 1022-4.

Urban, B. W., and M. Bleckwenn. 2002. 'Concepts and correlations relevant to general anaesthesia', *Br J Anaesth*, 89: 3-16.

Vanini, G., M. Bassana, M. Mast, A. Mondino, I. Cerda, M. Phyle, V. Chen, A. V. Colmenero, V. S. Hambrecht-Wiedbusch, and G. A. Mashour. 2020. 'Activation of Preoptic GABAergic or Glutamatergic Neurons Modulates Sleep-Wake Architecture, but Not Anesthetic State Transitions', *Curr Biol*, 30: 779-87 e4.

Vanini, G., B. L. Wathen, R. Lydic, and H. A. Baghdoyan. 2011. 'Endogenous GABA levels in the pontine reticular formation are greater during wakefulness than during rapid eye movement sleep', *J Neurosci*, 31: 2649-56.

Vanini, G., C. J. Watson, R. Lydic, and H. A. Baghdoyan. 2008. 'Gamma-aminobutyric acid-mediated neurotransmission in the pontine reticular formation modulates hypnosis, immobility, and breathing during isoflurane anesthesia', *Anesthesiology*, 109: 978-88.

Vardanyan, R. S., and V. J. Hruby. 2014. 'Fentanyl-related compounds and derivatives: current status and future prospects for pharmaceutical applications', *Future Med Chem*, 6: 385-412.

Varin, C., and P. Bonnavion. 2019. 'Pharmacosynthetic Deconstruction of Sleep-Wake Circuits in the Brain', *Handb Exp Pharmacol*, 253: 153-206.

Velly, L. J., M. F. Rey, N. J. Bruder, F. A. Gouvitsos, T. Witjas, J. M. Regis, J. C. Peragut, and F. M. Gouin. 2007. 'Differential dynamic of action on cortical and subcortical structures of anesthetic agents during induction of anesthesia', *Anesthesiology*, 107: 202-12.

Wang, W., J. Cai, Y. Lin, Z. Liu, Q. Ren, L. Hu, Z. Huang, M. Guo, and W. Li. 2014. 'Zinc fingers function cooperatively with KRAB domain for nuclear localization of KRAB-containing zinc finger proteins', *PLoS One*, 9: e92155.

Wei, Ziqiang, Bei-Jung Lin, Tsai-Wen Chen, Kayvon Daie, Karel Svoboda, and Shaul Druckmann. 2020. 'A comparison of neuronal population dynamics measured with calcium imaging and electrophysiology', *PLOS Computational Biology*, 16: e1008198.

West, A. E., E. C. Griffith, and M. E. Greenberg. 2002. 'Regulation of transcription factors by neuronal activity', *Nat Rev Neurosci*, 3: 921-31.

Whitlock, J. R., A. J. Heynen, M. G. Shuler, and M. F. Bear. 2006. 'Learning induces long-term potentiation in the hippocampus', *Science*, 313: 1093-7.

Wiegert, J. S., and H. Bading. 2011. 'Activity-dependent calcium signaling and ERK-MAP kinases in neurons: a link to structural plasticity of the nucleus and gene transcription regulation', *Cell Calcium*, 49: 296-305.

Wiegert, J. S., and T. G. Oertner. 2013. 'Long-term depression triggers the selective elimination of weakly integrated synapses', *Proc Natl Acad Sci U S A*, 110: E4510-9.

Wiegert, J. S., M. Pulin, C. E. Gee, and T. G. Oertner. 2018. 'The fate of hippocampal synapses depends on the sequence of plasticity-inducing events', *Elife*, 7.

Wiklund, A., S. Granon, P. Faure, E. Sundman, J. P. Changeux, and L. I. Eriksson. 2009. 'Object memory in young and aged mice after sevoflurane anaesthesia', *Neuroreport*, 20: 1419-23.

Yamakage, M., C. A. Hirshman, and T. L. Croxton. 1995. 'Inhibitory effects of thiopental, ketamine, and propofol on voltage-dependent Ca2+ channels in porcine tracheal smooth muscle cells', *Anesthesiology*, 83: 1274-82.

Yang, G., P. C. Chang, A. Bekker, T. J. Blanck, and W. B. Gan. 2011. 'Transient effects of anesthetics on dendritic spines and filopodia in the living mouse cortex', *Anesthesiology*, 115: 718-26.

Yang, G., F. Pan, and W. B. Gan. 2009. 'Stably maintained dendritic spines are associated with lifelong memories', *Nature*, 462: 920-4.

Yang, Y., Y. Cui, K. Sang, Y. Dong, Z. Ni, S. Ma, and H. Hu. 2018. 'Ketamine blocks bursting in the lateral habenula to rapidly relieve depression', *Nature*, 554: 317-22.

Yasuda, R., E. A. Nimchinsky, V. Scheuss, T. A. Pologruto, T. G. Oertner, B. L. Sabatini, and K. Svoboda. 2004. 'Imaging calcium concentration dynamics in small neuronal compartments', *Sci STKE*, 2004: pl5.

Yuzgec, O., M. Prsa, R. Zimmermann, and D. Huber. 2018. 'Pupil Size Coupling to Cortical States Protects the Stability of Deep Sleep via Parasympathetic Modulation', *Curr Biol*, 28: 392-400 e3.

Zhang, K., and K. Hashimoto. 2019. 'An update on ketamine and its two enantiomers as rapid-acting antidepressants', *Expert Rev Neurother*, 19: 83-92.

Zhang, Yan; , Márton; Rózsa, Daniel; Bushey, Jihong; Zheng, Daniel; Reep, and Gerard Joey; Broussard. 2020. 'jGCaMP8: a new suite of fast and sensitive calcium indicators'.

Zurek, A. A., E. M. Bridgwater, and B. A. Orser. 2012. 'Inhibition of alpha5 gamma-Aminobutyric acid type A receptors restores recognition memory after general anesthesia', *Anesth Analg*, 114: 845-55.

Zurek, A. A., J. Yu, D. S. Wang, S. C. Haffey, E. M. Bridgwater, A. Penna, I. Lecker, G. Lei, T. Chang, E. W. Salter, and B. A. Orser. 2014. 'Sustained increase in alpha5GABAA receptor function impairs memory after anesthesia', *J Clin Invest*, 124: 5437-41.

Wei, Ziqiang, Bei-Jung Lin, Tsai-Wen Chen, Kayvon Daie, Karel Svoboda, and Shaul Druckmann. 2020. 'A comparison of neuronal population dynamics measured with calcium imaging and electrophysiology', PLOS Computational Biology, 16: e1008198.

5.2 Statement of contribution

List of Contributions

Wei Yang produced all of the results with the exception of those listed below. Thy-1-GFP-M mouse line was collected from Prof. Michael Frotscher. In vivo two-photon imaging analysis were performed by Mattia Chini (figure 4,5,6) and Andrey Formozov (figure 6,9). In vivo LTP recordings were performed and analyzed by Jastyn Pöpplau (figure 7,8). Pupil and eyelid analysis were performed by Alexander Dieter (figure 14). Spine counting were performed with the help of Patrick Piechocinski and Cynthia Rais. All histology experiments were performed by Stefan Schillemeit. AAVs were produced by Dr. Ingke Braren. Prof. Simon Wiegert generated the concept of the project, supervised the project and provided funding. This work is funded by grants from the European Research Council (ERC-2016-StG 714762 to J.S.W) and scholarship to W.Y from China Scholarship Council.

5.3 Curriculum vitae

Personal information

Surname, first name: Yang, Wei

Date of birth: 06.10.1990

Gender: Female

Nationality: P.R.China

Education

07/2017-present PhD in Neurobiology at Hamburg University, Germany

laboratory of Prof. Simon Wiegert

10/2016-06/2017 Intership in Neurobiology at Hamburg University, Germany

laboratory of Prof. Dr. med. Dr. h. c.Michael Frotscher,

09/2013-06/2016 MSc in Biology at Peking Union Medical College, China

laboratory of Prof. Qi Xu

09/2009-06/2013 Bachelor in Biology at China Medical University, China

PUBLICATIONS

1. **Wei Yang**, Mattia Chini, Jastyn A Pöpplau, Andrey Formozov, Alexander Dieter, …, Ileana L Hanganu-Opatz, J Simon Wiegert. Anesthetics uniquely decorrelate hippocampal network activity, alter spine dynamics and affect memory consolidation. PLoS Biol 19(4): e3001146.

2. Alberto Perez-Alvarez, Brenna C Fearey, Ryan J O'Toole, **Wei Yang**, …, Eric R Schreiter, J Simon Wiegert, Christine E Gee, Michael B Hoppa, Thomas G Oertner. Freeze-frame imaging of synaptic activity using SynTagMA. Nat Commun 11, 2464 (2020).

3. **Wei Yang**, Chunyan Zhu, Yan Shen, Qi Xu. The pathogenic mechanism of dysbindin-1B toxic aggregation: BLOC-1 and intercellular vesicle trafficking. Neuroscience. 2016 Oct 1; 333:78-91.